Synthesis and Characterizations of Organic based Mechanoluminescent Materials

静岡大学博士論文

Synthesis and Characterizations of Organic based Mechanoluminescent Materials

有機材料を利用した応力発光材料の合成と特性評価

Ranasinghe Arachchilage Don Manoj Ranasinghe

大学院自然科学系教育部

光・ナノ物質機能専攻

2017 年 6 月

Abstract

This research devoted to study synthesis and characterization of an organic based mechanoluminescent (ML) materials. The organic europium-doped dibenzoylmethide triethylammonium (EuD_4TEA) is a well-known ML material and is used as a basis for this study. In this thesis, the enhancement of the ML properties and crystalline structure was investigated.

ML is a light-emission event that results from a mechanical action on a solid. Fracto-, plastico- and elastico-ML are various forms of ML. Among the various ML forms, fracto-ML is well known because most of the inorganic materials emit light when they are fractured. For example, mechanical stress relaxation during and prior the earthquake results in fractoluminescence. Additionally, plastico-ML can be observed by peeling an adhesive tape in a vacuum. When the crystal bonds are broken along oppositely charged planes and then reconnect, light is emitted as the charges pass through the gaps that were created from the fracture. Once the material is fractured, the electrons are excited to higher energy levels and then transition to the lower energy levels. The energy difference between the corresponding levels is emitted as a light with different wavelengths. The third type of ML mechanism, elastico-ML, results from a mechanical stress that produces a piezoelectric field on the surface of crystals. This electric field that is near the color centre is high because of changes in the local structure. These changes may reduce the carrier trap depth or effect band bending. After decreasing the carrier trap depth, the thermal de-trapping of the carriers may occur. Trapped charge carriers can tunnel to the conduction band because of the band bending. The electrons from the conduction band may be captured by the excited state of the activator ions. This may cause a de-excitation of the color centre and produce the emission. When plastico-mechanoluminescent materials are plastically deformed, a movement of dislocation occurs. Similarly, an electric field generated by the charge dislocation causes a bending of the valance, conduction and dislocation bands. Trapped electrons tunnel to the conduction band and the recombination of electrons and holes enables the light emission characteristic of the color centre. However, the conduction band electrons are trapped by the color center, and a potential energy transfer occurs as a result of the de-excitation of the rare-earth cation. Both functions occur, and electron-hole recombination is greater than that caused by the impact excitation. To date, many inorganic mechanoluminescent materials have been synthesized with various dopants.

Our group has synthesized a novel ML material with the addition of 1-ethenylpyrrolidin-2-one [(polyvinylpyrrolidone) (PVP)], which changed the ligand EuI_2, $EuBr_2$ and $EuCl_2$ of the mechanoluminescent material. This study investigated the ML substance structure, molecular orbital electron distributions of the ligands, ML mechanism and enhancement in the photoluminescence (PL) intensity with PVP. For the first time, the ML material structure was characterized using nuclear magnetic resonance spectroscopy (NMR), X-ray photoelectron spectroscopy (XPS), X-ray diffraction (XRD) and Gaussian DFT/B3LYP/6-31G(d,p) software. The ML properties were characterized using a Hamamatsu Photonic Multichannel Analyzer (PMA).

We have investigated the low-temperature effect on the form mechanoluminescent material with different ligands. The study revealed that ML intensity can be controlled by the addition of ligands with different oxidation state of Eu. The highest enhancement of the ML intensity is obtained by adding Eu^{+2} containing ligands. The higher ML intensity in case of Eu^{+2}, can be explained by higher flexibility of the coordinated structure, because Eu^{+2} has only two bonds with benzoyl groups. Therefore, higher flexibility of the coordinated structure, allows higher orbital overlapping and reduce the distance between cation, and ligand. Moreover, ML intensity is affected by different chalcogenide anions from Eu compounds – EuI_2, $EuBr_2$ and $EuCl_2$. The highest enhancement of the ML intensity is obtained by adding EuI_2, followed by $EuBr_2$ and the lowest ML intensity was observed in case of $EuCl_2$. The low ML intensity in case of $EuCl_2$, can be explained by the high electron affinity of Cl^- anions, which is disrupting EuD_4TEA band structure and reducing radiative recombination of electrons.

Since changing the valence of the ML, material occurs to varying the ML and PL intensity of the materials. However, DSC characterization depicted that glass transition of the ML material changes after treated with liquid nitrogen and occur to increase the crystallinity of the synthesized ML materials. Integrated materials were distinguished by using Differential scanning calorimetry (DSC), X-ray photon spectroscopy(XPS) and X-Ray diffractometer (XRD).

The material can be applied to the real-time visualization of the stress field near the tip of a crack, an ML light source, determination of laser and ultrasonic powers, secret message writing and earthquake-detection sensors. The further study concerned to fabricate the ML thin film without using any binder or resin. The first time we have achieved to form a thin film of the PVP-added EuD_4TEA. The thin films with different quantities of the PVP addition are

developed on an Al_2O_3 buffer layer fabricated on Ni substrate. The present study has examined a relationship among both the ML and the photoluminescence characteristics of thin films and the counting amount. For the first time, we have fabricated the ML thin film without any use of binder or resin. The results infer that the properties are entirely related to a crystallinity of the thin films. Also, we have succeeded to form a thin film with using synthesized ML nanoparticles. Research carried out about synthesis and fabricated the Mechanoluminescent thin film by using mechanoluminescent nanoparticles. Novel organic based mechanoluminescent material is incorporated by using polyvinylpyrrolidone with higher intensity.

Acknowledgement

With the deep sense of appreciation, I wish to express my sincere thanks to my Supervisor Professor Murakami Kenji, co-supervisors Professor Masaru Shimomura and Professor Kazuhiko Hara and for their excellent guidance and support throughout this work. I experienced very valuable and excellent academic training from them, which has stood in good stead while writing this thesis. Their unique, inimitable style has left an indelible impression on me. Their constant encouragement, help, and review of the entire work during the research of the investigation are invaluable. I would like to express my thanks to Associate Professor Masayuki Okuya and thesis Reviewer Associate professor Yasutaka Tanaka for their great supported to accomplished my research, Also I would like to express my heartfelt thanks to Professor R.M.G.Rajapakse who is gave excellent guidance to success my research studies. Nevertheless, it helped me to acquire and develop some of the skills and intricacies of much independent research. I must express my deep sensitivity and gratitude to Professor Hayakawa, associate professor Navaneethan and their laboratory students who given great support to achieve my research also, Technicians on the Department of optoelectronic and nanostructure's science in Shizuoka University, for their constant and selfless support at each stage of my project work. My sincere gratefulness to all the faculty members, research scholars and friends for their encouragement and kind help extended towards me. Last but not the least, I am very thankful to Dr. Viraj Priyanka whom currently working in an SPD laboratory in Hamamatsu for the design of the ML setup to succeed my research and my laboratory colleagues specially Edvīns Daukšta, Saveedya jayawardana, Hirulak siriwardana who gave neversent support and all my hall mates for their tremendous cooperation without whom my stay here would not have been memorable. Finally, I would like to share this moment of happiness with my family members for whom I do what I do.

List of Abreviations

ML.....Mechanoluminescent

T_1.....triplet excited state

S_0.....Singlet state

FML .....Fracto mechanoluminescent

PML .....Plastico mechanoluminescent

EML ..... Elastico mechanoluminescent

AHC .....

T_1..... Triplet Energy state

XPS .....X-ray Photoelectron Spectroscopy

ESCA .....Electron Spectroscopy for Chemical Analysis

KE .....Kinetic Energy

BE .....Electron Binding Energy

Φ ..... Spectrometer Work Function

DSC.....Differential scanning calorimetry

SEM ..... Scanning Electron Microscopy

XRD.....X-Ray Diffractometer

PMA..... Photonic multichannel analyzer

NMR .....Nuclear Magnetic Resonance spectroscopy

TEM .....Transmission electron microscope

CCD ..... charge couple device

EuD_4TEA ..... europium dibenzoylmethide triethylammonium

PVP .....polyvinylpyrrolidone

PL.....Photoluminescence

JCPDS.....Joint Committee on Powder Diffraction Standards

FESEM..... -Field Emission Scanning Electron Microscope

DBM .....Dibenzoylmethane

TEA..... Triethylamine

MO .....Molecular orbital

HOMO .....Higher occupied molecular orbital

LUMO.....Lower unoccupied molecular orbital

DFT .....Density Functional Theory

eV ..... Electron volt

CIE .....Commission on Illumination

Phen.....Phenanthroline

CONTENTS

Chapter 1 Introduction

1.1 General background

Luminescence is the usually define as an emission of light which is not an effect of elevated temperature[1]. So, luminescence can figure out as an expression of cold body radiation[2]. This radioactivity can unless being part of a chemical reaction or a matter of subatomic movements or stress on a crystal[3]. Another way to create emission is incandescence where a property transmits light as the result of heat[4]. Luminescence can be described as "a spontaneous transmission of radiation from an electronically induced species, not in thermal equilibrium with its environment[5]." The term of "luminescence" was invented in 1888 by Eilhardt Wiedemann, a German physicist. Luminescence can be grouped into two kinds of emission transitions define as fluorescence and phosphorescence[6]. Fluorescence is the light emission occurring from the

S_1 (singlet excited state) to S_0 (singlet ground state) transition and ends in 10^{-9}-10^{-7} s[7]. Phosphorescence is the emission resulting from the T_1 (triplet excited state) to S0 (singlet state) transition[8]. The electron transition happens between energy states with different spin multiplicities[9]. The emission lifetime is longer (10^{-3}-100 s) than fluorescence because it is a spin-forbidden transition[10]. The singlet excited states are reformed triplet excited states through intersystem crossing. The excitons can also decay non-radiatively, producing heat[11].The diagram explains the mechanism of luminescence[12].

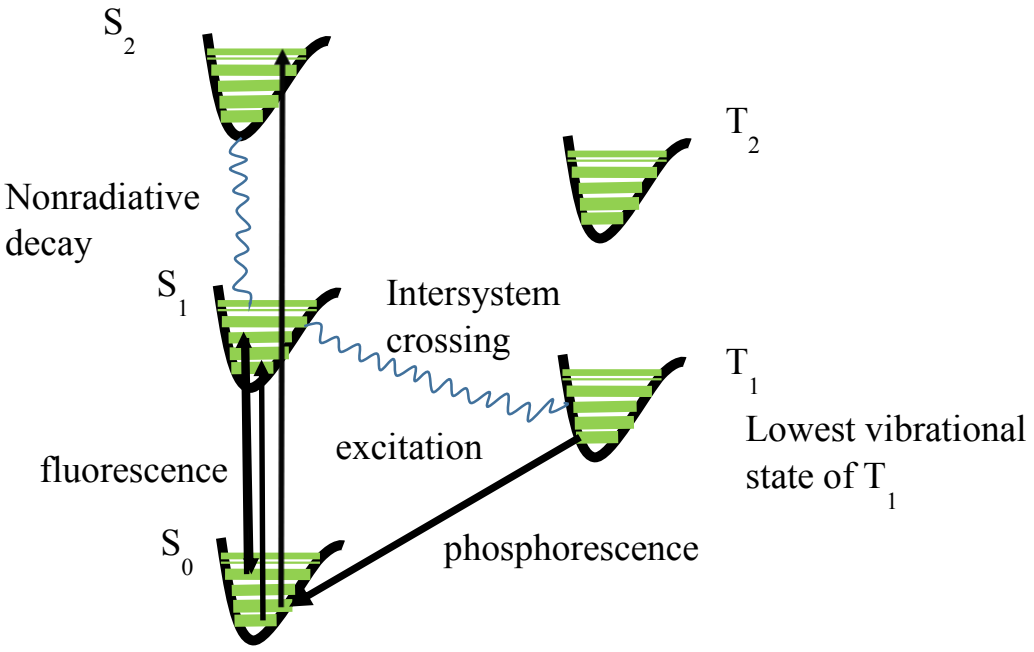

Figure 1 Energy level diagram and summary of photochemical process

1.2 Types of luminescence

1.2.1 Bioluminescence

Luminescence originated by a living organism[13]. The light is generating molecules be turned into excited by a chemical reaction. Bioluminescence is consequently correlated to chemiluminescence[14]. Some organic things like bugs, e.g. fireflies, denizens of the deep like anglerfish, some mushrooms and even bacteria can control this reaction[15]. They produce the chemicals pigment and an enzyme. The pigment reacts with oxygen to create light[16]. The enzymes act as a catalyst to speed up the reaction[17]

1.2.2 Chemiluminescence

Chemiluminescence generates resulting of some chemical or electrochemical reactions[18]. Required energy comes from the reaction enthalpy. The reaction produces some innovative molecule that can have its electrons in an excited state right after it was settled[19]. Decay to a ground state may then generate visible light or release the energy in some other way. The flash of light see when some dynamite detonates is not chemiluminescence despite so the energy comes from a chemical reaction but naturally black body radiation or incandescence from things getting hot very quickly[20].

1.2.3 Crystalloluminescence

infrequently performed during crystallization, it is another variant of chemiluminescence because the energy comes originally from bonding among the nucleus[21].

1.2.4 Electro-luminescence

Forms light in response to an electric current passing through some material Electroluminescence occurs radiative recombination of electrons and holes, typically in semiconductors[22]. Electroluminescence is the reformation regarding electrical energy to light[23]. In 1960 Electroluminescence in organic crystals was minted by Helfrich and Schneider[24]. In their investigation, they used electrolyte solutions containing anthracene cations (anode) and anions (cathode). They perceived a linear increment in emission intensity with enhancing current density.That emission typically occurred from the region near the anode, demonstrating that electrons from the cathode move through the crystal to combine with the holes from the anode. This indicates that charge injection electroluminescence occurs via bulk-controlled charge transport and recombination[25].

1.2.5 Cathodoluminescence

Cathodoluminescence results when an electron beam bearings on a luminescent substance such as a phosphor[26]. Scientists are also converging at the cathodoluminescence that specimen show

in the electron beam of a Scanning Electron microscopeCathodoluminescence is applying for producing displays, traditional cathode ray tube or television tube that was lately redeemed by flat screen displays. Still, require cathodoluminescence for the electron microscope for simple designs. It can use as an analytical tool. The phosphors lead to be large bandgap semiconductors line as ZnO, because if the color does require like for an old type television, more concerned different materials emitting red, green, and blue are important[27].

Photoluminescence is produced by transferring electrons to energetically higher levels through the absorption of photons[28]. It is easily done in semiconductors with photons of energy greater than the bandgap, radiating recombination carriers than produce bandgap light[29].

1.2.6 Sonoluminescence

Sonoluminescence is the ejection of short discharges of light from imploding bubbles in a liquid when stimulated by sound. The mechanism is not remarkably clear at present, and somewhat unusual interpretations have been suggested by well know scientists[30].

1.2.7 Thermoluminescence

Describes the happening that particular crystalline materials transmit light when heated that is not black body radiation or radiance[31]. What occurs is that initially absorbed energy from a source excited electrons stays in higher energy states, consistently at defects. Thermoluminescence is an original way of defining some archeological artifactsIt is presented in the kind of light if some thermal energy releases the excited electrons to achieve the energy limit. Ceramic parts being appropriated gain some ionizing serving from radioactive elements in the soil or from cosmic rays that are comparative to their age and so is the energy of the luminescence generate consequent to heating[32].

1.2.8 Mechanoluminescence

Light-induced by any mechanical action called mechanoluminescent[33]. The ML has also been termed by many other names, such as deformation luminescence, triboluminescence, piezoluminescence, and stress-activated luminescence. Mechanoluminescent (ML) is a sort of luminescence produced by any mechanical performance on solids[34]. It can be induced by shivering, spreading, splitting, cleaving, waving, damaging, reducing, or mashing of solids. ML can further be effected by thermal shocks generated by radical cooling or heating of elements. On the other hand by the shock waves formed during expression of samples to powerful laser pulses. ML also performs during the deformation prompted by the phase transformation or growth of specific crystals as well as during dissociation of two different materials in contact. Since the designation mechanoluminescent is associated in a usual way with varying mechanical intellection, such as fracto, plastico, elastico, deformation, piezo, tribo, stress, cutting, crushing, There are three main categories of mechanoluminescent materials. Fracto mechanoluminescent (FML), Plastico mechanoluminescent(PML), Elastico mechanoluminescent(EML)[35].

1.2.8.1 Fracto mechanoluminescent

The light is transmitting from the material After the material getting fracture called fracto mechanoluminescent. Figure 2 shows the Langevin model for the creation of charged surfaces

While the movement of a crack in a PC (Langevin, 1921). The piezoelectric constants and the stress wanted to break the surfaces of crystals are usually of the order of 10^{-12}-10^{-11} coulombs CN^{-1} and 108 Nm^{-2}, consequently. Thus, the charge density γ of the lately formed surfaces is of the order of 10^{-4}-10^{-3} C m^{-2} The electric field among the contrarily charged surfaces will be $\gamma/80$, where 80 defining permittivity of free space, equal to 8.85 x 10^{-12} C^2 N^{-1} m^{-2}. Hence, an electric field of the order of 107 -108 V m^{-1} may be formed between the newly created oppositely charged surfaces. This electric field may produce the dielectric breakdown of the intermediate gasses and indeed may give rise to gaseous discharge ML. The potential may also cause the

dielectric breakdown of the crystals, and the recombination of free carriers may increase to activate the luminescence. Furthermore, the accelerated electrons moving from negatively charged surfaces toward the positively charged surface may trigger the cathodoluminescent[36].

1.2.8.2 Plastico mechanoluminescent

Thermal excitation mechanism to explain PML in noncolored AHC. According to this mechanism, there is a possibility that thermally activated electronic transitions can occur in regions of high stress when, upon fluctuational displacements along the configuration coordinate, the potential curves of the ground and excited states cross each other. This effect is the inverse of thermal radiation less quenching of excited states. Low-energy excitons like electronic excitations that are formed can dissociate at dislocations, giving rise to electrons and holes in the dislocation bands. To explain the emission phenomena, one must assume that the centers that are formed are mobile and can move away from where they are formed along the dislocation bands. These dislocation electrons and holes are captured by anion and cation vacancies, respectively. The recombination of these centers lead to the excitation of luminescence[37].

1.2.8.3 Elastico mechanoluminescent

The elastic deformation makes bending of the dislocation segments. The electric field of the charged dislocation fragments creates bending of the valance band and conduction band as well as dislocation bands. Consequently, the electrons from the electron trap sites de-trapping and tunnel to the conduction band. The recombination of electrons with the holes gives rise to the light emission characteristic of the activator centers. The phenomenon of the piezoelectrically-stimulated electron de-trapping model of the elastico $SrAl_2O_4$: Eu^{+3} crystals may be identified in the following way, The deformation of $SrAl_2O_4$: Eu^{+3} nanocrystals generates piezoelectric field since crystal structure of $SrAl_2O_4$ is non-centrosymmetric. Because of the shrinkage in the trap-

depth due to the piezoelectric field, the de-trapping of electrons from filled-electron traps demands place, and therefore, electrons arrive the conduction band. The electrons reaching the conduction band may recombine with the holes trapped in the defect centers, or they may bounce to the valence band, and consequently, energy may be discharged non-radiatively. The energy freed non-radiatively during charge carriers recombination may be transferred to the color center, whereby lanthanide ions may get excited.[38]

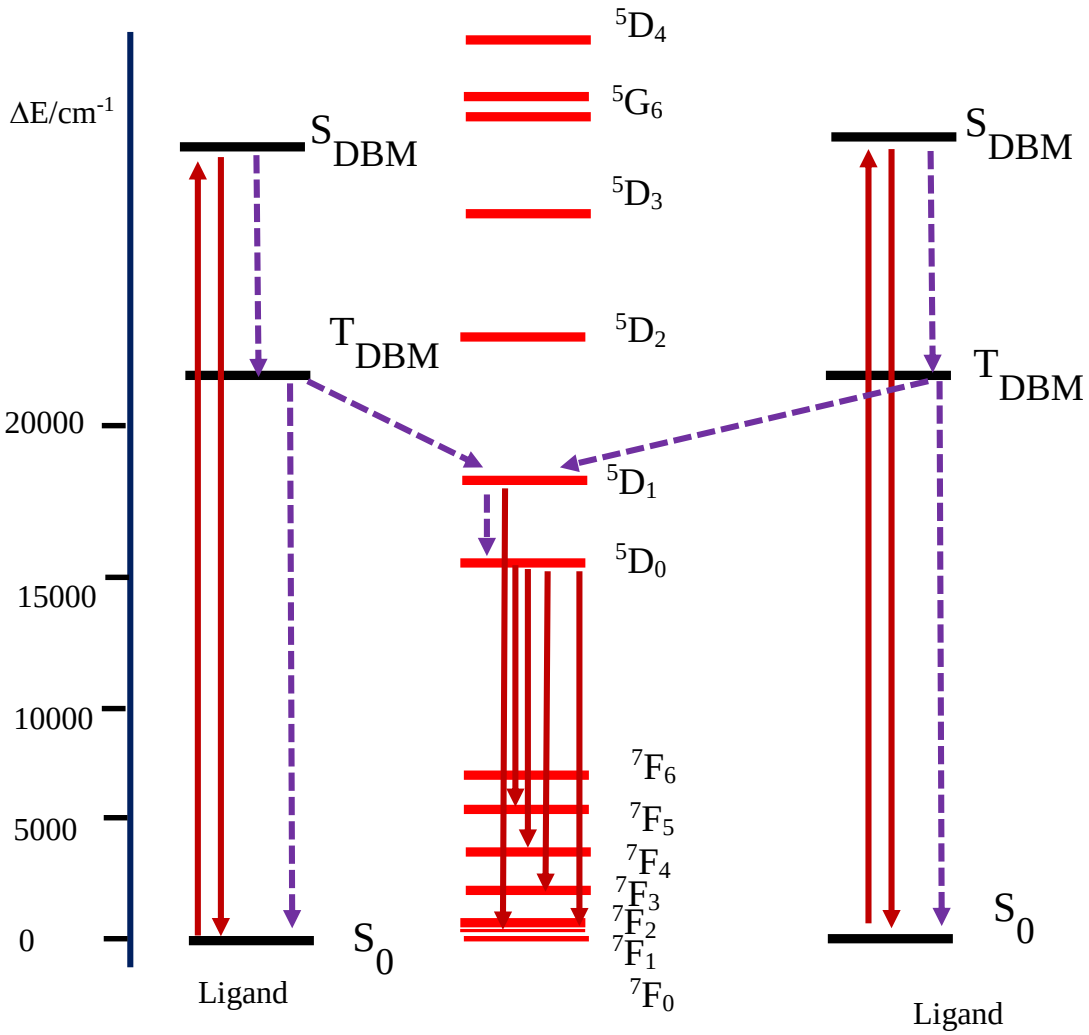

Figure 2 Electron transition mechanism of Mechanoluminescent material

1.3 Motivation and composition of the thesis

Many researchers have synthesized the mechanoluminescent material using rare earth dopants. Different dopants and ligands peer to present the distinct colour of Mechanoluminescent (ML) light intensity. Most of the scientists have synthesized the ML material based on the inorganic compounds. However, materials have been synthesized at higher temperatures, mostly above 1000˚C. The higher quantity of energy consuming causes big problems from the point of view of energy saving. Furthermore, the high temperature requires the experiments in a reducing atmosphere to prevent from the oxidizing. Therefore, we have focused on a synthesis of the organic based ML materials at the low temperature. We have also attempted to enhance the ML intensity for the practical applications. Mostly the enhancement of ML intensity has been attempted by an investigation of synthesis method. In the present study, we have paid our attention a ligand included in the ML material. As a result, the synthesis with the different ligands have realized visual ML intensity in the daylight. We have also realized an ML thin film without any resin or binder. Usually, the ML thin film is formed with the aid of resin and/or binder resulting in a reduced intensity because the resin and/or binder prevent an extensive amount of applied stress from transferring directly to the ML material. Although a sputtering technique allow to coat the ML material directly on a substrate, the technique is not adoptable to the organic materials. We have succeeded to form the ML thin film on a Ni substrate with an Al_2O_3 buffer layer by using a spray pyrolysis deposition technique. Finally, we have investigated a structure of the synthesized ML materials by using the different characterization methods.

Objectives of this thesis

1. We are focused to synthesized organic based ML materials at Low temperature.
2. We are focused to enhance the ML intensity by changing the different ligands.
3. By using various characterizations, we are concentrated to investigate the structure of the ML material.
4. Analyzing the Glass transitions temperature of the ML materials focused to investigate the low temperature effect to the ML materials.
5. We are confocal to fabricate the ML thin film without using any kind of resin or a binder.

1.4 Reference

1. Ahn, T.S., et al., *Self-absorption correction for photoluminescence quantum yields from integrating sphere measurements.* Rev Sci Instrum, 2007. **78**.
2. Janulevicius, M., et al., *Luminescence and luminescence quenching of highly efficient Y2Mo4O15:Eu3+ phosphors and ceramics.* Scientific Reports, 2016. **6**: p. 26098.
3. Dothager, R.S., et al., *Cerenkov Radiation Energy Transfer (CRET) Imaging: A Novel Method for Optical Imaging of PET Isotopes in Biological Systems.* PLOS ONE, 2010. **5**(10): p. e13300.
4. Wurfel, P., *The chemical potential of radiation.* Journal of Physics C: Solid State Physics, 1982. **15**(18): p. 3967.
5. Katsumi, Y., et al., *Thermochromism, Photochromism and Anomalous Temperature Dependence of Luminescence in Poly(3-Alkylthiophene) Film.* Japanese Journal of Applied Physics, 1988. **27**(4A): p. L716.
6. Goldberg, M.C. and E.R. Weiner, *The Science of Luminescence*, in *Luminescence Applications*. 1989, American Chemical Society. p. 1-22.
7. Enomoto, K., J.A. LaVerne, and M.S. Araos, *Heavy Ion Radiolysis of Liquid Pyridine.* The Journal of Physical Chemistry A, 2007. **111**(1): p. 9-15.
8. Liu, Y., et al., *Photophysics of Monodisperse Platinum-Acetylide Oligomers: Delocalization in the Singlet and Triplet Excited States.* Journal of the American Chemical Society, 2002. **124**(42): p. 12412-12413.
9. Reiher, M., O. Salomon, and B. Artur Hess, *Reparameterization of hybrid functionals based on energy differences of states of different multiplicity.* Theoretical Chemistry Accounts, 2001. **107**(1): p. 48-55.
10. Georgescu, S., et al., *Excited-state-absorption in low concentrated Er : YAG crystals for pulsed and cw pumping.* Journal of Luminescence, 2001. **93**(4): p. 281-292.
11. Duffy, D.M., S.L. Daraszewicz, and J. Mulroue, *Modelling the effects of electronic excitations in ionic-covalent materials.* Nuclear Instruments and Methods in Physics Research Section B: Beam Interactions with Materials and Atoms, 2012. **277**: p. 21-27.
12. Carey, F.A. and R.J. Sundberg, *Advanced Organic Chemistry: Part A: Structure and Mechanisms*. 2007: Springer Science & Business Media.
13. Widder, E.A., *Bioluminescence in the Ocean: Origins of Biological, Chemical, and Ecological Diversity.* Science, 2010. **328**(5979): p. 704-708.
14. Xu, Y., D.W. Piston, and C.H. Johnson, *A bioluminescence resonance energy transfer (BRET) system: Application to interacting circadian clock proteins.* Proceedings of the National Academy of Sciences, 1999. **96**(1): p. 151-156.
15. Matsumoto, M., *Advanced chemistry of dioxetane-based chemiluminescent substrates originating from bioluminescence.* Journal of Photochemistry and Photobiology C: Photochemistry Reviews, 2004. **5**(1): p. 27-53.
16. Rees, J.F., et al., *The origins of marine bioluminescence: turning oxygen defence mechanisms into deep-sea communication tools.* Journal of Experimental Biology, 1998. **201**(8): p. 1211.
17. Shimomura, O., F.H. Johnson, and Y. Saiga, *Extraction, Purification and Properties of Aequorin, a Bioluminescent Protein from the Luminous Hydromedusan, Aequorea.* Journal of Cellular and Comparative Physiology, 1962. **59**(3): p. 223-239.
18. Elliott, C.M., et al., *Highly Efficient Solid-State Electrochemically Generated Chemiluminescence from Ester-Substituted Trisbipyridineruthenium(II)-Based Polymers.* Journal of the American Chemical Society, 1998. **120**(27): p. 6781-6784.

19. Leland, J.K. and M.J. Powell, *Electrogenerated Chemiluminescence: An Oxidative‐Reduction Type ECL Reaction Sequence Using Tripropyl Amine.* Journal of The Electrochemical Society, 1990. **137**(10): p. 3127-3131.
20. Jiang, Q., et al., *Chemiluminescent energy transfer conjugates and their uses as labels in binding assays*. 2000, Google Patents.
21. Weiser, H.B., *Crystalloluminescence.* The Journal of Physical Chemistry, 1917. **22**(7): p. 480-509.
22. Chung, C.T., et al., *Organic electro-luminescence element used in a display device*. 2005, Google Patents.
23. Toyama, T., et al., *Hot-electron induced electroluminescence and avalanche multiplication in hydrogenated amorphous silicon.* Journal of Non-Crystalline Solids, 1996. **198**: p. 198-201.
24. Kido, J. and T. Matsumoto, *Bright organic electroluminescent devices having a metal-doped electron-injecting layer.* Applied Physics Letters, 1998. **73**(20): p. 2866-2868.
25. Karg, S., et al., *Transient electroluminescence in poly(p-phenylenevinylene) light-emitting diodes.* Synthetic Metals, 1994. **67**(1): p. 165-168.
26. Mariano, A.N. and P.J. King, *Europium-activated cathodoluminescence in minerals.* Geochimica et Cosmochimica Acta, 1975. **39**(5): p. 649-660.
27. Wu, X.L., et al., *Photoluminescence and cathodoluminescence studies of stoichiometric and oxygen-deficient ZnO films.* Applied Physics Letters, 2001. **78**(16): p. 2285-2287.
28. Werts, M.H.V., *Making sense of lanthanide luminescence.* Science Progress, 2005. **88**(2): p. 101-131.
29. Vanheusden, K., et al., *Mechanisms behind green photoluminescence in ZnO phosphor powders.* Journal of Applied Physics, 1996. **79**(10): p. 7983-7990.
30. Prosperetti, A., *A new mechanism for sonoluminescence.* The Journal of the Acoustical Society of America, 1997. **101**(4): p. 2003-2007.
31. Nakashima, K., et al., *Thermoluminescence mechanism of dysprosium-doped β-tricalcium phosphate phosphor.* Journal of Luminescence, 2005. **111**(1–2): p. 113-120.
32. Watanabe, S., et al., *Thermoluminescence Mechanism In Li2B407:Cu.* Radiation Protection Dosimetry, 1996. **65**(1-4): p. 79-82.
33. Chandra, B.P., et al., *Fracto-mechanoluminescence and mechanics of fracture of solids.* Journal of Luminescence, 2012. **132**(8): p. 2012-2022.
34. Carpenter, M.A., et al., *Elastic anomalies due to structural phase transitions in mechanoluminescent SrAl2O4:Eu.* Journal of Applied Physics, 2010. **107**(1): p. 013505.
35. Chandra, B.P. and A.S. Rathore, *Classification of Mechanoluminescence.* Crystal Research and Technology, 1995. **30**(7): p. 885-896.
36. Dickinson, J.T., et al., *Fracto-emission from deuterated titanium: Supporting evidence for a fracto-fusion mechanism.* Journal of Materials Research, 2011. **5**(1): p. 109-122.
37. Chandra, B.P., V.K. Chandra, and P. Jha, *Piezoelectrically-induced trap-depth reduction model of elastico-mechanoluminescent materials.* Physica B: Condensed Matter, 2015. **461**: p. 38-48.

Chapter 2 Experimental and Instrumental Technique Used

2.1 X-ray photoelectron spectroscopy (XPS)

X-ray Photoelectron Spectroscopy (XPS), also perceived as Electron Spectroscopy for Chemical Analysis (ESCA) is a widely-used manner to study the chemical composition of surfaces. X-ray Photoelectron spectroscopy, based on the photoelectric effect,1,2 was formed in the mid-1960's by Kai Siegbahn and his research association at the University of Uppsala in Sweden.

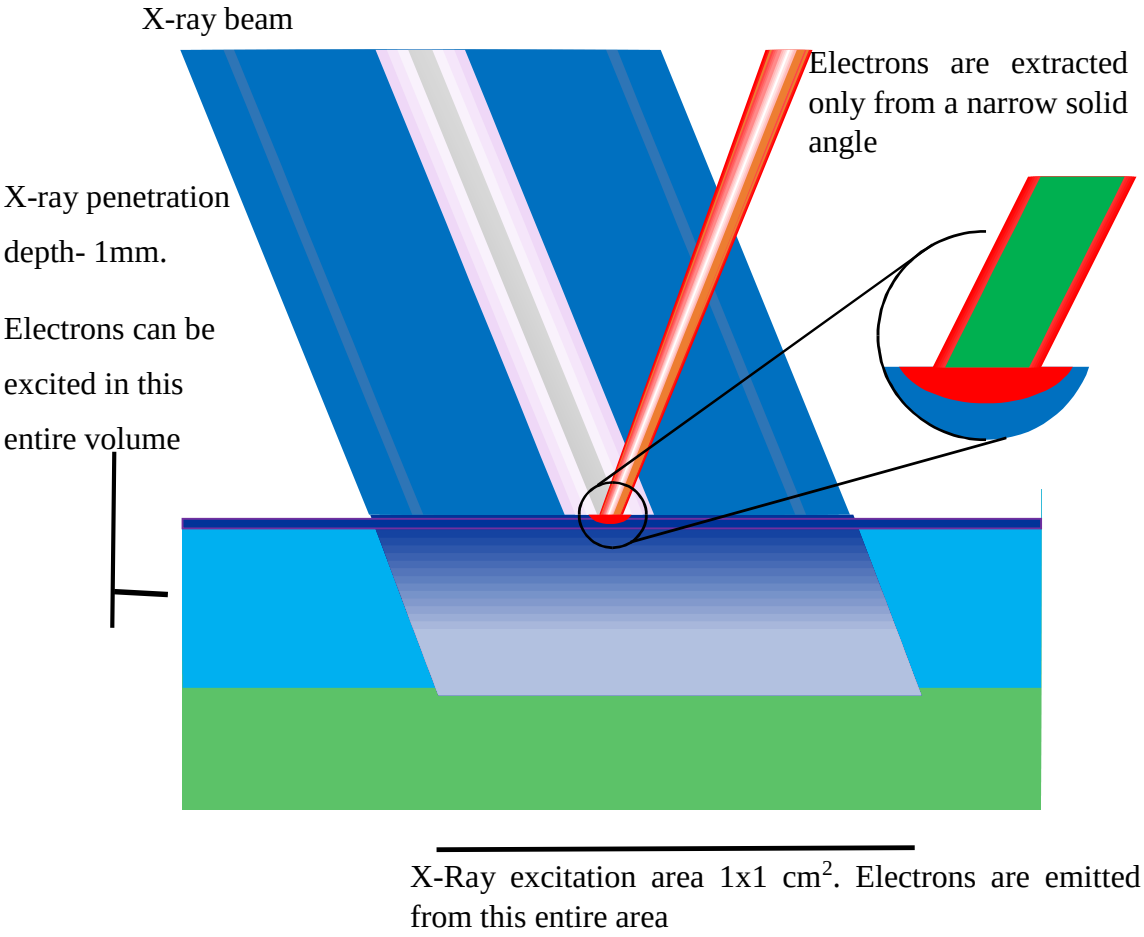

Figure 3 Schematic diagram of X-ray photoelectron spectroscopy small area detection

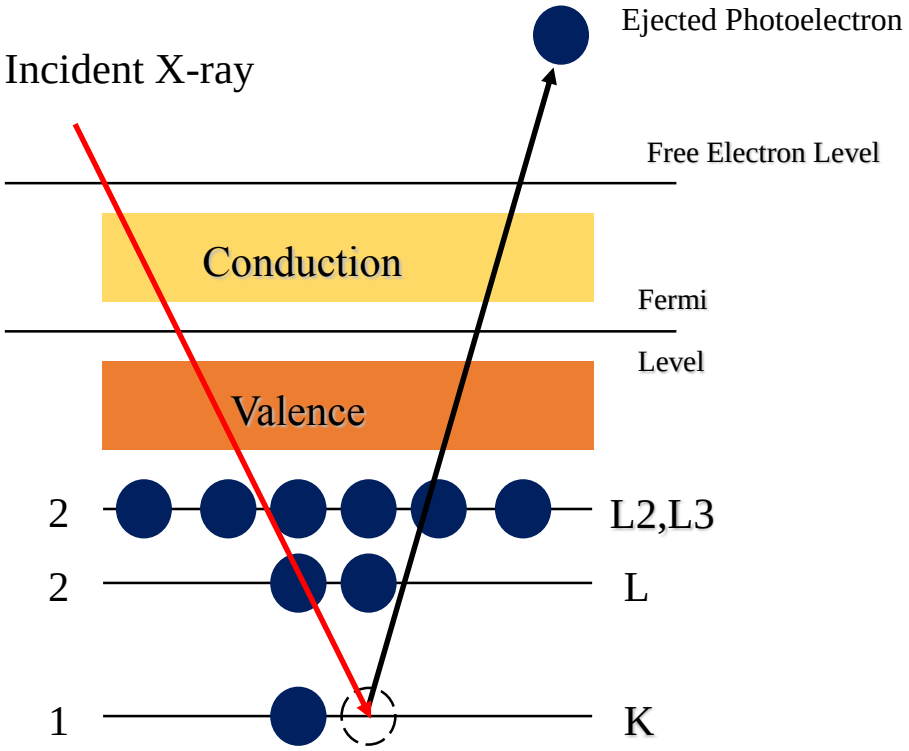

Figure 4 schematic diagram of Photoelectric process

XPS spectral lines are distinguished by the shell from whatever the electron was emitted (1s, 2s, 2p, …). The emitted photoelectron has kinetic energy

$$KE=hv-BE-\Phi$$

Following this method, the atom will discharge energy by the ejection of an Auger Electron. The XPS instrument measures the kinetic energy of all accumulated electrons. The electron signal incorporates participation from both photoelectron and Auger-electron lines.

Where: BE= Electron Binding Energy

KE= Electron Kinetic Energy

Φ = Spectrometer Work Function

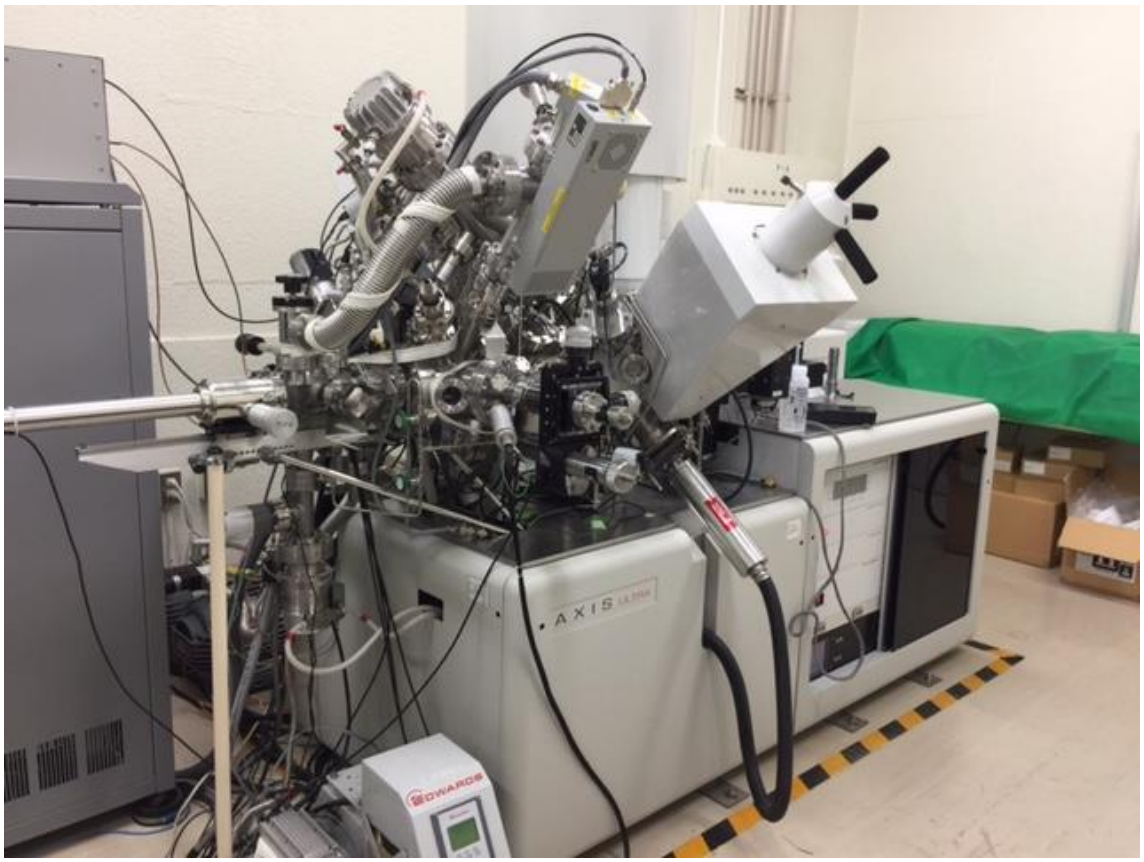

Figure 5 X-ray photoelectron spectroscopy set up (KRATOS AXIS Ultra OLD.)

Photoelectron line energies are dependent on photon energy. However, Auger electron line energies are Not dependent on photon energy. If XPS spectra were performed on a kinetic energy scale, one would need to know the X-ray source energy utilized to accumulate the data to correlate the chemical states in the specimen with data collected using the different source.

$BE = hv - KE - \Phi spec$

Where: BE= Electron Binding Energy

KE= Electron Kinetic Energy

Φ_{spec}= Spectrometer Work Function

Photoelectron line energies are not reliant on photon energy. Auger electron line energies are dependent on photon energy. The binding energy scale was reaped from making uniform illustrations of chemical states straight forward.

2.2 Differential scanning calorimetry (DSC)

Differential scanning calorimetry is a kind of method to examine glass transition temperature, melting temperature and decompose temperature. Those investigate mention that analyzing the thermal shifts of a polymer and what the thermal transitions are the transformations that take place in a polymer when heat it. On the other hand softening of a crystalline polymer is one case. The glass transformation is also kind of thermal transition. So how do we read what follows to a polymer when we heat it is, the first step would be to heat it, certainly. Moreover, that is what we do in differential scanning calorimetry(DSC) for short

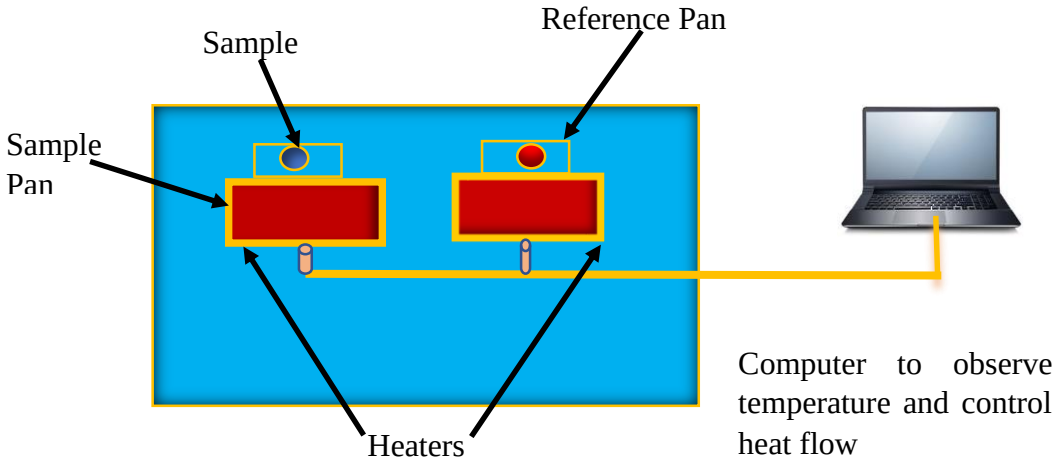

Figure 6 Schematic diagram on Setup Of differential scanning calorimetry

There are two pans. In one pan, the sample pan put the polymer sample. The other one is the reference pan. Transmit it empty. Each Pan remains on top of a heater. Then switch to the processor to turn on the heaters. When the computer turns on the heaters, and change it to heat the two pans at a particular rate, regularly being like 10 ^{o}C per minute. The computer makes sure that the heating the rate waits for the equivalent during the experiment. However, besides importantly, it presents sure that the two separate pans, with their two assign heaters, heat at the equivalent rate as each other. One container has polymer in it, and one doesn't. The polymer sample implies there is extra material in the specimen pan. Having extra material implies that it will take more heat to preserve the temperature of the specimen pan improving at the same rate as the reference pan. So, the heater beneath the sample pan has to serve harder than the heater underneath the reference pan. It need insert out extra heat. By estimating just how considerable more heat it need put out is what we estimate in a DSC analysis.

Precisely, what we do is this, make a plot as the temperature increases. On the x-axis, we sketch the temperature. On the y-axis, we plot variation in heat output of the two heaters at a presented temperature. Differential Scanning Calorimeter (DSC) is a dominant and accomplished thermal analyzer that provides for quality determinations on a broad difference of substances from -150 to 600°C. The DSC determines the temperature and heat flow correlated with material changes as a variable of time and temperature. It further gives quantitative and qualitative data on endothermic (heat absorption) and exothermic (heat evolution) processes of substances while physical changes that are caused by phase transitions, melting, glass transitions, crystallization, oxidation, and other heat related differences. This report helps the scientist or engineer recognize processing and end-use achievement. The DSC apparatus works in connection with a controller and associated software to allow for data acquisition and interpretation.

The quantity of heat required to improve temperature of matter the essential under the DSC peak, $(dH/dt)_{sample}\, dt=\Delta H_{sample}$

If the heat capacity of the reference is constant over the temperature range covered by the peak, $\Delta H_{reference}$ will cancel out because the integral above the baseline is taken. The heat capacity defines as

$$Cp = (dq/dt)_p = (dh/dt)_p$$

Temperature scan rate is dt/dT

Using the chain rule

$$Cp = (dH/dT) = dH/dt \times dt/Dt$$

Where dH/dt is the change in the baseline of the thermogram and the end derivative is just the opposite of the scan rate. For differential measurements, we define the difference in the heat capacity of the specimen and the reference

$$\Delta Cp = Cp(sample) - Cp(reference)$$

$$\Delta Cp = \Delta(dH/dT) = dH/dt \times dt/Dt$$

2.3 Scanning Electron Microscopy (SEM)

The scanning electron microscopy (SEM, JOEL 6320 F) was used to study about the particle size and surface morphology of the Mechanoluminescent materials.

Figure 7 Scanning Electron Microscope set up, JOEL 6320 F

2.3.1 Fundamental Principles of Scanning Electron Microscopy (SEM)

Accelerated electrons in a SEM carry notable amounts of kinetic energy, and this energy is consumed as a variety of signals generated by when the incident electrons are hinder in the solid sample. These signals comprise secondary electrons, backscattered electrons, diffracted backscattered electrons, photons, visible light, and heat. Secondary electrons and backscattered electrons are usually used for imaging samples .secondary electrons are extremely relevant for confirming morphology and topography on samples, and backscattered electrons are

considerably significant for illustrating contrasts in the composition in multiphase samples. X-Ray generation is offered by inelastic collisions of the incident electrons with electrons in discrete shells of atoms in the specimen. As the excited electrons restore to lower energy states, yield X-rays that are of a fixed wavelength. Particular X-rays are performed for each component in a mineral that is excited by the electron beam. SEM interpretation is deemed to be non-destructive, that is, x-rays formed by electron correlation do not lead to volume loss of the specimen, so it is permissible to analyze the similar materials frequently.

2.4 X-Ray Diffractometer (XRD)

Figure 8 X-Ray Diffractometer-D5000

2.4.1 Fundamental principle of X-Ray Diffractometer

In 1912 Max von Laue invented that crystalline elements act as three-dimensional diffraction gratings for X-ray wavelengths comparable to the spacing of planes in a crystal lattice. X-ray diffraction is presently a standard technique for the investigation of crystal structures and atomic spacing. X-ray diffraction is established on constructive interference of monochromatic X-rays and a crystalline specimen. These X-rays are formed by a cathode ray tube, filtered to generate monochromatic radiation, collimated to concentrate, and focused toward the sample. The

correlation of the incident rays with the specimen gives constructive interference when conditions provide Bragg's Law (2dsin Θ = n λ), where n is the order of diffraction and λ is the wavelength of the X-Ray. This law associates the wavelength of electromagnetic radiation to the diffraction angle and the lattice spacing in a crystalline specimen. These diffracted X-rays are then identified, processed and computed. By scanning the specimen through a range of 2Θ angles, all reasonable diffraction directions of the lattice should be succeeded due to the random adjustment of the powdered substance. Reformation of the diffraction peaks to d-spacings provides an association of the mineral because each mineral has a set of individual d-spacings. Typically, this is accomplished by distinguishing of d-spacings with regular reference patterns.

2.5 Multichannel spectroscope(Hamamatsu-photonic) (PMA/C8808-01)

The PMA-11/C8808-01 is compact spectral estimation apparatus that connects a spectrometer and optical detector within one unit. An optical fiber is utilized, since of the high responsiveness, spectra can be collected easily just by producing the optical fiber close to the specimen in typical applications, outwardly a particular light gathering system. Considering the spectrometer and photo-detector are fixed, the PMA-11 is durable and can be applied with certainty for extended periods of time. The wavelength axis and spectral response components are already calibrated so that spectral measurements can be conducted simply and accurately

Figure 9 Multichannel spectroscope(Hamamatsu-photonic) (PMA/C8808-01)

2.6 Nuclear magnetic resonance spectroscopy

2.6.1 Fundamental principal of Nuclear magnetic resonance

Nuclear Magnetic Resonance spectroscopy (NMR) is a powerfull method used in quality control and research for a figure out the content and purity of a specimen as well as its molecular formation. For example, NMR can quantitatively examine mixtures comprising known compounds. For unknown compounds, NMR can either be applied to match against spectral libraries or to assume the primary structure straightly. Once the primary structure is known, NMR can be employed to determine molecular formation in solution as well as examining physical features at the molecular level such as conformational exchange, solubility, phase changes, and diffusion. To accomplish the wanted results, a variety of NMR routines are available. The fundamentals of NMR are defined here. The principle following NMR is that many nuclei have spin and all nuclei are electrically energized. If an external magnetic field is implemented, an energy transfer is possible between the base energy to a higher energy level. The potential transfer takes place at a wavelength that agrees to radio frequencies, and the spin reverses to its base level, energy is transmitted at the corresponding frequency. The signal that rivals this transfer is estimated in many ways and processed to generate an NMR spectrum for the nucleus concerned.

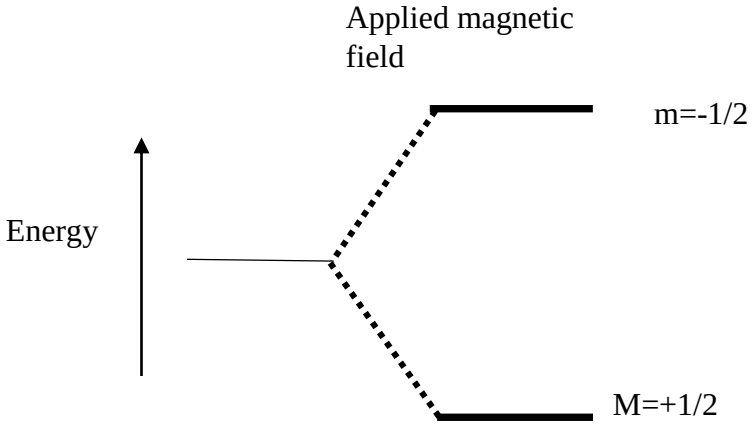

Figure 10 Energy state diagram for a nucleus with spin quantum number 1/2

2.7 Transmission electron microscope (TEM)

2.7.1 Fundamental principle of Transmission electron microscope

Transmission electron microscope (TEM), the source of flame is a beam of electrons of remarkably tiny wavelength, transmitted from a tungsten filament at the top of a cylindrical column regarding about 2 m high. The entire optical arrangement of the microscope is implanted in a vacuum. Air must be removed from the column to create a vacuum so that the interference of electrons with air fragments and therefore the scattering of electrons is avoided. Along the column, at particular intervals, magnetic coils are installed. Just as the light is sharpened by the glass lenses in a light microscope, certain magnetic coils in the electron microscope adjust the electron beam. The magnetic coils fixed at specific intervals in the column acts as an electromagnetic condenser lenses system. The sample stained with an electron dense substance and is located in the vacuum. The electron beams are routes through the specimen and scattered by the internal formations. The heated filament discharges electrons which are then stimulated by a voltage in the anode. A higher anode voltage will produce the electrons a greater velocity. Thus, the electrons will have a shorter de Broglie wavelength corresponding to the equation, $\lambda = h/mv$. The resolving power of a microscope is straightly associated with the wavelength of the irradiation, which utilized to form an image. The accelerated the electrons travel, the shorter their wavelength. As the wavelength is decreased, the resolution is improved. Therefore, the resolution of the microscope is raised if the accelerating voltage of the electron beam is improved.

TEM involves a high voltage beam of the electron transmitted by a cathode and determined by magnetic lenses. The beam of the electron that has been partially transmitted through the thin specimen carries details about the formation of the specimen. The spatial variation in this details is then amplified by a group of magnetic lenses until it is reported by hitting a photographic, plate fluorescent screen, or light sensitive sensor. The image identified by the CCD may be displayed in real time on a monitor or computer. The TEM has the capability to define the locations of atoms within substances which has made an essential tool for Nanotechnologies investigation and progress in many fields, including heterogeneous catalysis and the improvement of semiconductor devices for photonics and electronics.

There are four parts for a transmission electron microscope

1. Electron source
2. Electromagnetic lenses system
3. Sample holder
4. Imaging system

The electron source is an electron injector which consists of a tungsten filament. This filament discharges electrons when it is heated. The beam of electrons is the centered on the specimen by the condenser which exists of electromagnets named magnetic lenses. The specimen holder consists of a mechanical arm which contains the specimen. The imaging system also exists of electromagnetic lens arrangement and a screen which has a phosphorescent plate. The plate glows when tapped by the electrons after moving through the specimen.

Figure 11 Transmission electron microscope set up

2.8 Experimental technique

2.8.1 Crystal Quality

The most encouraging crystals are apparent and sharp edged with the favored dimensions 0.1 to 0.4mm. Agreeable crystals may be generated serendipitously from the preparative route. The first visual inspection is also used to check the consistency of the sample. Different colors or shapes of the crystal may designate unreacted origin material or by-products, and more report about the preparative process may be needed. If the specimen is not of sufficient nature, it may be essential to use an another crystallization manner.

2.8.2 Crystal growing

The intention is to produce single crystals of a proper size in at least two of the three dimensions. The dimension of the crystals can be examined by several factors, for example, the solubility of the specimen in the preferred solvent, the number of nucleation sites and time. If desirable, a solvent should be determined in which the specimen is moderately soluble. The crystal growing vessel should be washed since dust contributes infinite nucleation sites and may initiate interfering crystal growth. Avoiding agitation of the container is essential. Vibration or frequent change to check the sample tends to point to inferior quality crystals.

2.8.3 Crystal growing Techniques

Frequently used methods include solvent evaporation, slow cooling of the solution, solvent and non-solvent diffusion, vapor diffusion an sublimation and many variations on these themes. The procedure may be prescribed by the quantity of specimen.

2.8.3.1 Solvent Evaporation

This kind of simplest procedure for air stable samples. A nearly saturated solvent is prepared in a proper solvent. The specimen can then be dropped in a sample vessel that has a perforated cap. The size of the perforations is an experimental shifting that depends on some limit on the evaporation of the specimen. It is acceptable to tilt the tube so that some of the crystals grow on the surface of the tube. This promotes easier removal of fragile crystals without damage. Other

changes in this process are to transfer some of the solutions to a crystallization plate and shield with perforated Al foil or to confine some of the solutions between microscope slides.

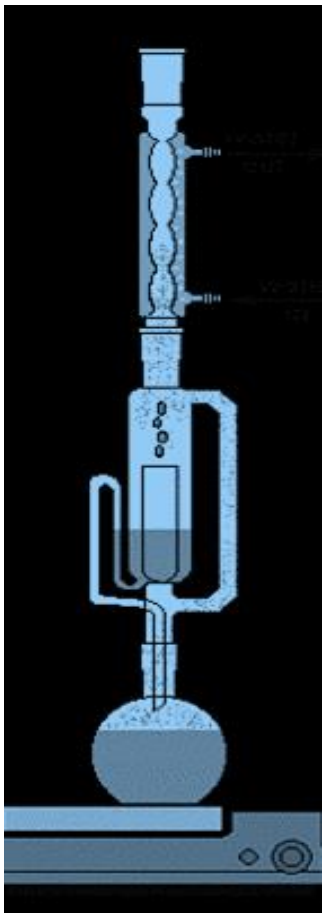

Figure 13 Soxhlet apparatus

Evaporation

Figure 12 Schematic diagram of crystal growing in evaporation

2.8.3.2 Slow Cooling technique

This is one of good method for limited soluble solute-solvent operations where the boiling point of the solution is in the range 30 - 90 ^{0}C. Make a saturated solution which is the solvent is heated to quite below the boiling point. Shift the solution to a stoppered tube then keep this tube to a Dewar including water at a temperature also quite below the boiling point of the solvent. The

water level should pass the solvent level but beneath the stopper. The Dewar should be lidded and left for several days.

Both the above methods may be developed by using solvent saturation. The process may also be used to tailor crystal form. Pretty fine needles or extremely thin plates present poor diffraction data. Modification of solvent composition may inhibit or promote growth of particular crystal faces and hence yield crystals of suitable morphology.

2.8.3.3 Solvent Diffusion

The process is relevant to mg amounts of the specimen that are air or solvent sensitive. A solution is located in a specimen tube then a second less dense solution is particularly dropped down the side of the tube applying either a pipette or a syringe to produce a discreet layer. A suitable solvent mixture is CH_2Cl_2/CH_3CH_2OH provided the specimen is near insoluble in the ether. Crystals appear at the edge where the solvents gradually diffuse.

2.8.3.4 Vapour Diffusion

This method is like the previous method and applicable to miligramme amounts of the specimen. In this situation, a solution of the specimen contained in a small sample tube is located in a larger tube holding a second less efficient solvent. The tube then sealed. The process works fine if the solution solvent is the limited volatile and thus predominately the second solvent diffuses into the sample solution.

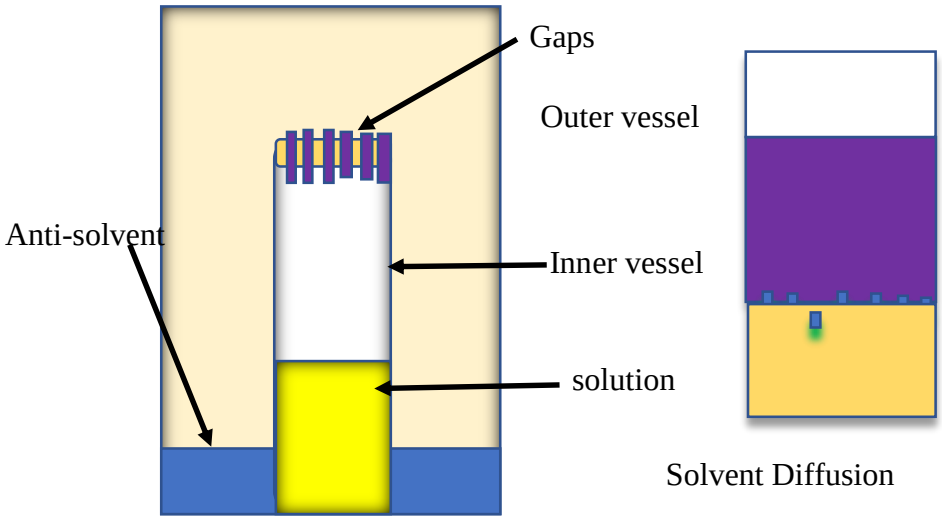

Figure 14 Schematic diagram of vapor diffusion crystal growing

2.8.3.5 Vacuum Sublimation

Many composites can be stately to form fine crystals. There are diverse modifications of this process utilizing either static or dynamic vacuum. A plenty amount of specimen sealed under vacuum in a Pyrex tube can be directed to a temperature gradient in each number of methods. A simple process that often achieves is to place the tube in a warm oven. The small temperature inclination can be enough to create crystals in hours or probably weeks depending on the evaporation of the sample and the nature of the vacuum. The dynamic vacuum works fine for less volatile specimens. Vacuum sublimation is ideal for much air sensitive composites as the tubes can be placed in dry boxes.

Figure 13 shows Standard Mechanoluminescent setup for characterizing the ML intensity at the room temperature. The instrument can be adjusted motor speed, the number of cycles apply pressure and utilize to identify the stability of the ML material, intensity variation of the ML material and ML intensity variation with applying pressure.

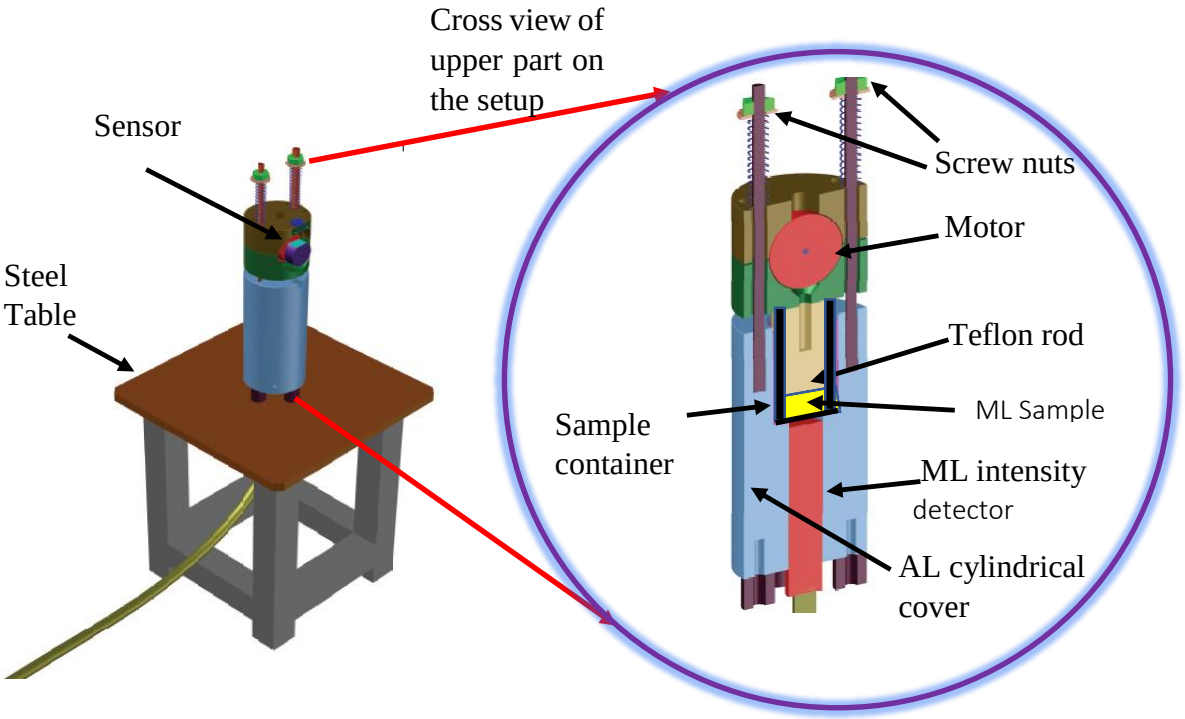

Figure 15 Mechanoluminescent intensity analyzing apparatus

ML intensity is characterized by using ML setup by following procedure.1 g of ML material insert in to the container and motor speed set up at 0.02 rpm. ML setup connect to the Multichannel spectroscope and experiment carried out 50 ms exposure time.

Chapter 3 Synthesis of Europium Dibenzoylmethide Triethylammonium Mechanoluminescent Material

3.1 Introduction

Mechanoluminescence (ML) is a phenomenon that light emission induced by a mechanical action on a solid[39]. There are several forms of ML materials such as elastico, plastico and fracto, usually denoted by the method used to excite the electrons[40]. Compare with other luminescence materials elastico ML elements are most abundant of them because of constant intensity is emitted while it is crushing[41]. Things what happen in here crystal bonds are broken along the planes with opposite charge, and when they are re-connected light is emitted as the charges pass through the separations created through the fractures[42]. ML also can be prepared by using peeling off the tape in a vacuum, as a result of plate force during and just earlier than to Erath quake[42]. When ML material structure is fractured, then electrons are excited to the higher energy levels, after that they are fallen to the lower energy levels. Energy different between corresponded each energy state emitted light in different wavelength region[43]. The light is emitted by several distinct it depends on the material and synthesized mechanism. The emission spectrum of sugar mentioned that the light comes from the atmospheric nitrogen that fills the Gap during fracture[44]. In 1999, Sage and Geddes utilized the characteristic of ML to the application for a sensor possessing the ability of locations of impact. They are used different kind of ML materials could be used and arranged at various places. The main advantage of this is when an Impact takes place, its location could be identified according to corresponded wavelength emitted[45].How ever consider the available mechanoluminescence materials' intensity is very low. Resulting light cannot detect easily also in dark light[45]. In last few years, Fontenot and Hollerman et al. have been worked with europium tetrakis dibenzoylmethide triethyl ammonium. The first practical europium tetrakis dibenzoylmethide triethyl ammonium

ML material was synthesized by Hurt et al[46]. The crystal form of this material has been studied by using methanol and dichloromethane were evaporation in room temperature[47]. There are so many mechanoluminescence materials has been synthesized by using various kinds of inorganic materials with different dopents[48]. Such as $SrAl_2O_4$:Eu[49], $BaAl_2O_4$:Eu[50], $SrAl_2O_4:Eu^{+3}$ Dy^{+3} [51], $ZnS:Mn^{+2}$ [52]. Problem is all of them are synthesized at higher temperature normally above the

1000 °C[52]. We are focused to synthesize the ML material at low temperature. This paper is discussed about europium tetrakis dibenzoylmethidetriethylammonium synthesized at 70°C in temperature and compare the intensity of the synthesized material with commercially available ML material.

3.2 Experimental

The synthesis began by 0.106 mol dibenzoylmethane(1,3-diphenylpropane-1,3dione, $C_{15}H_{12}O_2$),(98.0%, Wako) and 1.5 ml trimethylamine(99.0%,Wako) were dissolved in 80 ml of ethyl alcohol(99.5%, Wako) under vigorously stirred on the hot plate at 70°C for solute become completely dissolved. Then 0.0016 mol Europium(iii)nitratehexahydrate (99.9%, Wako) was added to the stirred solution and further stirred 20 minutes until the solution became apparent. The hot solution contained beaker was capped tightly then inserted into the thermos on treating on slow cooling effect for overnight. Precipitated synthesized ML material was filtered by using vacuumed filter and washed several time with ethyl alcohol. Finally synthesized ML material and commercially available ML materials intensity were characterized by using Multichannel spectroscope(Hamamatsu-photonic /PMA/C8808-01).

$$3C_{15}H_{12}O_2 + C_6H_{15}N \xrightarrow[\Delta/70^{\circ}C]{\text{Ethyl alcohol}} NC_{51}H_{51}O_6$$

(1,3-Diphenyl-1,3-propanedione) (Triethylamine)

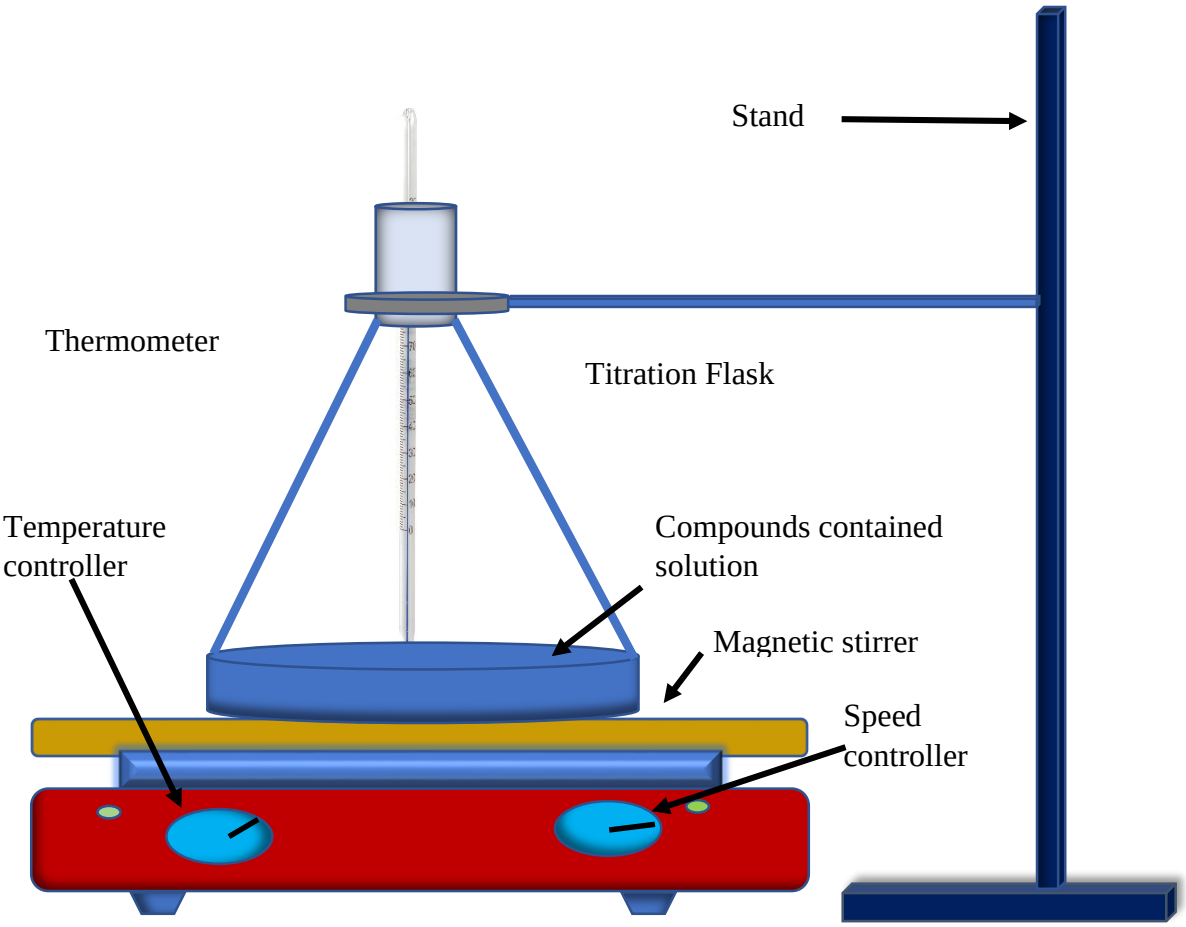

Figure 16 Schematic diagram of ML crystal growing apparatus setup

Figure 17 Image of the ML material in the bottom of the flask

Chapter 4 Effect of Additives on Synthesized Mechanoluminescent Material

4.1 Effect of Added Polyvinylpyrrolidone For Mechanoluminescence And Photoluminescence Intensity of Synthesized Material

4.1.1 Introduction

Mechanoluminescence (ML) is a phenomenon of light emission resulting from the mechanical action on a solid. There are various forms of ML such as fracto-, plastico- and elastico-ML, among the ML forms the fracto-ML is well identified because most inorganic materials transmit the light while they fracture such as a result of plate force throughout and just facing the earth quake [40, 42, 53]. The ML also can be followed by peeling an adhesive tape in a vacuum. When the crystal bonds are separated along the planes with counter charge and then re-connected, light is transmitted as the charges pass within the gaps generated from the fracture. When the material is cracked, electrons are stimulated to the higher energy levels accompanied by a transition to the lower energy levels. The energy separation between corresponding levels is transmitted as a light with distinct wavelengths [43, 54]. When we examine the tree type of ML substances mechanism of the eleasti-co ML supposes, When implementing the mechanical stress cause to perform the pizio-electric field on the surface of the crystals. This electric field quite high near to the color center since of the changing the local structure. This might be reducing the trap depth of the carriers, or it may be an effect on the band bending. When decreasing trap depth of the carriers, thermal de-trapping of the carriers may be produced. Trapped charge carriers can be a tunnel to the conduction band because of the band bending. Moving electron from the conduction band captured by excited state of the activator ions. This may cause to de-excitation of the color

center and might be produced the emission [55]. When we consider the plasti-co mechanoluminescent materials getting plastically deformed occurs movement of dislocation. Similarly, an electric field generated by the charge dislocation cause to bending of valance band and conduction band as well as dislocation band. Trap electron tunnel to the conduction band and recombination of electrons with holes gives rise to the light emission characteristic of the color center. However, conduction band electron digest by color center occurs to the de-excitation of the color center. Both functions are happening, and electrons holes' recombination is more as compared to that cause by the impact excitation. Consider the frac-to ML material it believes that mechanism quite different. When fracturing the material, newly created two surfaces generated on the opposite charge surfaces this can be generated an electric field and cause di-electric brake down of the surrounding gasses and in turn may provide rise to the gaseous discharge ML. Also, electric field cause to dielectric break down of the crystals and the recombination of the free carrier's may contribute rise to recombination luminescence. So far, various inorganic mechanoluminescent materials have been integrated with various dopants [56]. Such as $BaAl_2O_4$: Eu, $SrAl_2O_4$: Eu, Dy, $SrAl_2O_4$: Eu and ZnS: Mn Nevertheless, the problem is that they are regularly synthesized at extreme temperatures over 1000˚C [57].

We are concentrated to synthesize the ML material at a low temperature based on organic substances such as europium dibenzoylmethide triethylammonium (EuD_4TEA)[41]. We have accomplished to form the EuD_4TEA at an extremely low temperature of 70 °C by utilizing a dominated slow cooling method. This paper has examined the effect of an addition of polyvinylpyrrolidone (PVP) to the EuD_4TEA on the ML properties.

4.1.2 Experimental

First 80ml ethyl alcohol (99.9%, Wako) was heated to 70˚C, and then 0.8mmol 1, 3-diphenylpropane-1, 3-dione (99%, Wako) was added and agitated. After the solute was entirely

dissolved, 0.3mmol europium nitrate hexahydrate (99.9%, Wako) was added to the solution. 0.1 g PVP (99%, Wako) and 0.5 ml trimethylamine (99.8%) were added additional and suspension was kept at 70 °C for 20 min. Then the solution vessel was capped tightly and embedded in the thermos overnight. Controlled slow cooling in the thermos is efficient to grow fine crystals. For comparison, the EuD_4TEA based substance without PVP was also synthesized. Photoluminescence (PL) and ML characteristics were measured for both synthesized materials at the room temperature.

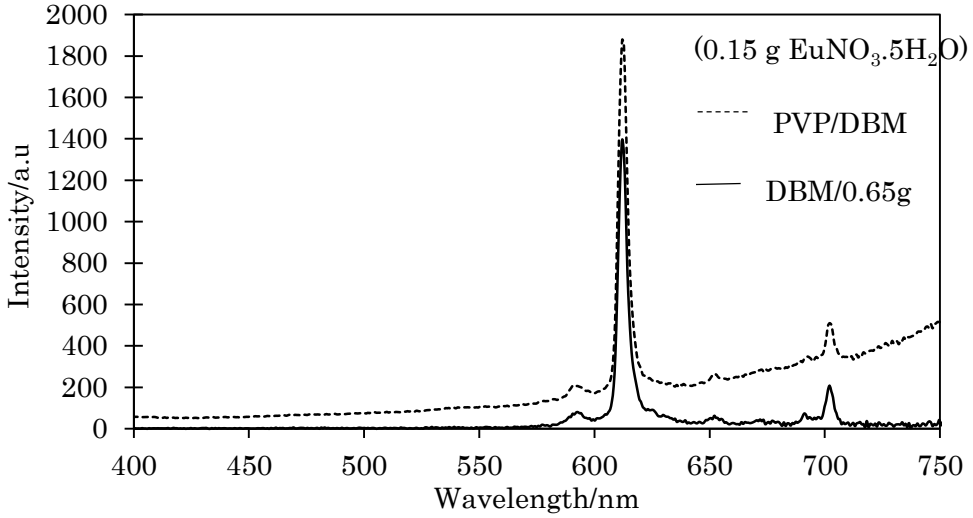

Figure 18 Mechanoluminescence intensity spectra of europium dibenzoylmethidetriethylammonium synthesized adding and without adding PVP

Figure 16 shows ML intensity correlation for specimens before and after addition of PVP polymer. These spectra obviously show an improvement Of ML intensity subsequent addition of PVP. Black curve matches to the ML intensity of the material with the higher amount of europium nitrate hexahydrate. However, a small amount of europium nitrate hexahydrate with the addition of PVP results in much higher ML intensity (red curve). PVP polymer makes coordination bond with Eu^{+3} and it is the reason for the higher electron transition rate, hence more excitation. Also, results suggest that the local environment around the Eu^{+3} ion was more disordered hence the degree of polarization for Europium doped dibenzoylmethidetriethylammonium was higher when PVP impregnated into the ML material, This further led to a higher probability for the electronic dipole allowed transitions.

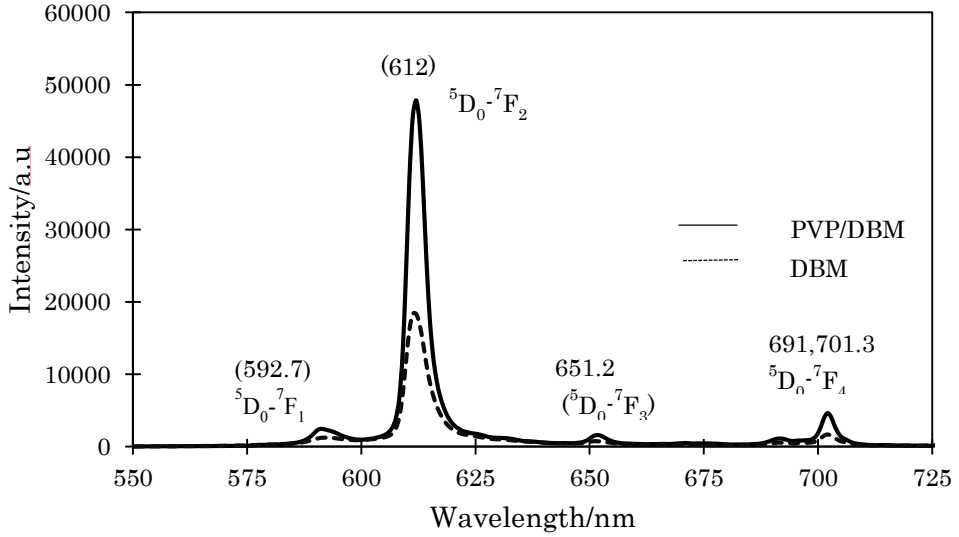

Figure 19 Comparison of Photoluminescence intensity spectrums on ML substance after and before adding PVP

Figure 17 agrees to the PL spectra of synthesized ML substance earlier and after enhancement of PVP polymer. The PL emission series with 357.0 nm excitation are 592.7 nm, 612.0 nm, 651.2 nm and 702.3 nm. Those emission lines belong to the $^5D_0$ to ^7F_n (n= 1,2,3,4) electron shifts. After incorporating of PVP to the synthesized material, ML and PL emission intensity are enhanced.

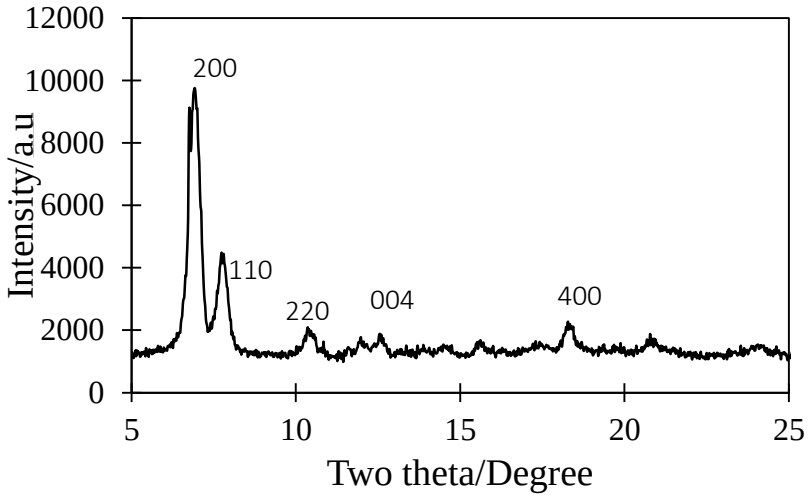

Figure 20 XRD pattern of the ML material without PVP

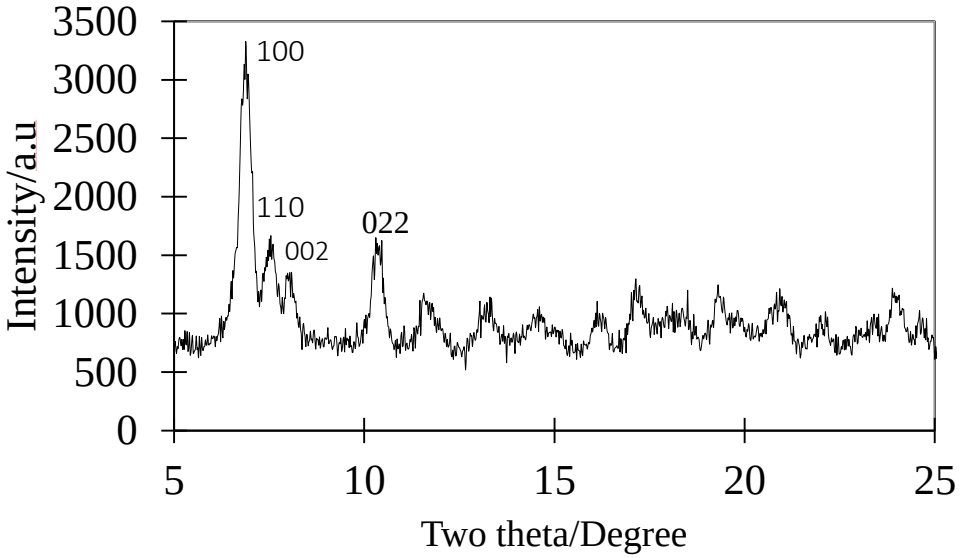

Figure 21 XRD pattern of the ML material with PVP

Figure 18 and 19 shows XRD patterns of EuD_4TEA with and without PVP. It is proof for the crystallinity of the lately synthesized mechanoluminescent material. Mean defect concentration in the crystalline material results in better electron transport qualities, without trapping besides recombination. Lately integrated EuD_4TEA substance with PVP incorporate

has shown higher ML and PL intensity than without PVP. Subsequent the adding PVP crystallinity of the ML material has increased since electron density of the unit cell has improved caused by the higher ML intensity.

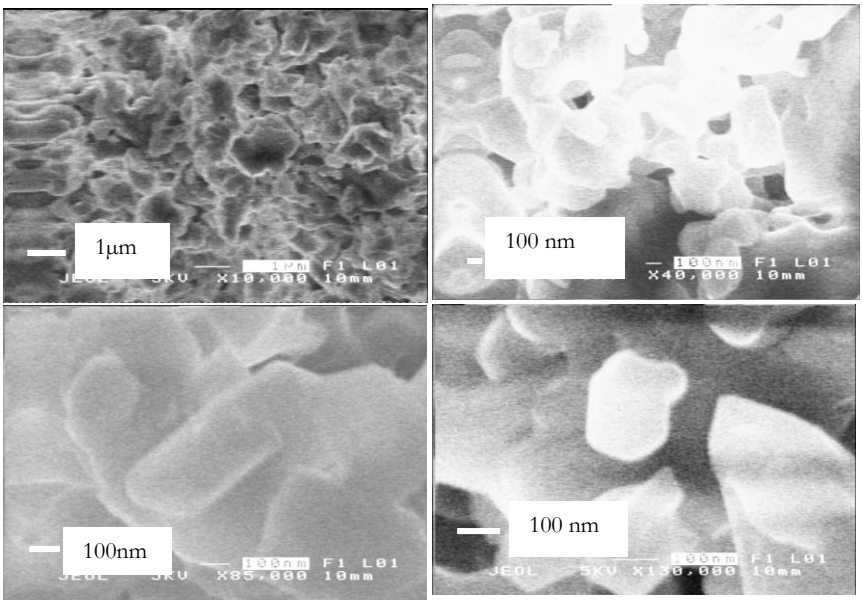

Figure 22 SEM images on ML material without adding PVP

Figure 20 shows SEM micrographs of the ML material without adding PVP. It is evidence for the size of the particles are around 50nm-200nm. When the particle size on without ML substance, compare with the novel ML material (with PVP) is a quiet lager. This is caused by the electron transition trough the material. When the particle size is getting decrease molecular orbital overlapping is increased therefore electron can easily transition to the higher energy level and lower energy level. It is believed that the after adding the PVP ML intensity is quite high. The also theory behind of the mechanism of the mechanoluminescent material is unknown. The intensity of the ML material depends on the energy difference

between the electron transition state. In the ML it depends on the flexibility of the ligand molecule which coordinates to the color center. Trimethylamine is much suitable flexible inorganic molecule compare with others. When giving the stress on the ML material ligand molecule can quickly move every direction and because of that molecular orbital overlapping and electron transit to the higher energy level and unsteady electrons fall to the lower energy. The energy difference between those energy state illuminating as a light. Eu^{+3} Coordinated polyvinylpyrrolidone molecules have quite a flexibility property so, therefore, it is a help to much increase the intensity of the ML material.

4.1.3 Conclusions

We have successfully synthesized ML material at a low temperature at 70°C without addition and with an addition of PVP. ML and PL intensity are defined by using Multichannel spectroscope(Hamamatsu-photonic) (PMA/C8808-01). PL spectrum with 357 nm excitation consists of emission lines at 592.7 nm, 612.0 nm, 651.2 nm including 701.3 nm. This discharge wavelength belongs to electron transition between $^5D_0$ to ^7F_n (n=1,2,3,4) energy levels. Corresponded XRD and TEM patterns are evidence for novel material have good crystallinity rather than without PVP material. More electron orbital over lapping, the flexibility of ligand molecules and higher dipole moment of the PVP caused to increase the ML, and PL intensity of the novel synthesized ML material. Lately integrated EuD_4TEA material with addition of PVP has much higher PL and ML intensity than without PVP

4.1.4 References

40. Chandra, B.P., *Mechanoluminescence*, in *Luminescence of Solids*, D.R. Vij, Editor. 1998, Springer US: Boston, MA. p. 361-389.

41. Fontenot, R.S., et al., *Synthesis and characterization of highly triboluminescent doped europium tetrakis compounds.* Journal of Luminescence, 2012. **132**(7): p. 1812-1818.
42. Fontenot, R., et al., *Luminescent properties of lanthanide dibenzoylmethide triethylammonium compounds.* Journal of Theoretical and Applied Physics, 2013. **7**(1): p. 1-10.
43. Chandra, V.K. and B.P. Chandra, *Suitable materials for elastico mechanoluminescence-based stress sensors.* Optical Materials, 2011. **34**(1): p. 194-200.
53. Tsuguo, I., et al., *Fracto-Luminescence of Rare Earth Element-Doped Hexacelsian (B a A l 2 S i 2 O 8).* Japanese Journal of Applied Physics, 1997. **36**(6B): p. L781.
54. Chandra, B.P., V.K. Chandra, and P. Jha, *Models for intrinsic and extrinsic fracto-mechanoluminescence of solids.* Journal of Luminescence, 2013. **135**: p. 139-153.
55. Chandra, V. and B. Chandra, *Dynamics of the mechanoluminescence induced by elastic deformation of persistent luminescent crystals.* Journal of Luminescence, 2012. **132**(3): p. 858-869.
56. Zhang, J.-C., et al., *Controlling elastico-mechanoluminescence in diphase (Ba,Ca)TiO3:Pr3+ by co-doping different rare earth ions.* RSC Advances, 2014. **4**(77): p. 40665-40675.
57. Mathur, V.K. and J.L. Price, *Color switchable stress-fracture sensor for damage control*. 2007, Google Patents.

4.2 Structural Characterizations of Organic-Based Materials With Extensive Mechanoluminescence Properties

4.2.1 Introduction

Mechanoluminescence (ML) is a light-emission event that results from a mechanical action on a solid[58]. Fracto-, plastico- and elastico-ML are various forms of ML. Among the various ML forms, fracto-ML is well known because most inorganic materials emit light when they fracture as a result of the plate force during and prior to an earthquake [40, 59, 60]. Additionally, plastico-ML can be observed by peeling an adhesive tape in a vacuum [44, 61]. When the crystal bonds are broken along oppositely charged planes and then reconnect, light is emitted as the charges pass through the gaps that were created from the fracture [62, 63]. Once the material is fractured, the electrons are excited to higher energy levels and then transition to the lower energy levels [64, 65]. The energy difference between the corresponding levels is emitted as a light with different wavelengths [54]. The third type of ML mechanism, elastico-ML, results from a mechanical stress that produces a piezoelectric field on the surface of crystals[43, 66, 67]. This electric field that is near the color center is high because of changes in the local structure. These changes may reduce the carrier trap depth or effect band bending [68-70]. After decreasing the carrier trap depth, the thermal de-trapping of the carriers may occur. Trapped charge carriers can tunnel to the conduction band because of the band bending. The electrons from the conduction band may be captured by the excited state of the activator ions. This may cause a de-excitation of the color center and

produce the emission[71]. When plastico-mechanoluminescent materials are plastically deformed, a movement of dislocation occurs. Similarly, an electric field generated by the charge dislocation causes a bending of the valance, conduction and dislocation bands. Trapped electrons tunnel to the conduction band and the recombination of electrons and holes enables the light emission characteristic of the color center. However, the conduction band electrons are trapped by the color center and a potential energy transfer occurs as a result of the de-excitation of the rare earth cation. Both functions occur and electron-hole recombination is greater than that caused by the impact excitation[37]. The mechanism of the fracto-ML material is believed to be different. In this case, when the material fractures, two newly created, oppositely charged surfaces are generated, which produce an electric field and cause a dielectric breakdown of the surrounding gasses and, in turn, may give rise to gaseous discharge ML. Additionally, the electric field that caused the dielectric breakdown of the crystals and the recombination of the free carriers may lead to recombination luminescence [33, 72]. To date, many inorganic mechanoluminescent materials have been synthesized with various dopants[56, 73, 74], such as Eu, dialuminum strontium oxygen(2-)$SrAl_2O_4$: Eu[75], Eu, Barium($^{2+}$), oxido(oxo)aluminum $BaAl_2O_4$: Eu[50], Eu, Dy, dialuminum strontium oxygen($^{2-}$)$SrAl_2O_4$: Eu, Dy[51] and zinc sulfide, ZnS: Mn[76]. However, the difficulty is that they are typically synthesized at high temperatures that are greater than 1000 °C[77].

Our study is focused on the structure of the synthesized material, the ML and the mechanism for the increase in PL intensity. We have determined the structure of this synthesized ML material using nuclear magnetic resonance spectroscopy (NMR), X-ray photoelectron

spectroscopy (XPS) and the molecular orbital diagram of the ligands. This paper has reviewed the structure of the synthesized ML material, mechanism of the intensity enhancement and crystallinity of the ML material.

4.2.2 Crystallography and Structural studies

Figures 21 and 22 show the X-ray diffraction patterns for EuD_4TEA without and with PVP, respectively. In Figure 21, the 2θ values at 6.68, 6.87, 7.00 and 7.60 correspond to the (100), (200), (110) and (011) Millar planes, (JCPDS card number 96-711-8092).

The Crystal structure matched the europium, 2,2′-bipyridine 5,5′-dicarboxylic acid compound and the crystal system was monoclinic. Figure 22 depicts that the XRD profile for the synthesized ML material with PVP and the 2θ values at 6.79, 6.88 and7.41 correspond to the (100), (200), (110) Millar planes, respectively, respectively,

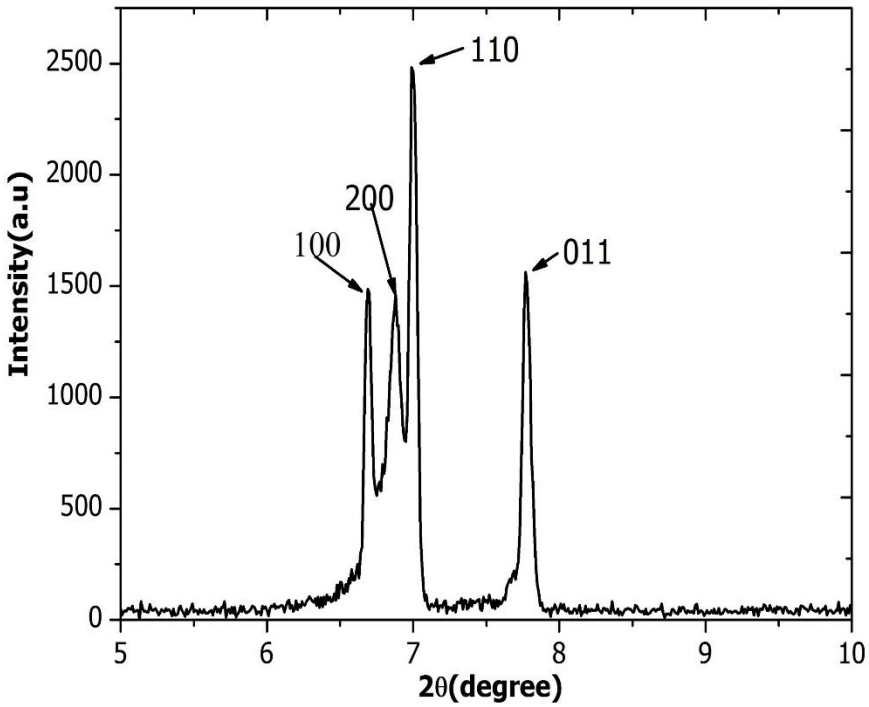

Figure 23 XRD pattern of the ML material without PVP

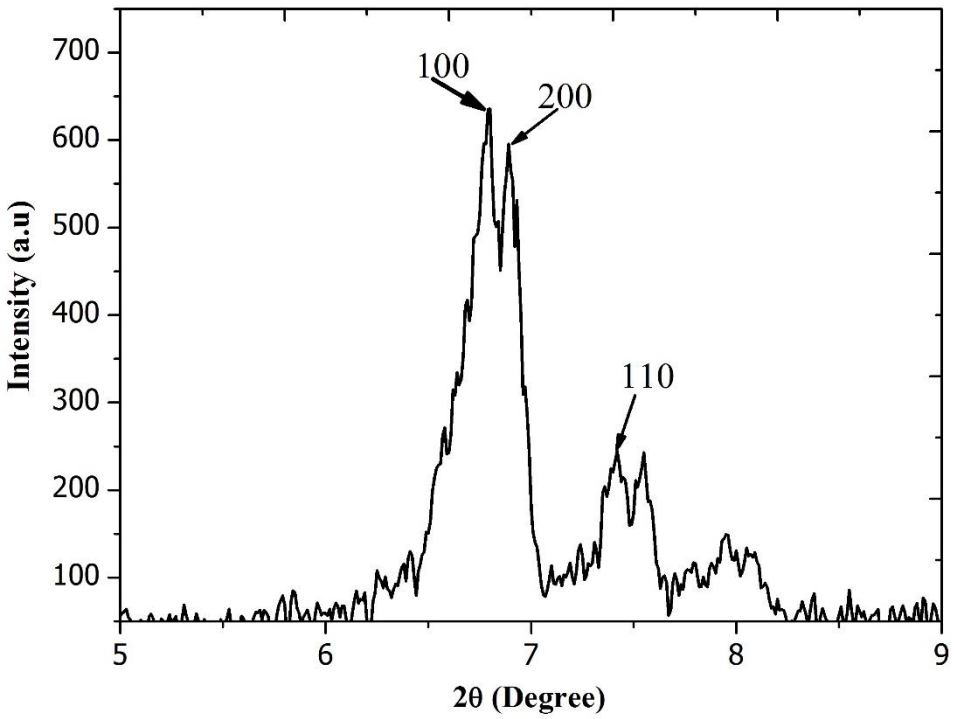

Figure 24 XRD pattern of the ML material with PVP

(JCPDS card number 96-711-8093). The crystal system was monoclinic and similar to europium,2,2′-bipyridine 5,5′-dicarboxylic-Cu.

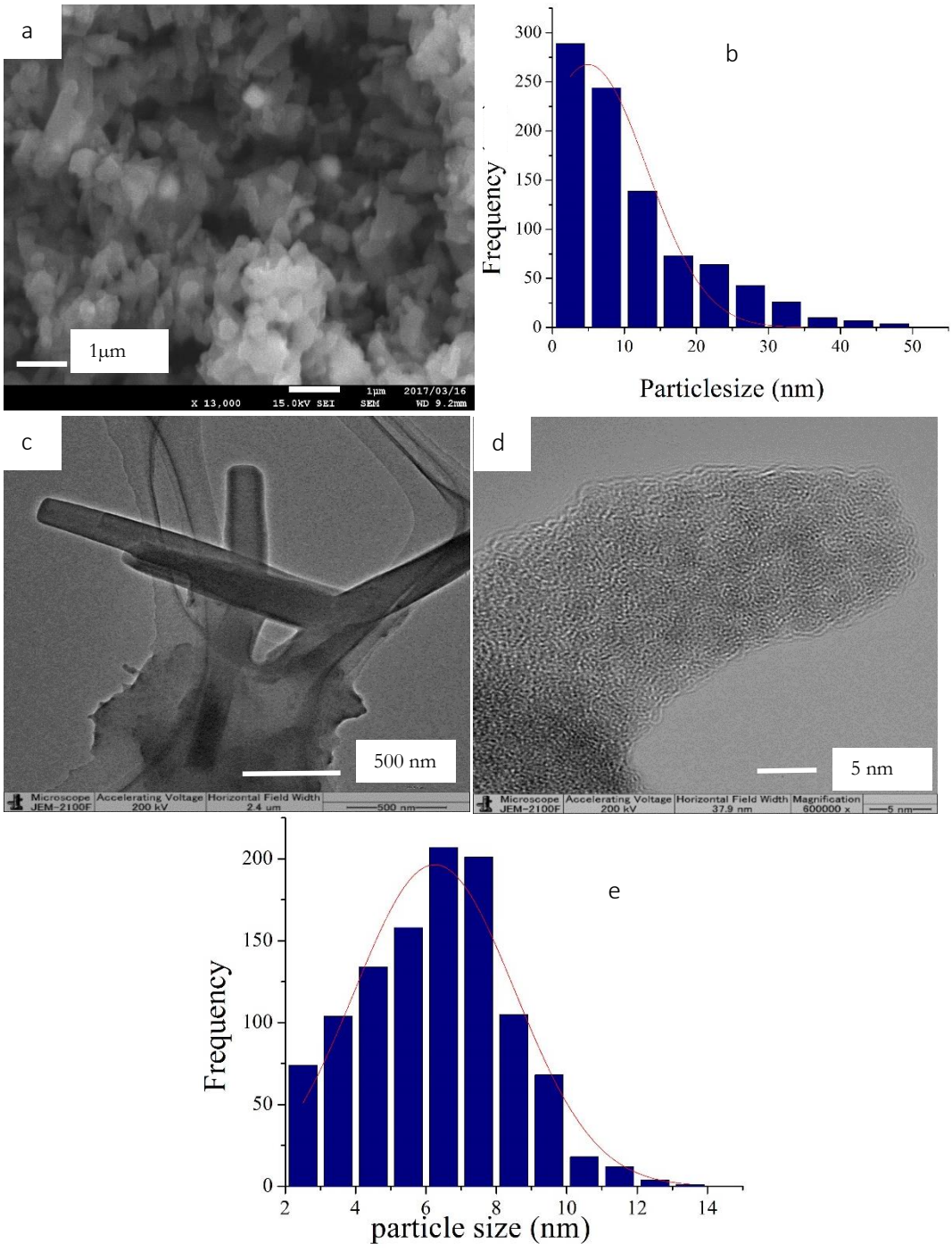

Figure 25 (a) FESEM, **(b)** histogram obtained by using FESEM micrograph, **(c)/(d)** TEM micrographs and (e) histogram correlated to TEM micrographs of the synthesized ML material without PVP

A comparison with the TEM micrograph in Figure 23(c) clearly shows that the structure has grown along the vertical c-axis and has a rod-like shape. Therefore, the monoclinic structure was confirmed. The mean value of the grain size in the synthesized materials before the addition of PVP was calculated to be approximately 7 nm using the de Debye-Scherer equation. A comparison with the histograms in Figures 23(e) and 24(d) confirmed that the particle size was comparable to that revealed by the XRD calculation. After the addition of PVP, the TEM micrographs in Figure 24(a) and (b) clearly show an unchanged structure and an increase in the nanorod-shaped structures in the novel material. The TEM images depict fine ML particles and the corresponding histogram (Figure 24(d)) shows a mean value of 4 nm for the calculated particle size. A comparison with the XRD profiles of the calculated grain size showed similar results and also provided evidence for the crystallinity of the newly formed organic-based mechanoluminescent material. The low defect site concentration in the crystalline material resulted in better electron transport properties without trapping and recombination. The newly synthesized EuD_4TEA material with PVP has shown higher ML and PL intensities than without PVP. After the addition of PVP, the crystallinity of the ML material increased and the enhanced electron density of the unit cell caused a higher ML intensity. Figure 23 shows TEM micrographs of the synthesized ML material without PVP and with fine particles. Image Figure 23(d) shows the small particles that correspond to a 7-nm size.

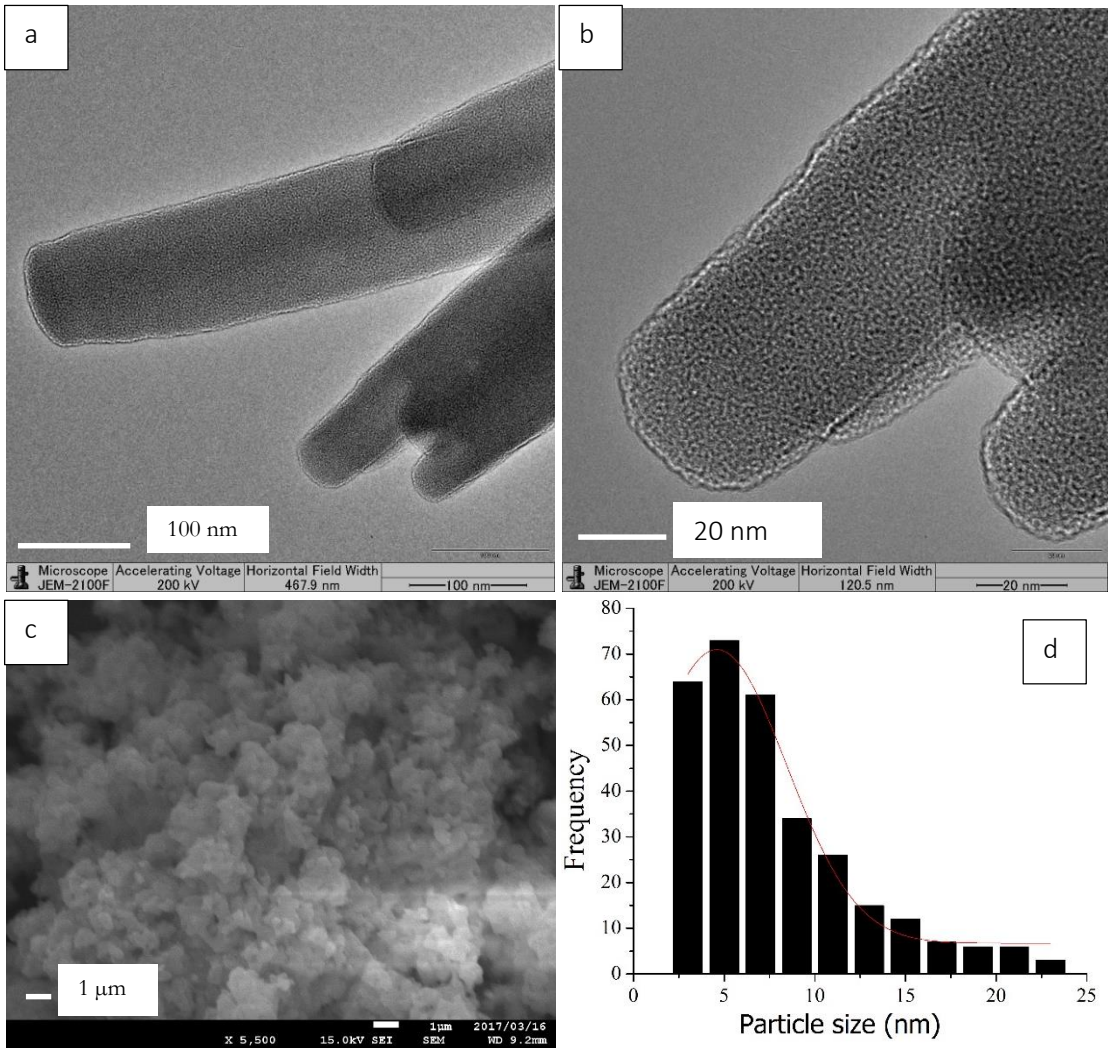

Figure 26 (a)/(b) TEM micrographs, **(c)** FESEM micrograph and (d) histogram correlated with TEM image (**b)** of the synthesized novel ML material with PVP

Figure 23 (c) reveals that the structure of the material exhibits a nanorod-like shape and the rod-like structure is integrated with the fine particles. However, a comparison with the histogram of the SEM micrograph in Figure 23(a) indicates that the average particle size was approximately 7 nm. In Figure 24, the TEM micrographs and corresponding histogram (Figure 24(d)) reveal that the particle sizes became finer after the addition of PVP and their average size was approximately 4 nm. Particle size analysis was performed using ImageJ software[78]. According to the TEM micrographs, the PVP molecules were attached to each crystal and these results were also confirmed by the XPS data. This molecular attachment caused an intensity enhancement because of the reduced electron back-transfer rate when the electron crossed the intersystem from the singlet excited state to the triplet energy state. The ML intensity depends on the critical distance of the ligand material, color center and electron's intersystem-crossing and back-transfer rates. Particle sizes of a few nanometers enable the convenient intersystem crossing of the electrons and may have caused the electrons to be captured by the color center. Because the distance between the ligand and color center was small, the electron orbital overlap increased. After adding PVP, the ML crystal size was approximately 4-5 mn and therefore there was in an increase of the intensity compared with the synthesized material without PVP.

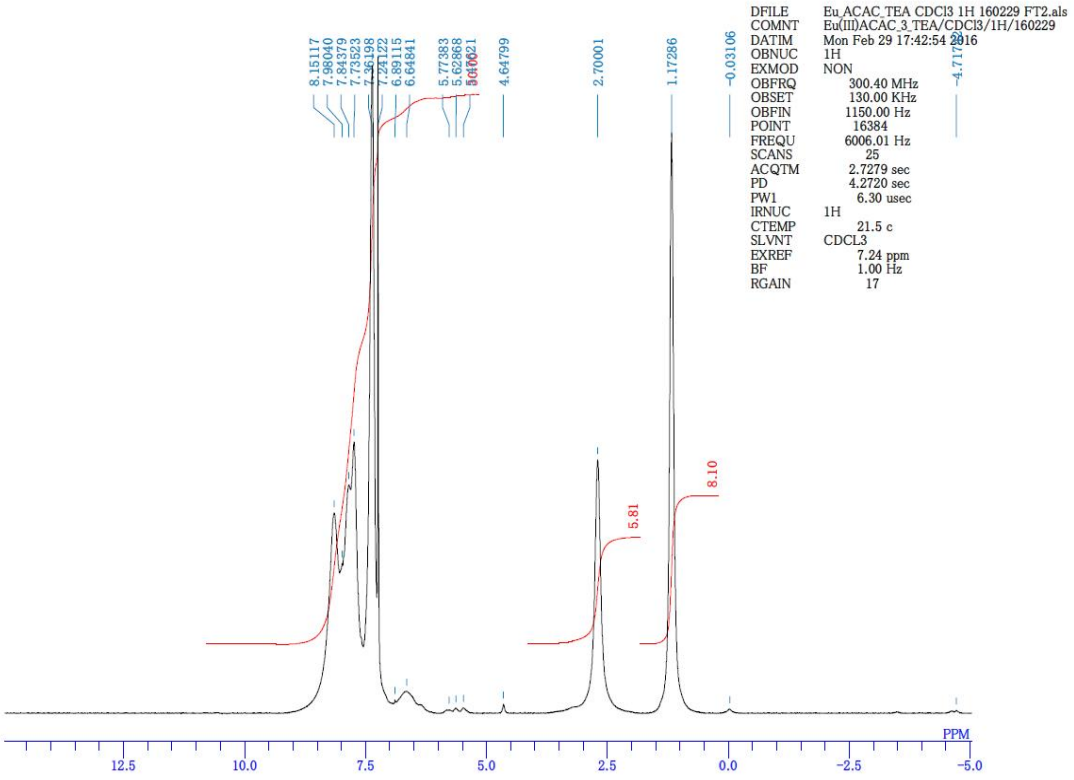

Figure 27 1H NMR spectrum of the ML material without PVP

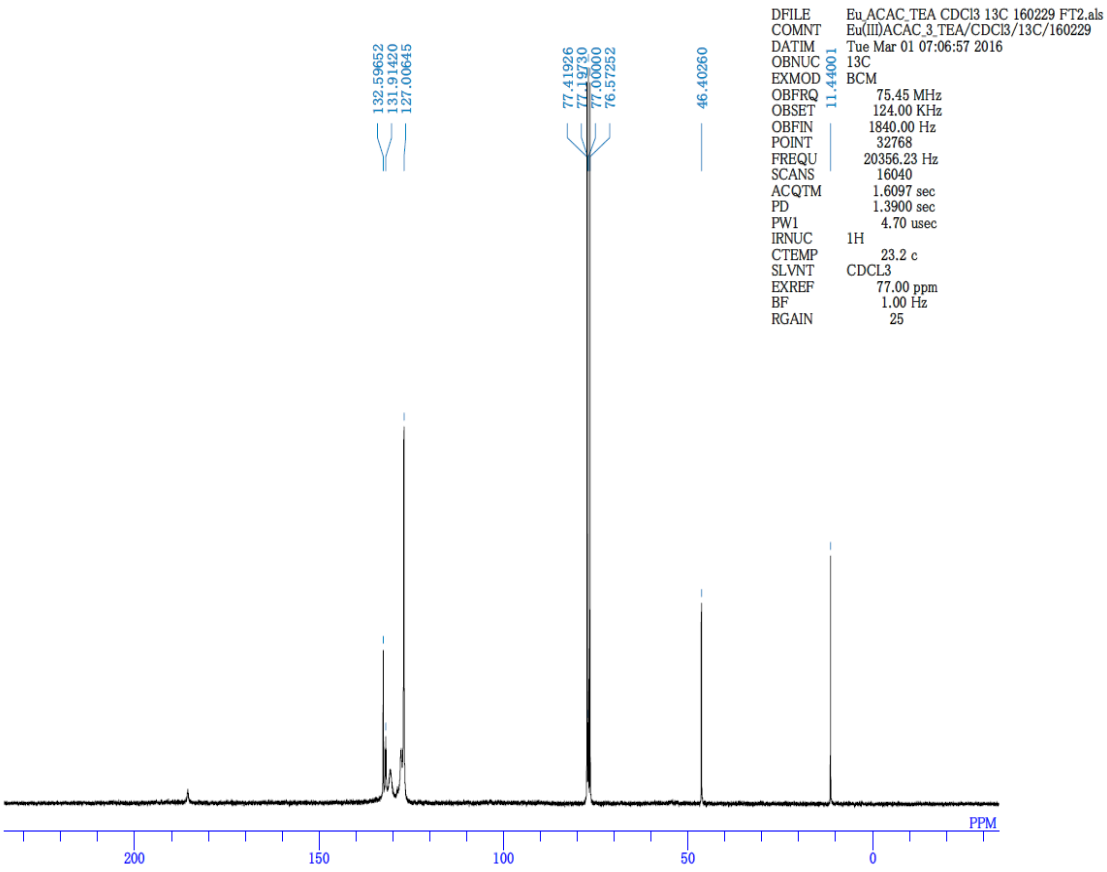

Figure 28 ^{13}C NMR spectrum of the ML material without PVP

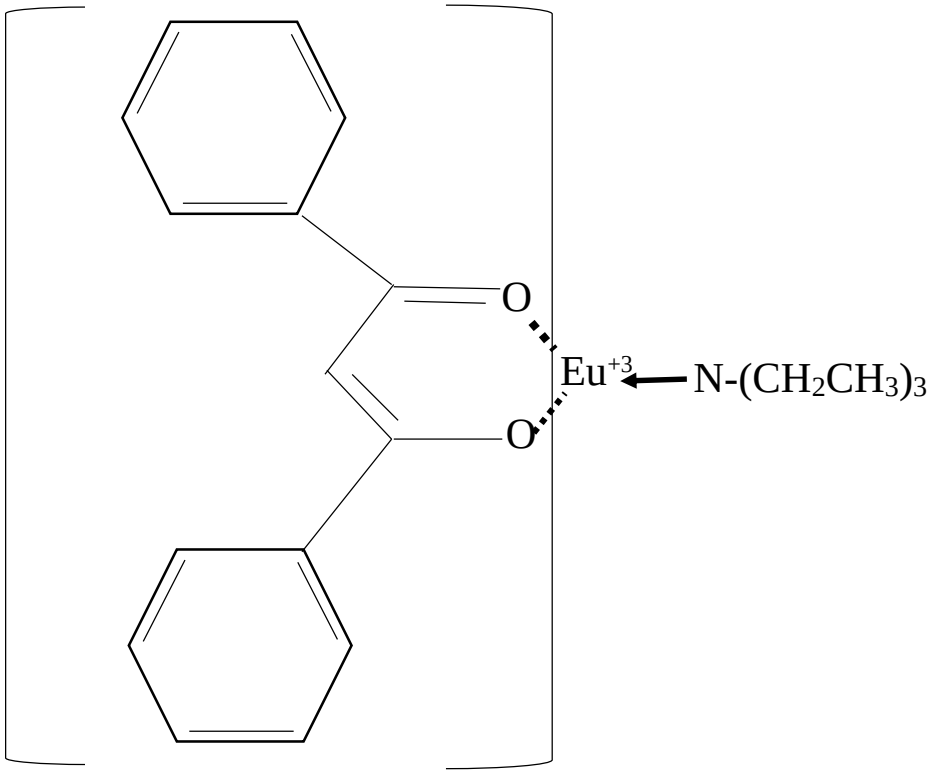

Chemical structure of the ML material

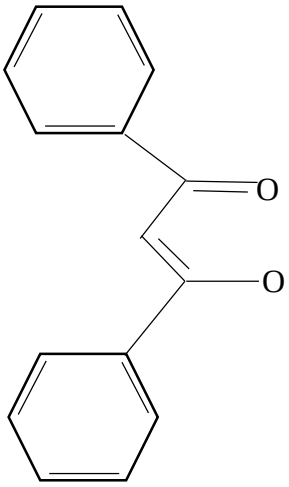

Chemical structure of the 1,3-diphenylpropane-1,3dione

N-(CH2CH3)3

Chemical structure of the Triethylamine

Figure 25 displays the ^{1}H NMR spectrum of the ML material without PVP. For the first time, an NMR analysis of the structure of the EuD_4TEA ML material was performed. The peaks at 1.17286 ppm and 2.7001 ppm correspond to the proton in the CH_3 and CH_2 groups, respectively. In Figure 25, the peaks at 11.4401 ppm and 46.40260 ppm correspond to ^{13}C in the CH_3 and CH_2 groups, respectively. The peaks between 7.24122 ppm and 8.15117 ppm in the ^{1}H spectrum and 127.00645 ppm and 132.59652 ppm in the ^{13}C spectrum revealed a dibenzoylmethane group. In Figure 26, the peaks from 76.57252 pm to 77.41926 ppm belong to Trichloro(^{2}H) methane ($CDCl_{3)}$. However, we used TEA and DBM; therefore, the total number of protons in TEA should be 15.

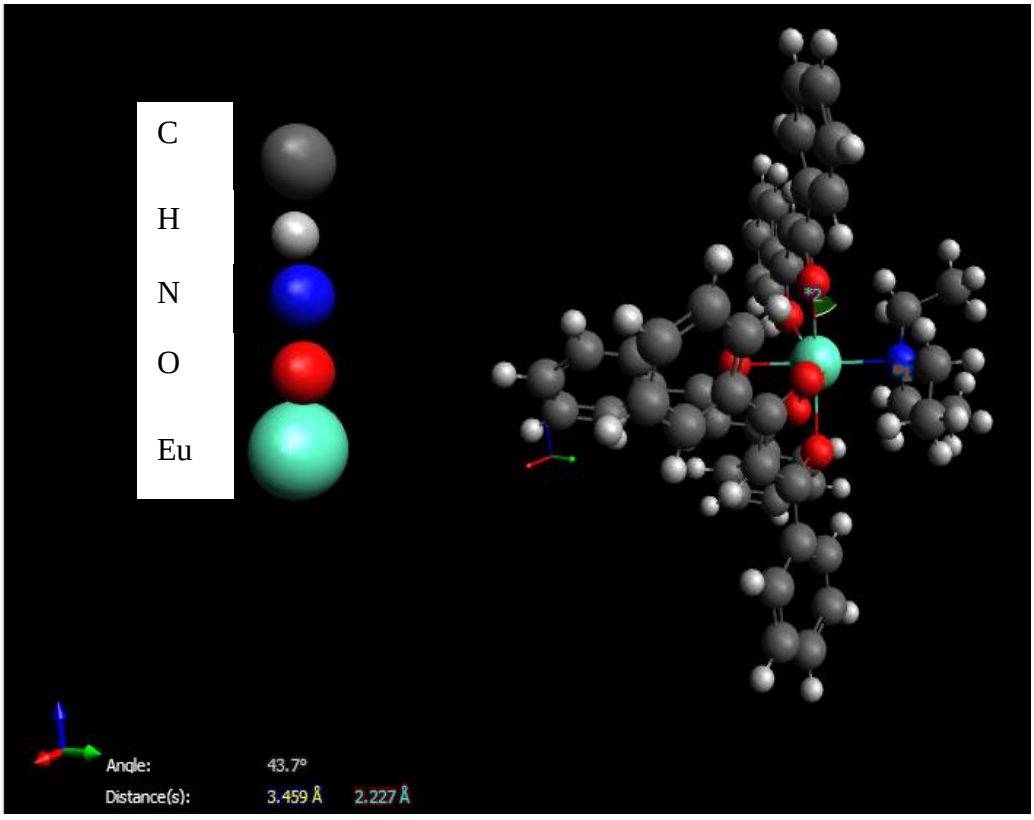

Figure 29 The crystal structure of the synthesized ML material that was illustrated using Avogadro 1.0.1software

Figure 27 revealed that the total number of protons that belong to the methyl and ethyl groups are approximately 14. Therefore, those peaks correspond to TEA. The total number of protons in the DBM molecule is 11 and ^{1}H proton NMR spectrum shows 30 protons that correspond to the DBM peak region. Therefore, 3 DBM molecules are represented and it is believed that smallest ratio between TEA and DBM to coordinate with Eu^{+3} is 1:3. However, if the color coordination number on Eu^{+3} ratio is considered, then the ratio can be 2:6.

4.2.3 Molecular orbital study

We performed theoretical calculations to analyze the electronic structures of triethylamine (TEA), polyvinylpyrrolidone (PVP) and dibenzoylmethane (DBM).

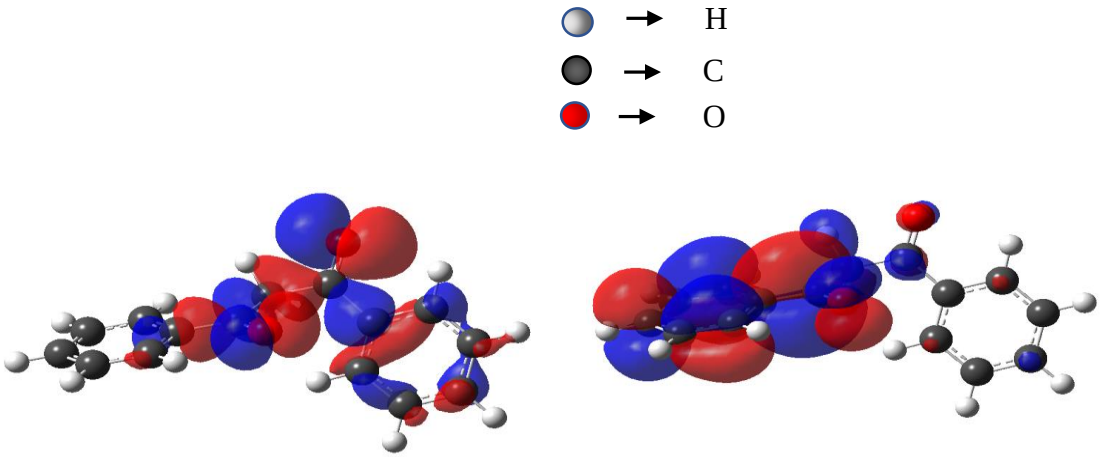

Dibenzoylmethane HOMO

Dibenzoylmethane LUMO

Figure 30 MC at were calc

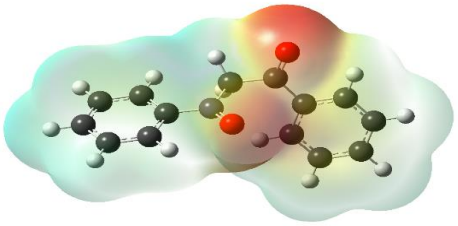

Dibenzoylmethane electron density mapping

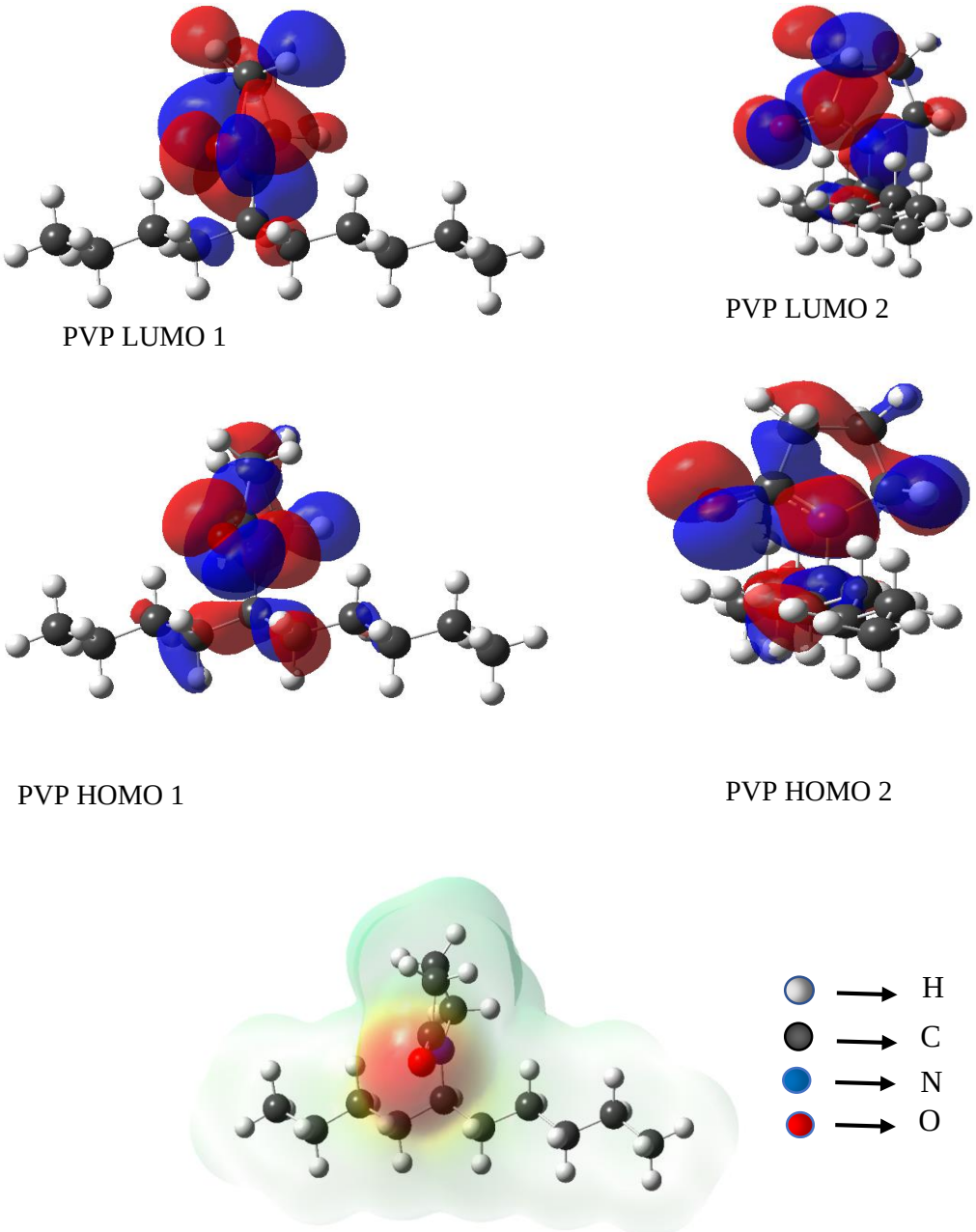

Figure 31 MO contour plots of PVP that were calculated using DFT methods

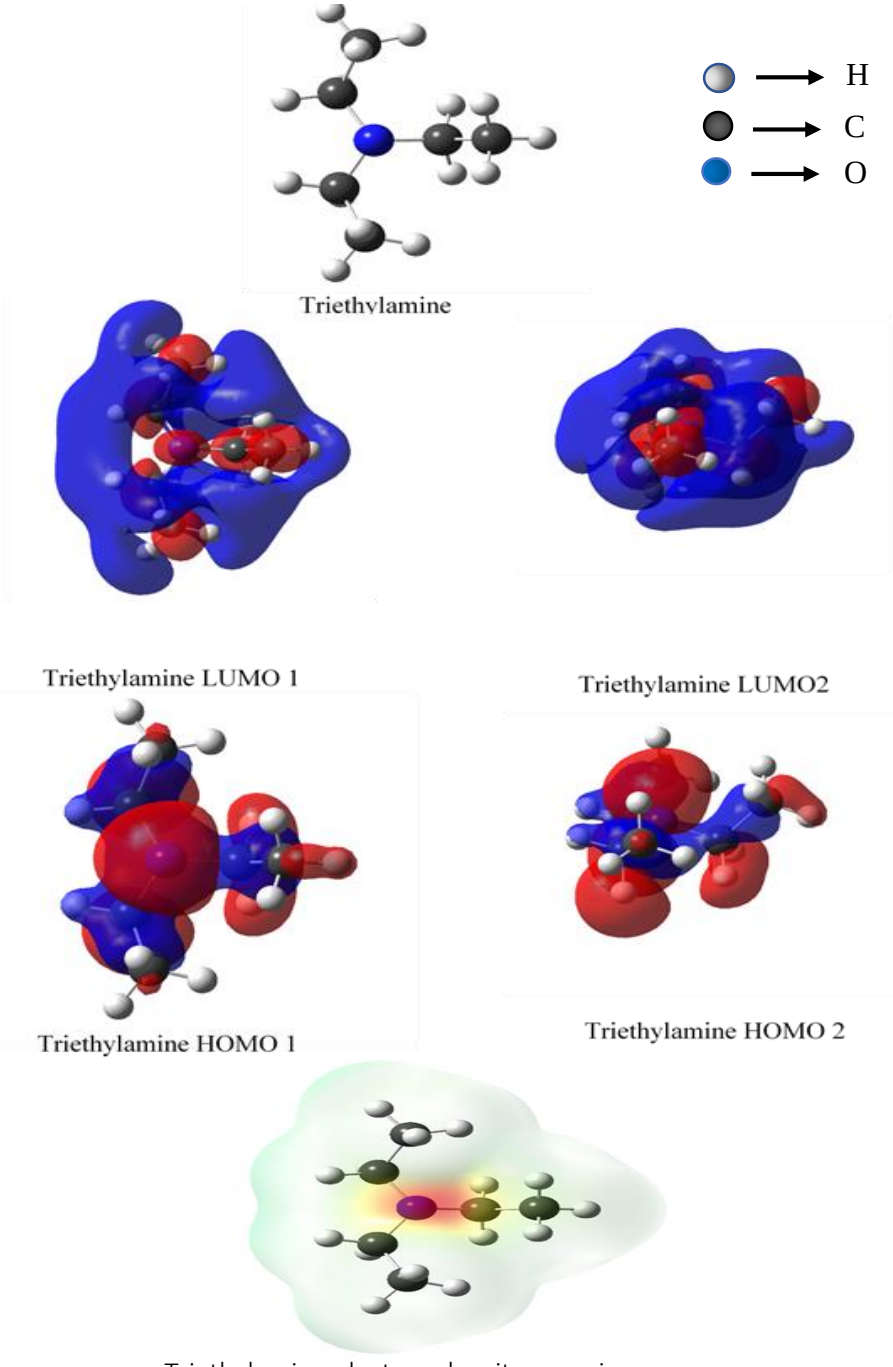

Figure 32 MO contour plots of the triethylamine that were calculated using DFT methods

Figures 28, 29 and 30 show the absolute value of the molecular orbitals (MOs), highest occupied molecular orbital (HOMO) and lowest unoccupied molecular orbital (LUMO) images for PVP, TEA and DBM, respectively. In Figure 28, the MOs of DBM are localized near the phenyl groups and according to the DBM electron density mapping, the electron density surrounding the two oxygen atoms is higher. Material under stressing, distance between europium cation and two oxygen atoms getting reduce and its leads to easily electron transfer to the cation. Oppositely under stretching distance between cation and the ligands increase and peer to reduce the electron affinity and decrease the ML intensity. Figure 29 demonstrated that the HOMO and LUMO of PVP are localized near the pyrrole group and a higher density of electrons are localized around the N and O atoms. These molecular orbital diagrams exhibit the strong possibility that PVP and DBM will coordinate with the europium color center. Figure 30 revealed that the HOMO and LUMO levels of trimethylamine surround all the atoms and the electron density is localized near the N atom.

Figure 23(a) shows SEM images of the ML material without PVP and the micrographs clearly demonstrate that material has a rod-like structure. The TEM micrograph in Figure 23 (c) also confirms that the material exhibits a rod-like structure after the addition of PVP. However, the homogeneity of the fine particles is uneven, and the particle size distribution that ranged from approximately 10 nm to 40 nm of particles distribution was increased. The material structure was larger compared with the structure of the ML material with PVP. This increase was caused by an electron transition through the material. When the particle size decreases, the molecular orbital overlap is increased. Therefore, the electron can easily

transition to the higher and lower energy levels. It is believed that after the addition of PVP, the ML intensity was high. Additionally, the theory behind the mechanism of the

mechanoluminescent material is unknown. The intensity of the ML material depends on the energy difference of the electron transition state. ML depends on the flexibility of the ligand molecule, which coordinates to the color center. Trimethylamine has a greater flexibility compared with the other inorganic molecules. When the ML material is under stress, the ligand molecule can easily move in all directions. Because of this movement, the molecular orbitals overlap and the electrons can transit to a higher energy level. However, the unsteady electrons fall to the lower energy levels. The energy difference between those energy states is illuminated as light. Eu^{+3}-coordinated polyvinylpyrrolidone molecules are highly flexible and therefore the intensity of the ML material significantly increased.

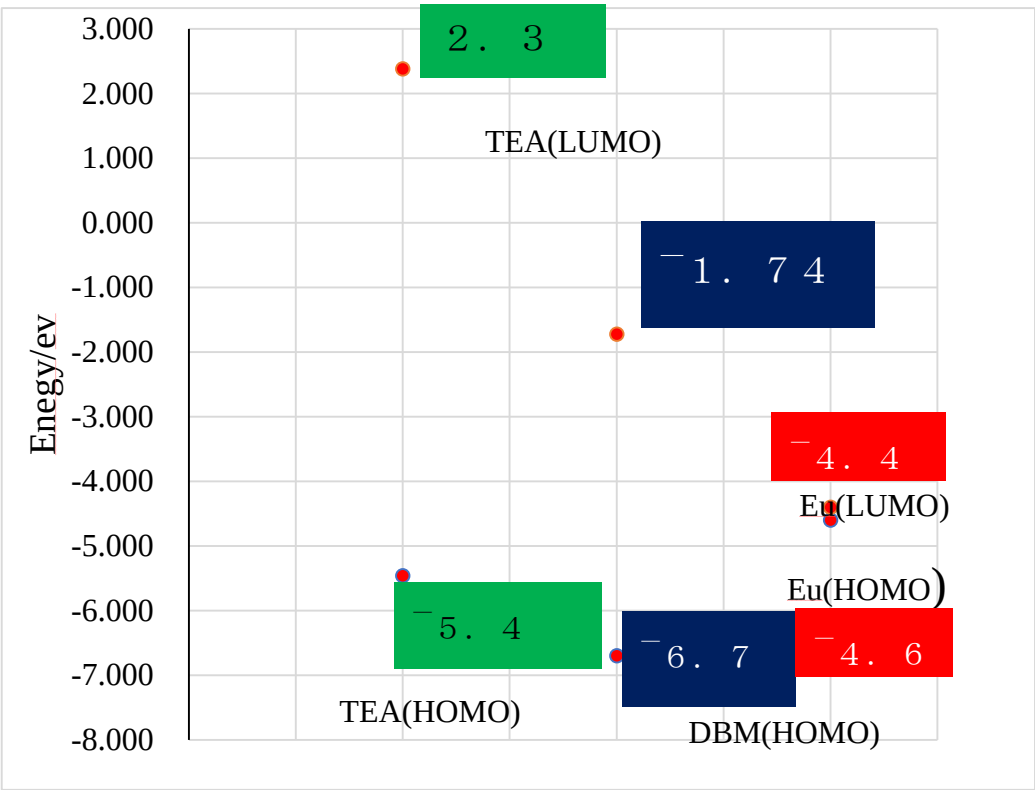

Figure 33 molecular Energy diagram of the molicules which contained the ML material

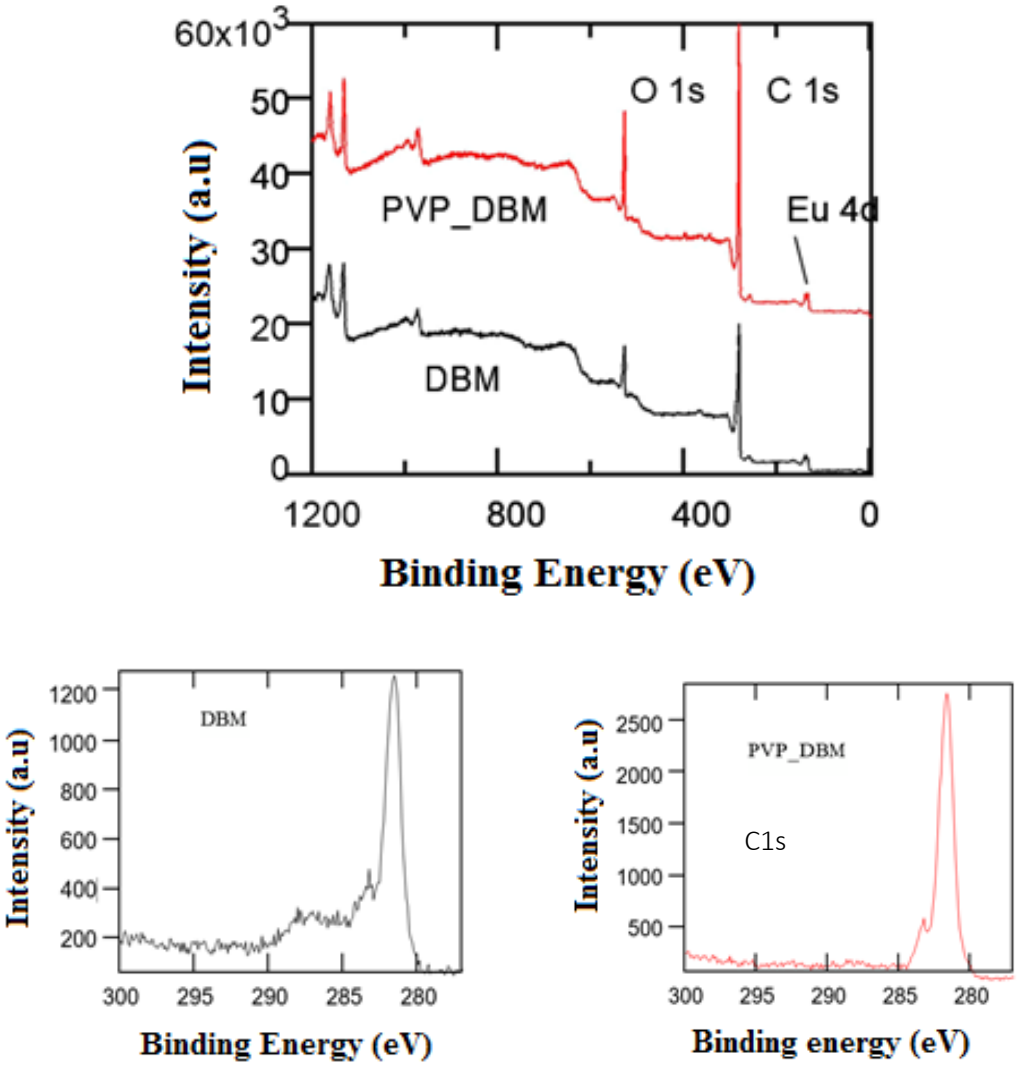

Figure 34 Comparison of XPS spectra obtained from the synthesized materials before and after the addition of PVP

Figure 31 depicts the XPS spectra of the ML materials synthesized both before and after the addition of PVP. The spectra clearly show that both materials have C, O, N and Eu. In the C1s spectra, the two main peaks between binding energies of 280 eV and 285 eV correspond to the C in dibenzoylmethane. A component that was higher than 5 eV from the main peak in the C1s spectra was found without PVP. This peak was assigned to the C=O functional group and disappeared with the addition of PVP. This disappearance confirms the decrease in coordination of the dibenzoylmethane group after the addition of PVP into the ML material and is caused by a larger amount of PVP molecules attached to the color center. In both materials, a component that is greater than 1 eV from the main peak was detected. This main peak can be assigned to a C-OH functional group, which can be attributed to water absorption on the synthesized ML material and to the intensity of that peak decreased with the addition of PVP. Furthermore, the PVP polymer material has a hydrophobic property, which caused

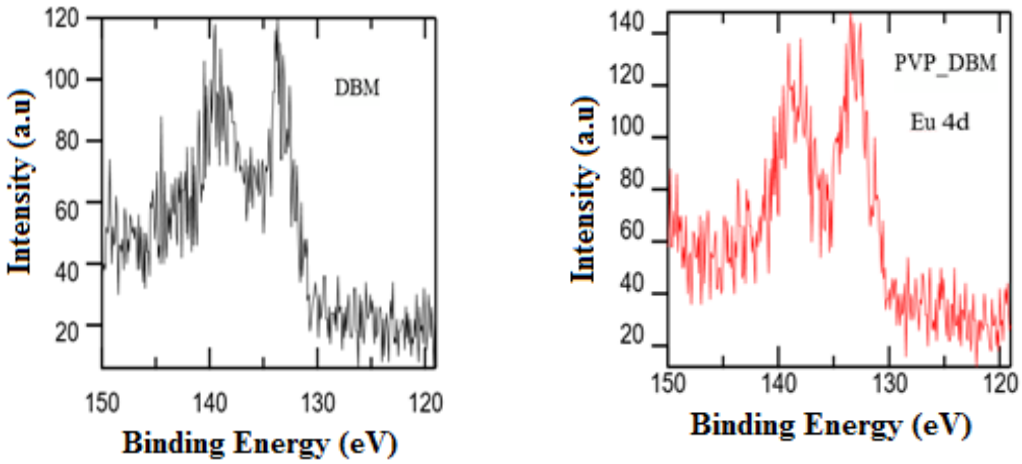

Figure 35 Comparison of Eu 4d spectra with and without PVP

a smaller amount of water absorption. There is not a significant difference in the Figure 32 Eu 4d spectra, but the peak area increased with the addition of PVP. The spectrum provides evidence that the Eu^{+3} valence is not changed with PVP.

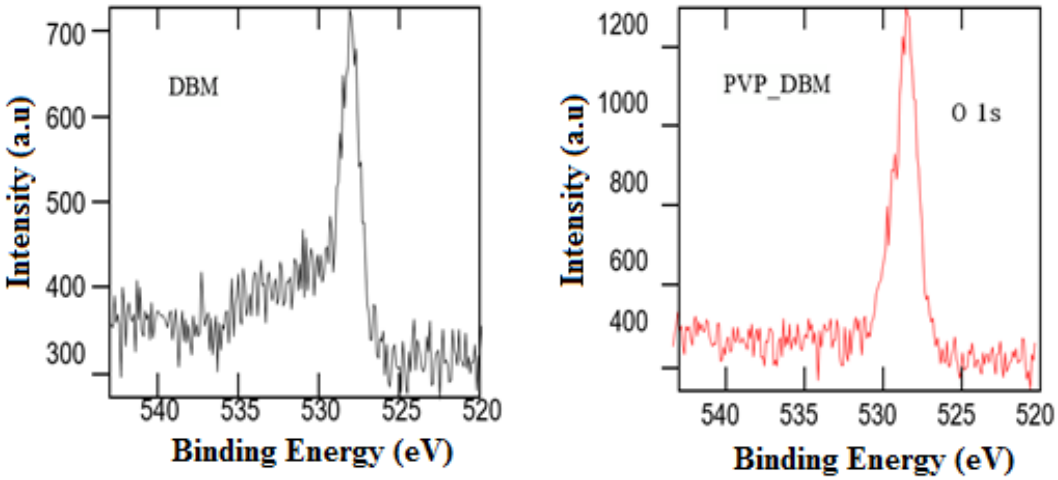

Figure 36 spectra with and without PVP

In Figure 33 the O1s spectra, a component that was higher than the main peak was found prior to the addition of PVP. This component was assigned to the C=O ∏ bond and disappeared after the addition of PVP. However, a higher number of molecules were coordinated with the Eu^{+3} color center with PVP. This highly intense new material can be used for various purposes, such as defect determination in pipes, stress sensor analyses, real-time visualization of the stress distribution in solids, internal visualization of artificial legs,

real-time visualization of the quasidynamic crack-propagation in solids, novel ML-driven solar cell systems, real-time visualization of the stress field near the tip of a crack, ML light sources, determination of laser and ultrasonic powers, secret message writing, EML-based safety-management monitoring systems, non-destructive testing of materials, earthquake detectors and sensors for the detection of cracks inside concrete beams.

4.2.4 Conclusions

For the first time, we have investigated the minimum ratio between TEA and DBM (1:3) from an analysis of ^{1}H and ^{13}C NMR spectra. The XPS results indicate that the materials have peaks that correspond to C, O, N and Eu. The ML and PL intensities were characterized using a Multichannel spectroscope(Hamamatsu-photonic) (PMA/C8808-01). The PL spectrum that was collected after a 357 nm excitation consisted of emission lines at 592.7 nm, 612.0 nm, 651.2 nm and 701.3 nm. Those emission wavelengths belong to an electron transition from the $^{5}D_0$ to $^{7}F_n$ (n=1, 2, 3, 4) energy levels. The corresponding XRD patterns provide evidence that the novel material has good crystallinity with PVP. The corresponding TEM images have confirmed that the material has a rod-like structure, and a histogram confirmed particle sizes at approximately 4 nm. The histogram from the TEM micrographs and XRD results of the material without PVP confirm a mean value of grain size from approximately 7 nm to 10 nm. After the addition of PVP, a decrease in the particle size was confirmed. The fine particle size and crystallinity of the synthesized ML material enabled a higher overlap in the electron orbitals. The greater electron orbital overlap, a flexibility of

the ligand molecules and a higher dipole moment of PVP resulted in an increase in the ML and PL intensities of the synthesized ML material. The newly synthesized EuD_4TEA material with PVP has higher PL and ML intensities compared with the material without PVP. Because the novel material has a higher ML intensity, it can be applied to defect detection in pipes, stress sensor analyses, real- time visualization of the stress distribution in solids, internal visualization of artificial legs, real-time visualization of the quasidynamic crack-propagation in solids, novel ML-driven solar cell systems, and real-time visualization of the stress field near the tip of a crack and used as an ML light source

4.2.5 References

58. Tiwari, N., V. Dubey, and R.K. Kuraria, *Mechanoluminescence Study of Europium Doped CaZrO3 Phosphor.* Journal of Fluorescence, 2016. **26**(4): p. 1309-1315.
59. Jha, P. and B.P. Chandra, *Survey of the literature on mechanoluminescence from 1605 to 2013.* Luminescence, 2014. **29**(8): p. 977-993.
60. Chandra, B.P., et al., *Sensing of shock-wave velocity and pressure using shock-wave induced mechanoluminescence of crystals.* Sensors and Actuators A: Physical, 2015. **235**: p. 203-209.
61. Teotonio, E.E.S., et al., *Mechanoluminescence of Coordination Compounds*, in *Triboluminescence: Theory, Synthesis, and Application*, O.D. Olawale, et al., Editors. 2016, Springer International Publishing: Cham. p. 39-63.
62. Reynolds, G.T. and R.H. Austin, *Mechanoluminescence of plastic scintillation counters.* Journal of Luminescence, 2000. **92**(1–2): p. 79-82.
63. Xu, C.N., et al., *Preparation and characteristics of highly triboluminescent ZnS film.* Materials Research Bulletin, 1999. **34**(10–11): p. 1491-1500.
64. Takada, N., et al., *Mechanoluminescence from piezoelectric crystals of an europium complex.* Synthetic Metals, 2000. **111–112**: p. 587-590.
65. Chandra, B.P., *Mechanoluminescence and high pressure photoluminescence of (Zn, Cd) S phosphors.* Pramana, 1982. **19**(5): p. 455-465.
66. Chandra, B.P., V.K. Chandra, and P. Jha, *Microscopic theory of elastico-mechanoluminescent smart materials.* Applied Physics Letters, 2014. **104**(3): p. 031102.

67. Jeong, S.M., et al., *Mechanoluminescence Color Conversion by Spontaneous Fluorescent-Dye-Diffusion in Elastomeric Zinc Sulfide Composite.* Advanced Functional Materials, 2016. **26**(27): p. 4848-4858.
68. Botterman, J., et al., *Mechanoluminescence in BaSi2O2N2:Eu.* Acta Materialia, 2012. **60**(15): p. 5494-5500.
69. Chandra, B.P., et al., *Real-time mechanoluminescence sensing of the amplitude and duration of impact stress.* Sensors and Actuators A: Physical, 2012. **173**(1): p. 9-16.
70. Wang, X., et al., *Dynamic Pressure Mapping of Personalized Handwriting by a Flexible Sensor Matrix Based on the Mechanoluminescence Process.* Advanced Materials, 2015. **27**(14): p. 2324-2331.
71. Rahimi, M.R., et al., *Effects of persistent luminescence decay on mechanoluminescence phenomena of SrAl2O4:Eu2+, Dy3+ materials.* Optics Letters, 2013. **38**(20): p. 4134-4137.
72. Li, D.G., N.S. McAlpine, and D. Haneman, *Surface barriers and potentials from luminescence on cleaved Si, GaAs, and InP.* Surface Science, 1993. **281**(1): p. L315-L320.
73. Lin, Y.-H., et al., *Studies on mechanoluminescence from SrAl2O4:Eu, Dy phosphor.* Materials Chemistry and Physics, 2003. **80**(1): p. 20-22.
74. Chandra, B.P., et al., *Strong mechanoluminescence induced by elastic deformation of rare-earth-doped strontium aluminate phosphors.* Journal of Luminescence, 2009. **129**(7): p. 760-766.
75. Imai, Y., R. Momoda, and C.-N. Xu, *Elasticoluminescence of europium-doped strontium aluminate spherical particles dispersed in polymeric matrices.* Materials Letters, 2007. **61**(19–20): p. 4124-4127.
76. Sharma, R., et al., *Mechanoluminescence and thermoluminescence of Mn doped ZnS nanocrystals.* Journal of Luminescence, 2011. **131**(10): p. 2089-2092.
77. Pust, P., et al., *Narrow-band red-emitting Sr[LiAl3N4]:Eu2+ as a next-generation LED-phosphor material.* Nat Mater, 2014. **13**(9): p. 891-896.

4.3 low-Temperature Treatment Effect on The Organic Based Mechanoluminescent Materials

4.3.1 Introduction

Mechanoluminescent (ML), is light discharge occurring from any mechanical movement on a solid[79]. This phenomenon has been recognized in distinct organic and inorganic solids with rare earth metal associate on their complexes[80]. Nevertheless, often ML materials lose their luminescent Intensity, either partially or entirely, by experimental and environmental impacts[81]. Therefore, their possible applications have not been broadly studied. Investigations on the effect of changing pressure, color center, temperature, impurities on the luminescence have been reported[82]. Despite, considering ML occurs in solids, Increasing the luminescence intensity, enhanced the lasting property, Crystal structure and understanding about the mechanism of the theory behind the intensity transmitted are required. For the crystallinity changing and increasing the size of the crystal, the cooling temperature is a most significant factor. In, this research carried out the low-temperature effect of to enhance the ML intensity and changing the crystal structure.

4.3.2 Experimental Method

The synthesis was began by 0.106 mol dibenzoylmathane(1,3-diphenylpropane-1,3dione, $C_{15}H_{12}O_2$),(98.0%, Wako) and 1.5 ml triethylamine(99.0%, Wako) were dissolved in 80 ml of ethyl alcohol(99.5%, Wako) under vigorously stirred on the hot plate at 70°C for solute

become completely dissolved. Then 0.02 mol l^{-1} Europium(iii)nitratehexahydrate (99.9%, Wako) was added to the stirred solution and further stirred 20 minutes until the solution became saturated. The saturated hot solution contained beaker was capped tightly then inserted into the thermos on treating on slow cooling effect for overnight. Precipitated synthesized ML material was filtered by using vacuumed filter and washed four-time with ethyl alcohol. The experiment was repeated with 0.02mol l^{-1}concentration of EuI_2, $EuBr_2$, and $EuCl_2$.Synthesized four different ML material's mechanoluminescent intensity were characterized by using Hamamatsu Photonic multichannel analyzer at the room temperature. Then 0.0013 mol l^{-1} Eu^{+3} contained a mechanoluminescent material insert into the ceramic pestle and put 10 ml liquid nitrogen on the sample. After the one minute, ML setup was run, and intensity was characterized by using Hamamatsu Photonic multichannel analyzer.process was repeated with 0.0013 mol l^{-1} concentration of other three different ML materials.

4.3.3 Result and Discussion

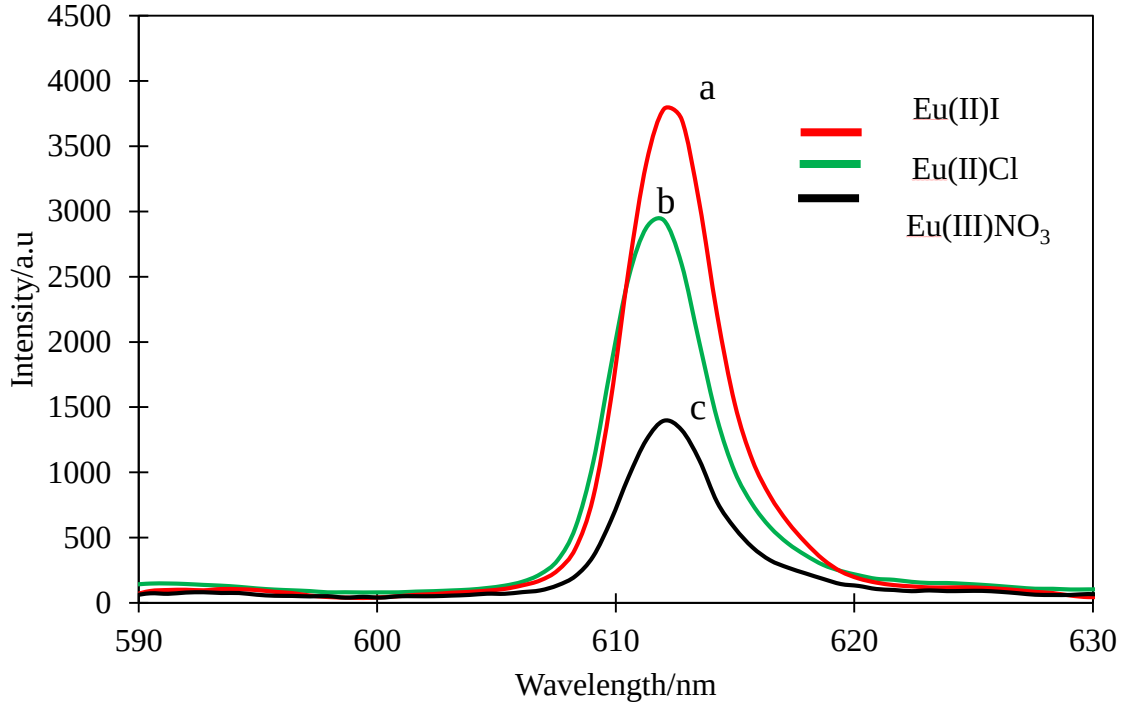

Figure 37 ML intensity comparison on three different ligands a) Eu(ii)I ligand contained ML b) Eu(ii)Cl ligand contained ML c) Eu(iii)NO3 contained ligand

Figure 34 show ML intensity comparison with three different ML material, which used to synthesize three different ligands. (a), (b) and (c) spectra correspond to the ML intensity with three different ligand Eu(ii)I, Eu(ii)Cl and Eu(iii)NO_3. Spectra Clearly reveal that ML intensity is changing according to the ligand changing and intense ML property corresponded to the Eu(ii)I ligand contained ML material. Central peaks reveal in wavelength 612 nm corresponded to the Eu $^5D_0$ to $^7F_2$ forbidden transaction. Since the ligand change caused to

differ on the oxidation state of the color center when using the Eu(ii)I and Eu(ii)Cl oxidation state of the europium is $Eu^{+2,}$ and it is for Eu(iii)NO_3 is Eu^{+3}.It is confirmed that valance band structure of the XPS data reveals that Eu^{+3} and Eu^{+2} band spectrum. According to the valance changing Higher occupied molecular orbital energy and Lower unoccupied molecular orbital energy difference is changed. Since energy difference occurs to the changing the ML intensity.

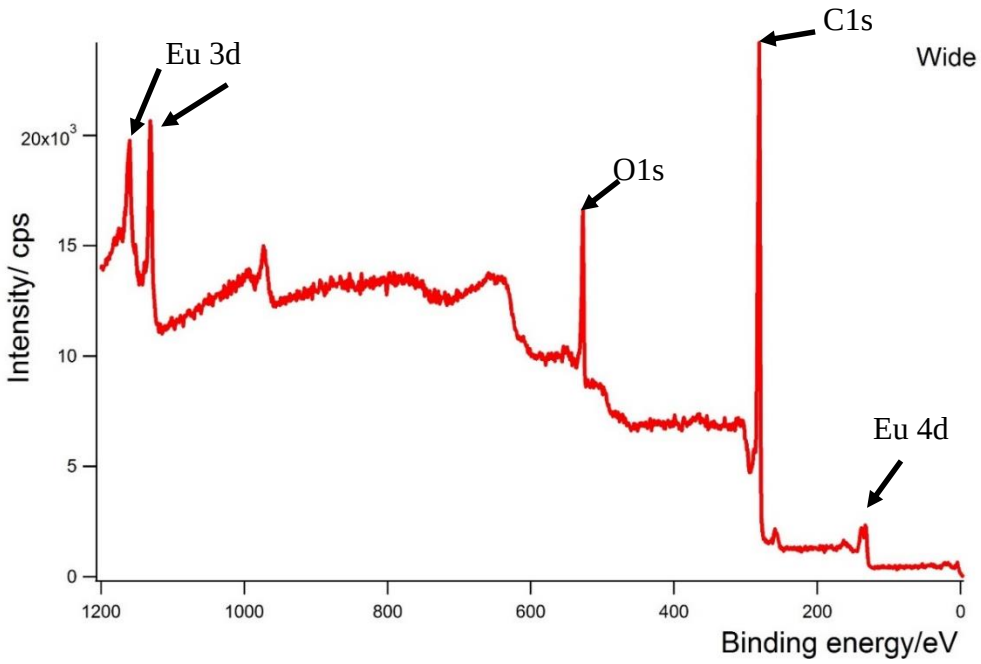

Figure 38 XPS wide spectrum on Eu^{+2} contained ML material

Figure 35 reveal that corresponding XPS wide spectrum of the Eu^{+3} ligand contained ML material. Spectrum clearly depicted that composition of synthesized ML material only have Europium, Carbon and Oxygen and its confirmed that the purity of the ML material.

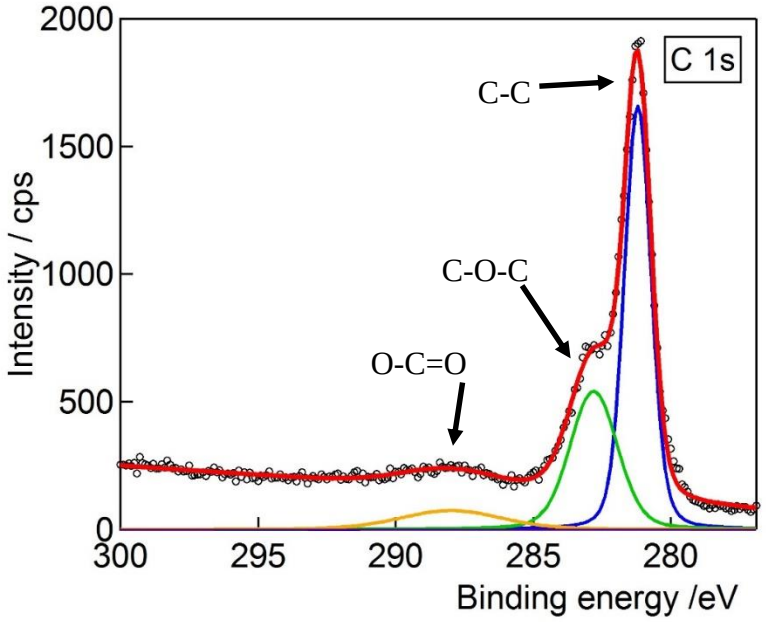

Figure 39 C1s spectrum on Eu^{+2} contained ML material

According to the Figure 36 C1s spectra is revealed binding energy at 282eVon that peak corresponded to the C from dibenzoyl methane and peaks at the 284eV and 287eV which can be assigned to the carbon to oxygen bond in dibenzoyl methane. When carefully study in Figure 37 which is a describing europium 3d spectrum, peaks at the binding energy on 1132eV assigning to the $Eu^{+2} – 3d_{5/2}$ and two peaks at the binding energy on 1153eV,1161eV be assigned to the Eu^{+2}-$3d_{3/2}$.In figure 38 we cannot clearly see the N1s peak corresponded to the triethylamine in ML material.However XPS measurement corresponded to the surface of the material, and it is possible to evaporate triethylamine because of the higher energy of the X-ray.

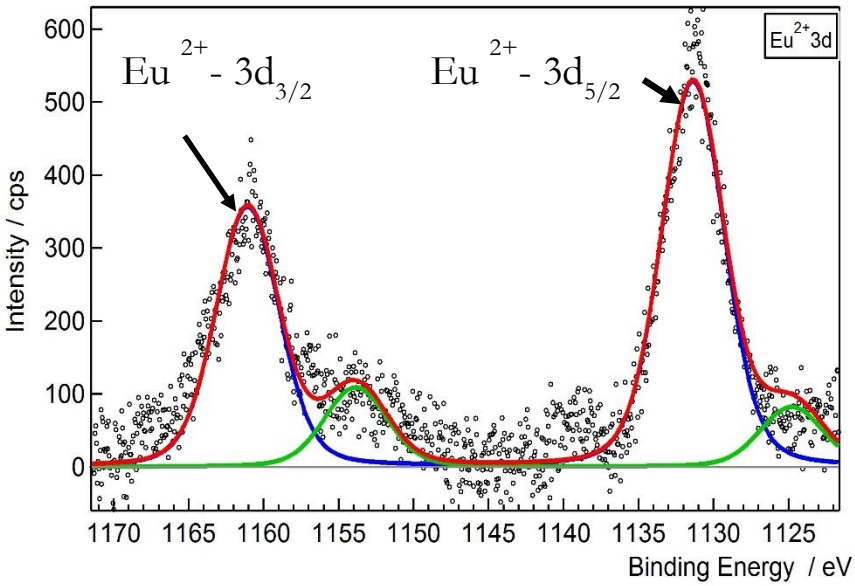

Figure 40 Eu 3d fitting spectrum on Eu^{+2} included ML material

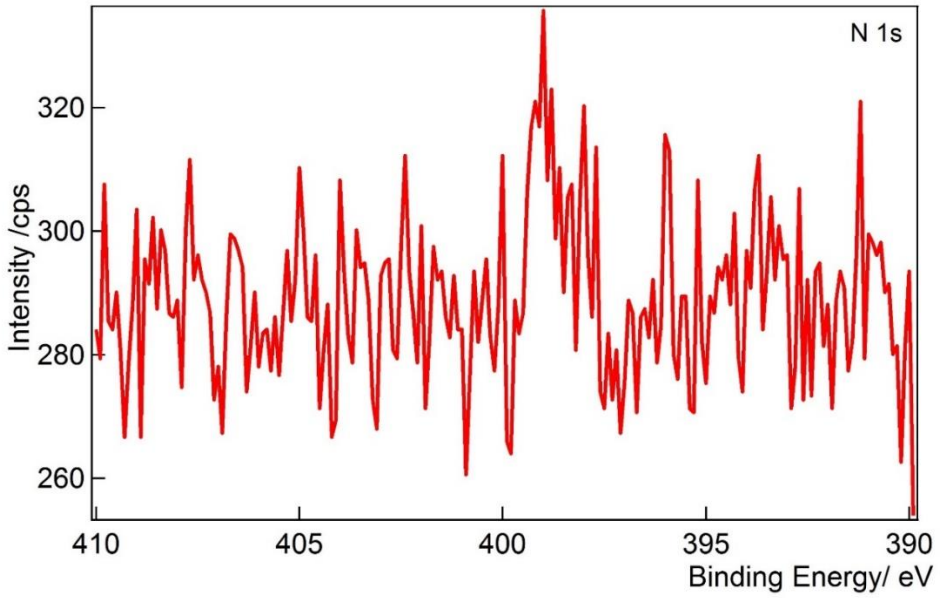

Figure 41 XPS spectrum corresponds to the N1s

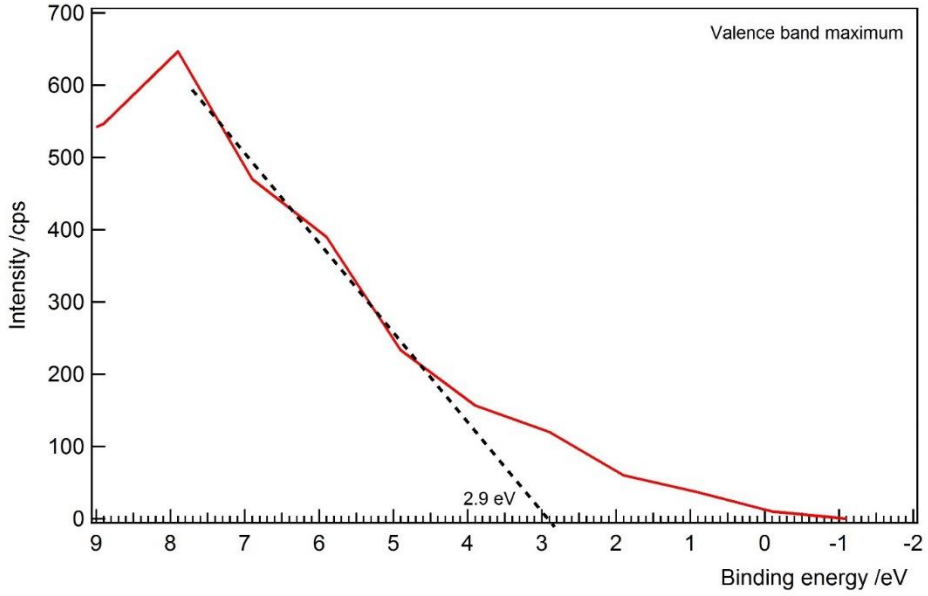

Figure 42 XPS wide spectrum region in between binding energy -1 eV to 9 eV

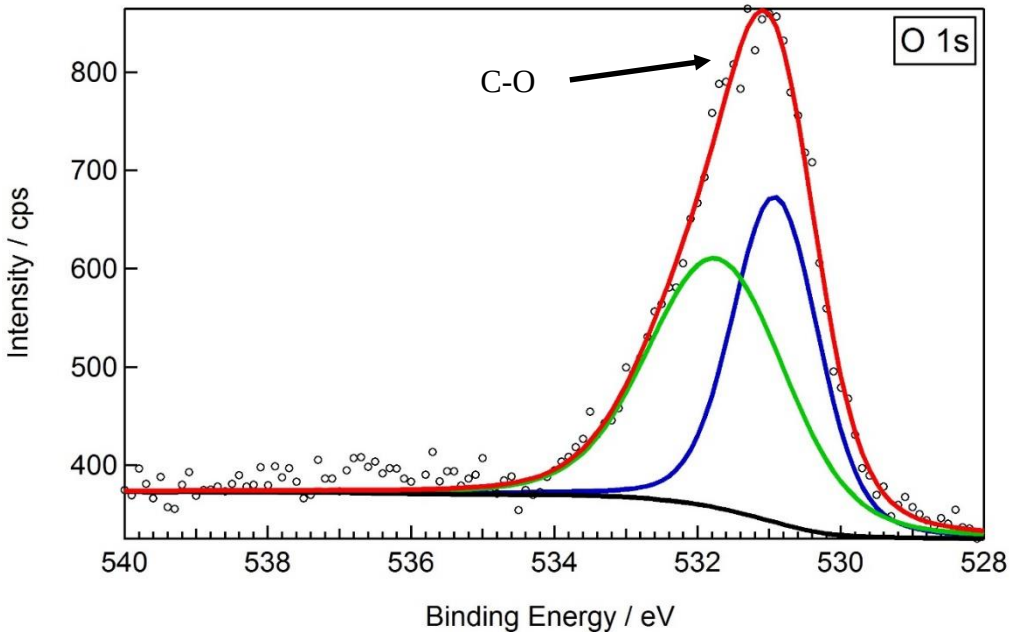

Figure 43 O 1s spectrum on Eu^{+2} contained ML material

In Figure 39 XPS spectrum reveal that valence band maximum of the Eu^{+2} provided ML material and its 2. 9ev.Figure 40 O1s spectrum depicted that fitted curve in binding energy at 531eV corresponded to the C-O bond in dibenzoyl methane. XPS spectrum showing in Figure 41 corresponds to the C1s of the Eu^{+3} contained ML. The component at the binding energy 281 eV is evidence that of the C in dibenzoyl methane and compare with the C 1s XPS spectrum on the Eu^{+2} contained ML material it's not different. However, component higher than the 1eV from the strong peak reveals that O-C-O bond in dibenzoyl methane. The peak at the binding energy of 288 eV corresponds to C=O bonds in dibenzoyl methane. In Figure 42 depicted that binding energy at 1133eV corresponds to the Eu^{+3} $3d_{5/2}$ and 1153eV, 1162 eV for Eu^{+3} $3d_{3/2}$.

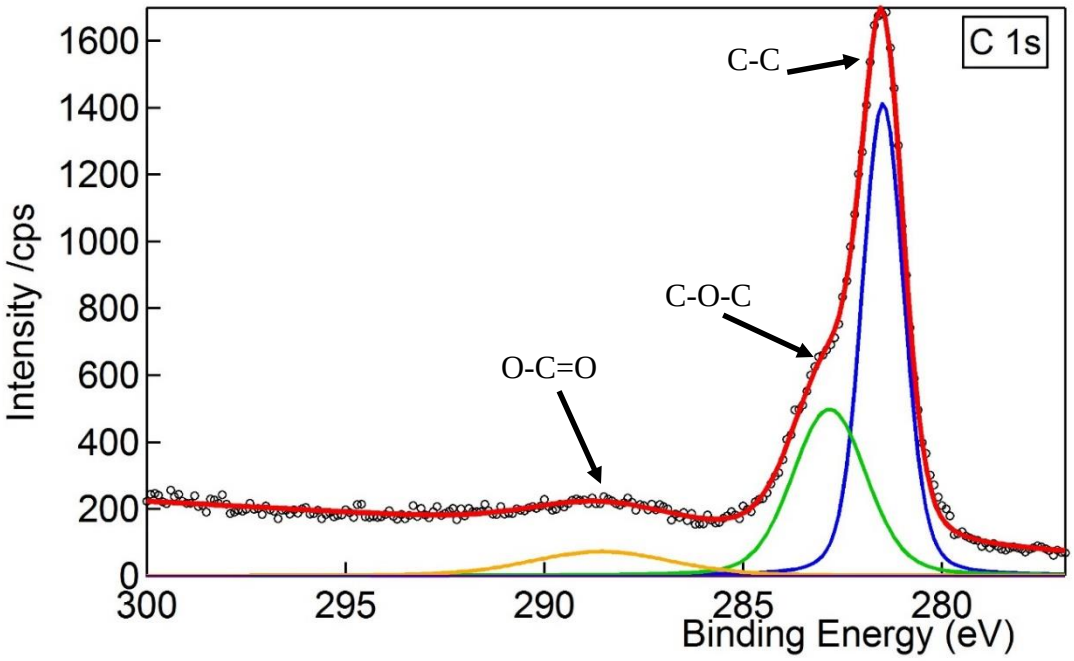

Figure 44 C1s spectrum on Eu+3 contained ML material

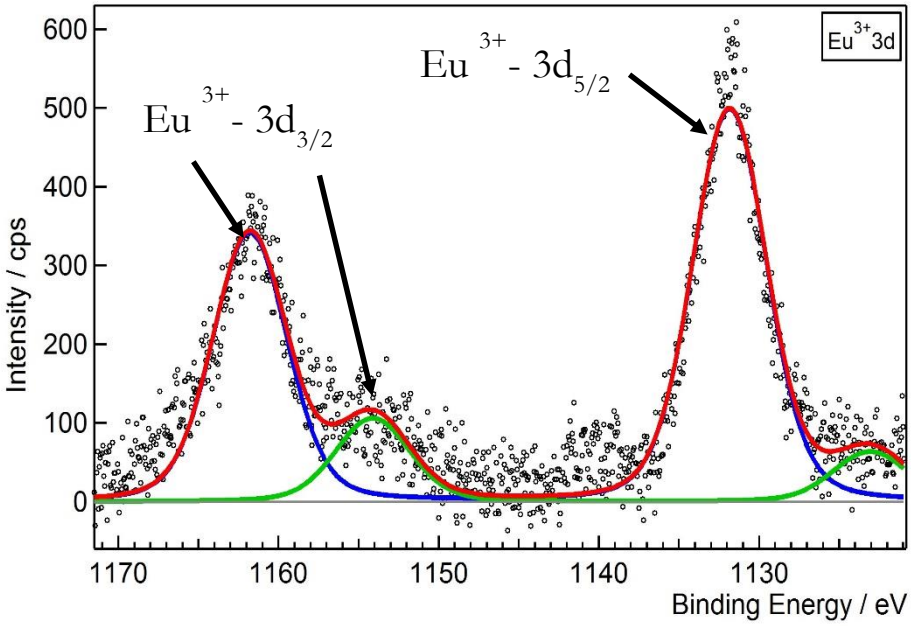

Figure 45 Eu 3d fitting spectrum on Eu^{+3} included ML material

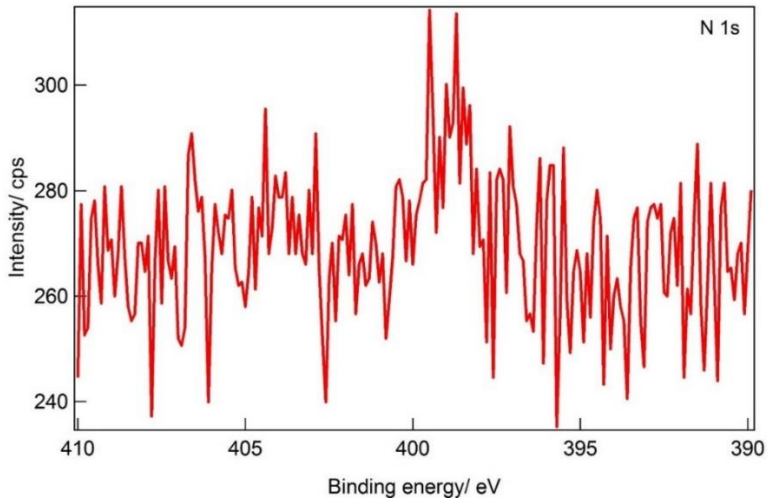

Figure 46 XPS spectrum for N1s

Figure 43 is identical N1s spectrum which is perceived from the XPS characterization for Eu^{+3} included ML material, and peaks cannot identify fluently because triethylamine chance to have to lead the evaporation because of the higher energy of the X-Ray source. In Figure 44 peak at binding energy, 527eV is disclosed that the C which is belonging to dibenzoyl methane. Carefully analysis the both ML material with Eu^{+2} and Eu^{+3}, C peak intensity is higher since base material is dibenzoyl methane for the both synthesized ML material.

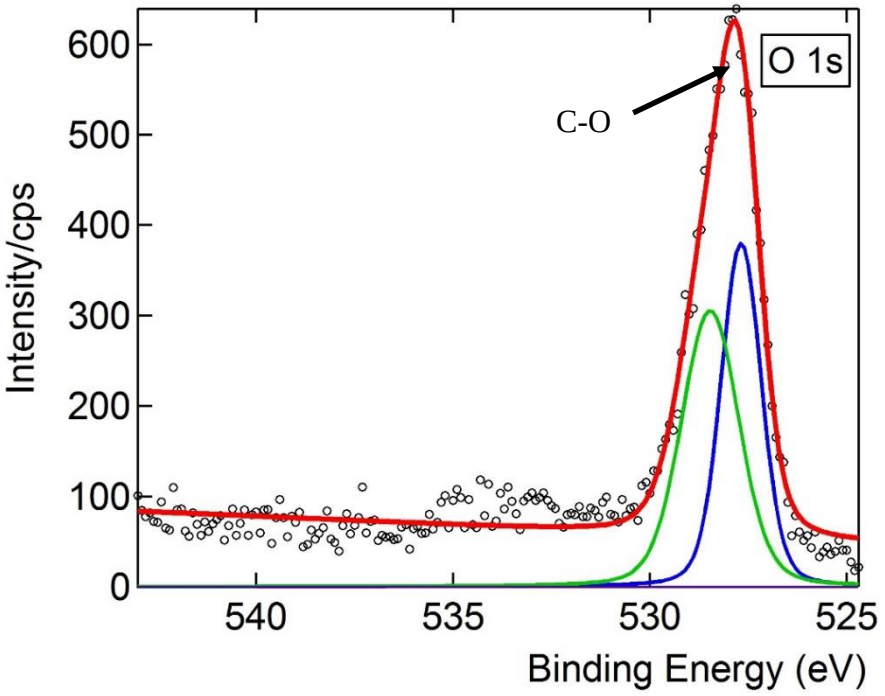

Figure 47 O1s spectrum on Eu+3 contained ML material

In Figure 44 revealed that peak at binding energy on 528eV C-O bond which is evidence to C-O bond in benzoyl group. Changing the ligand in ML material according to Eu^{+3} oxidization sate Figure 45 shown valence band maximum is becoming 1.7eV and it is confirming according to the ligand changing valence band electronic structure is change.

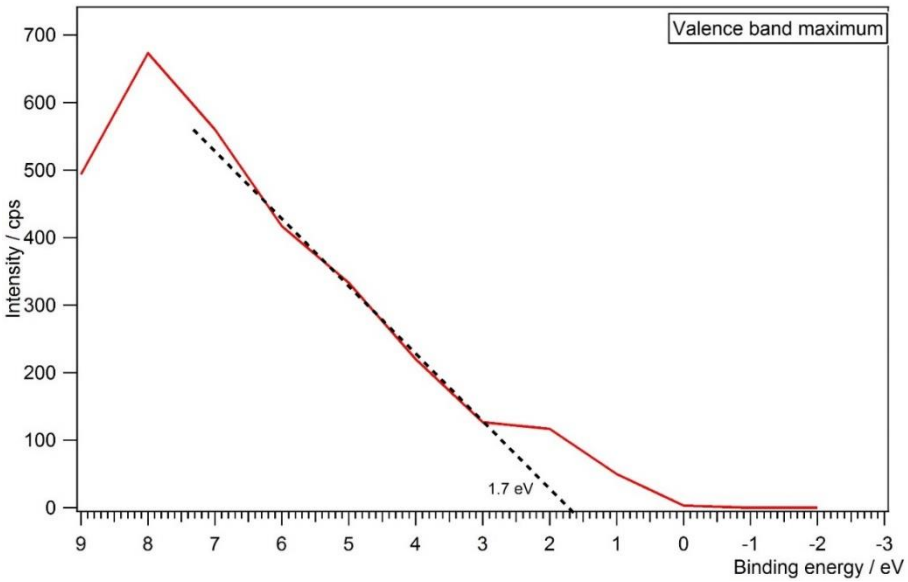

Figure 48 XPS wide spectrum region in between binding energy -2 eV to 9 eV

Carefully studying with Figure 46 and 47 which is revealing comparison of the valence band electronic structures energy difference between two bands about 1eV.HOMO and LUMO energy difference occur to the changing intensity of the ML material.

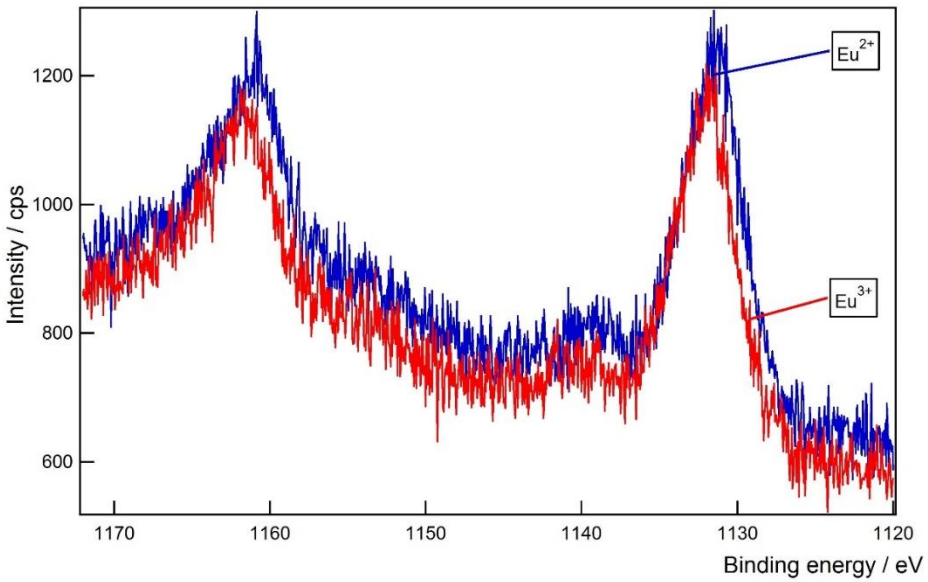

Figure 49 comparison of XPS spectrums on valence band structure for the Eu^{+2} and Eu^{+3}

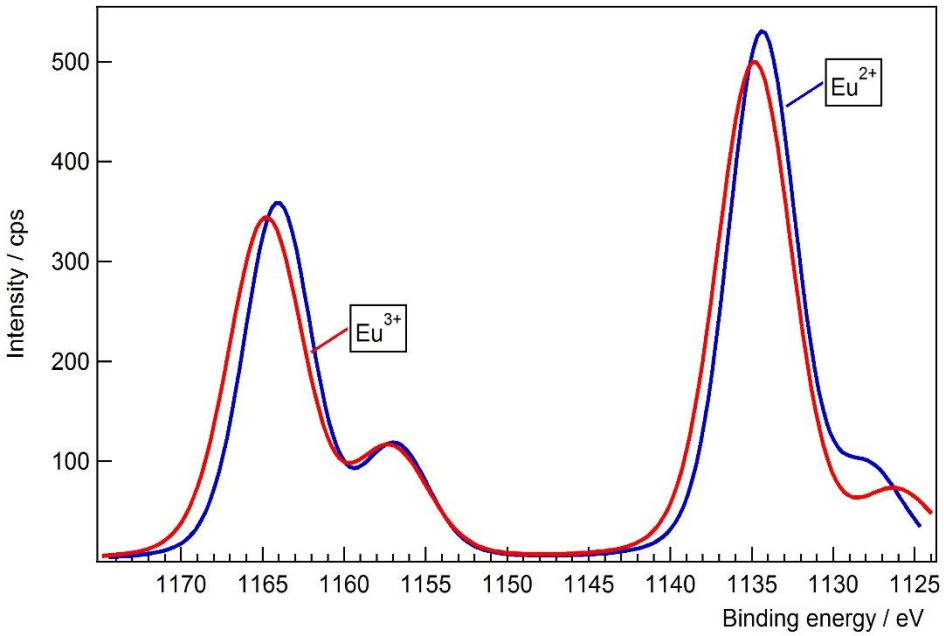

Figure 50 comparison of XPS fitted spectrums on valence band structure for the Eu^{+2} and Eu^{+3}

XPS valence structures of the both material (**Figure47**) a it is proved that HOMO and LUMO band energy difference is change according to the ligands changing. Therefore Eu^{+2} included ML material assign to the orange-yellow color light emitting ML material.

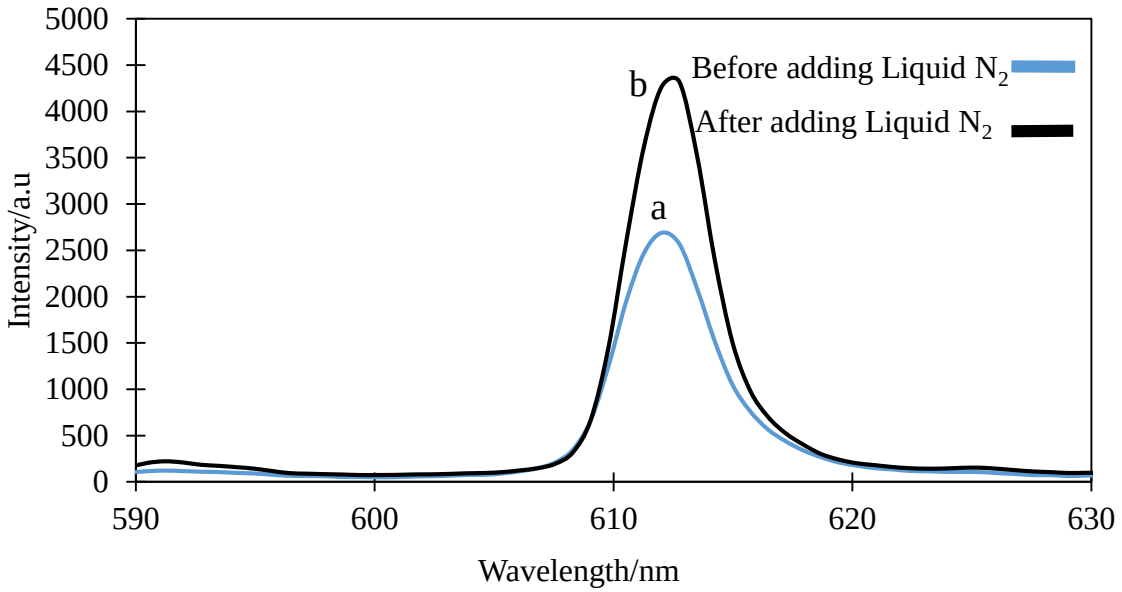

Figure 51ML intensity spectrums on Eu(ii)Cl Ligand contained ML material a) without treatment of Liquid Nitrogen b) with treatment of liquid nitrogen

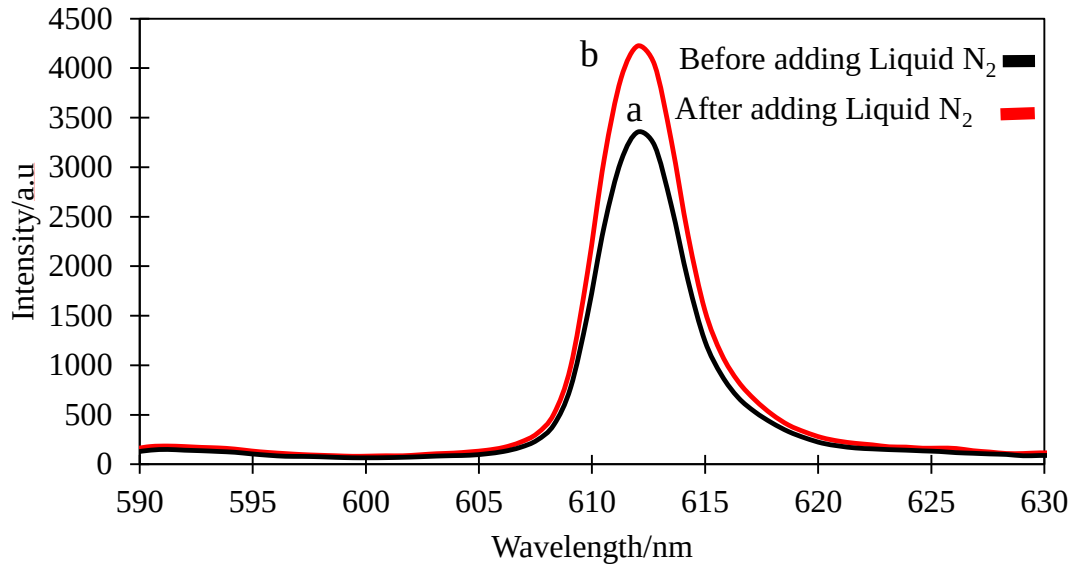

Figure 52 ML intensity spectrums on Eu(ii)Br Ligand contained ML material **a)** without treatment of Liquid Nitrogen **b)** with treatment of liquid nitrogen

Figure 49,50, and 51 are depicted that ML intensity variation with treatment with liquid nitrogen for different ligand contained ML materials. Carefully studied with the for spectrums its clearly revealed that after treated with liquid Nitrogen ML intensity is increased comparably. Highest mechanoluminescent intensity is provided that Eu(ii) I ligand contained ML material since treated with nitrogen ML intensity was two times increased. Mechanism happening in here synthesized materials are not the fully crystallized and some part are besides in amorphous phase. After treated with liquid nitrogen amorphous parts transfer to the crystalized, and it is lead to the electrons affinity from ligand to rare earth metal

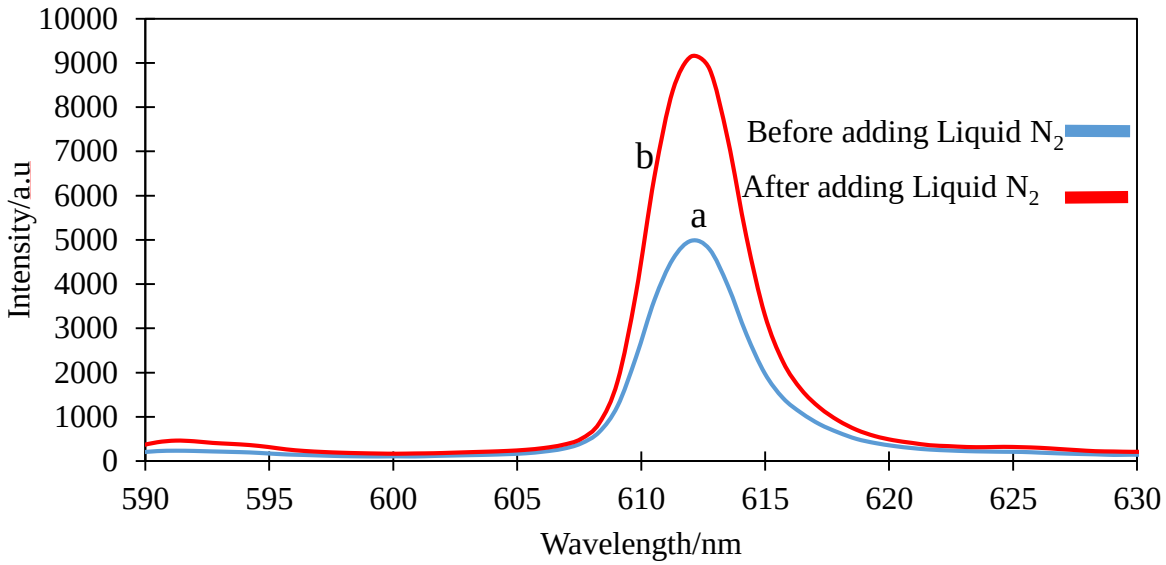

Figure 53 ML intensity spectrums on Eu(ii)I Ligand contained ML material **a)** without treatment of Liquid Nitrogen **b)** with treatment of liquid nitrogen

(europium cation) electron transitions, and much amount of electron de-trapped from the trap site and lead to increase the intensity.

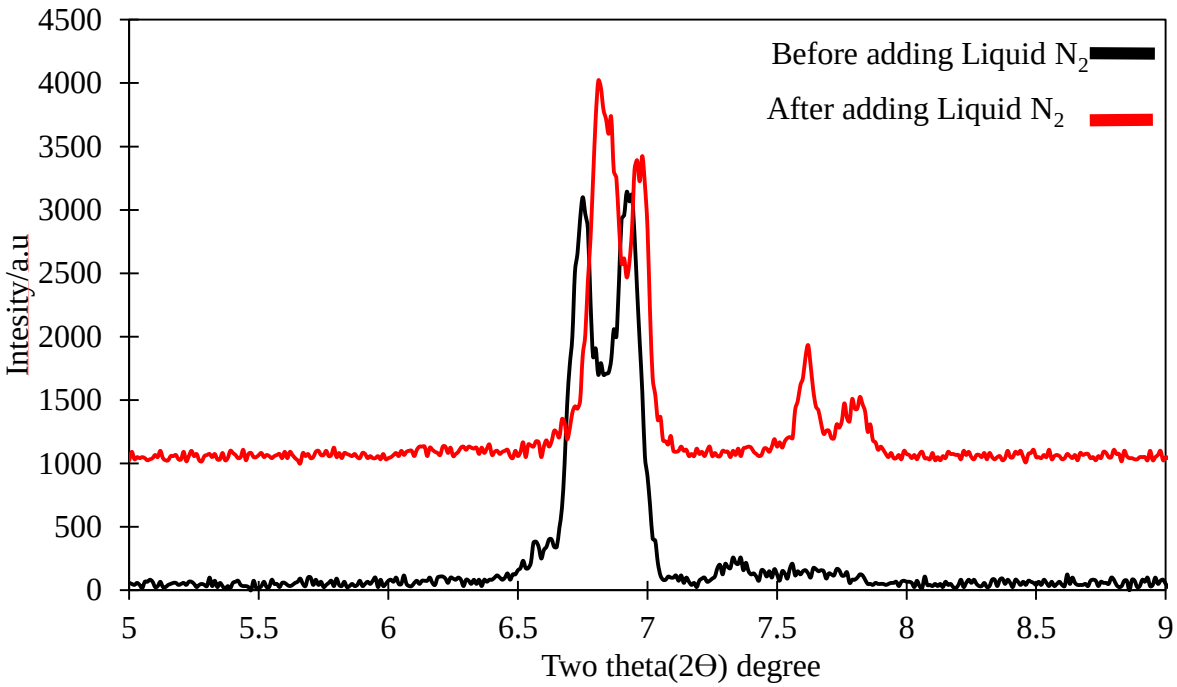

Figure 54 XRD profile on Eu(ii)Cl ligand contained ML material a) with treatment of Liquid Nitrogen b) without treatment of Liquid Nitrogen

Figure 52 reveal that X-ray diffraction patterns on the Eu(ii)Cl ligand included ML material with and without treatment of the liquid Nitrogen. After treated with Liquid Nitrogen, (b) XRD profile showed that crystallinity of the material was changed. Carefully studying of the XRD pattern in Figure 53 and 54 and 55 same mechanism happened, and we have observed crystallinity of the material is changed after treated the by the liquid nitrogen. We believe

that in the low temperature some part of the amorphous phase in the crystal converted to the crystalline phase and led to change the crystallinity of the whole ML material.

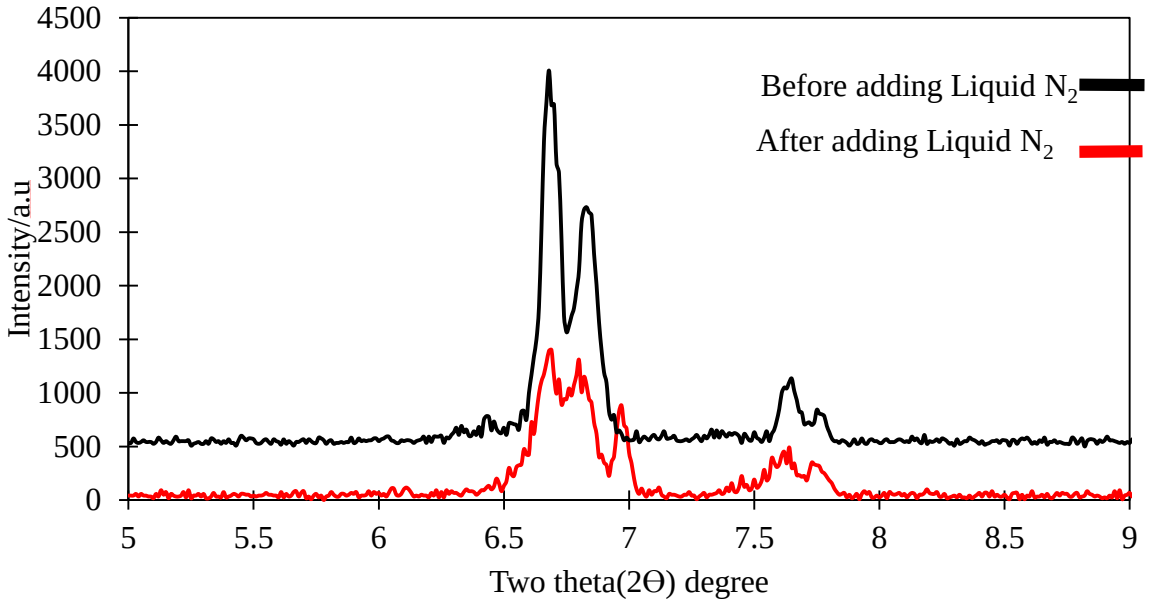

Figure 55 XRD profile on Eu(ii)I ligand contained ML material a) with treatment of Liquid Nitrogen b) without treatment of Liquid Nitrogen

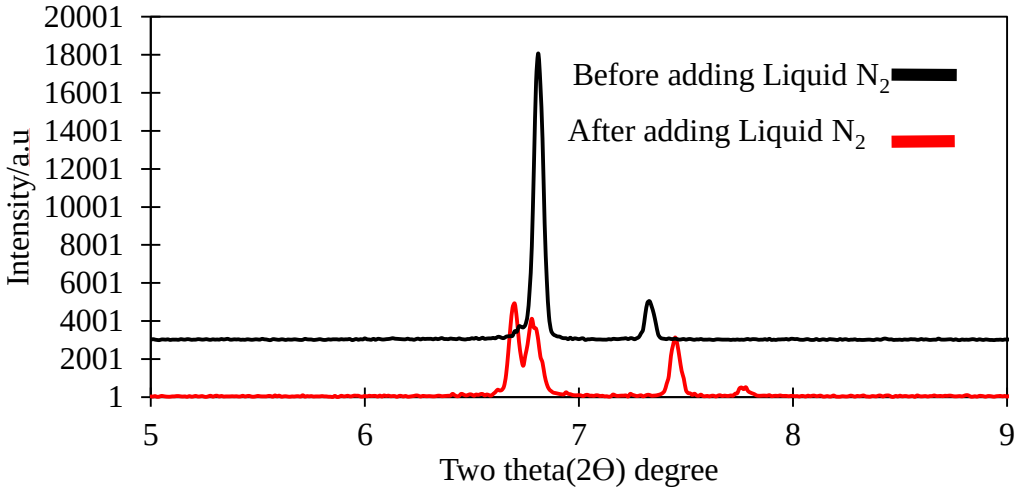

Figure 56 XRD profile on Eu(ii)Br ligand contained ML material a) with treatment of Liquid Nitrogen b) without treatment of

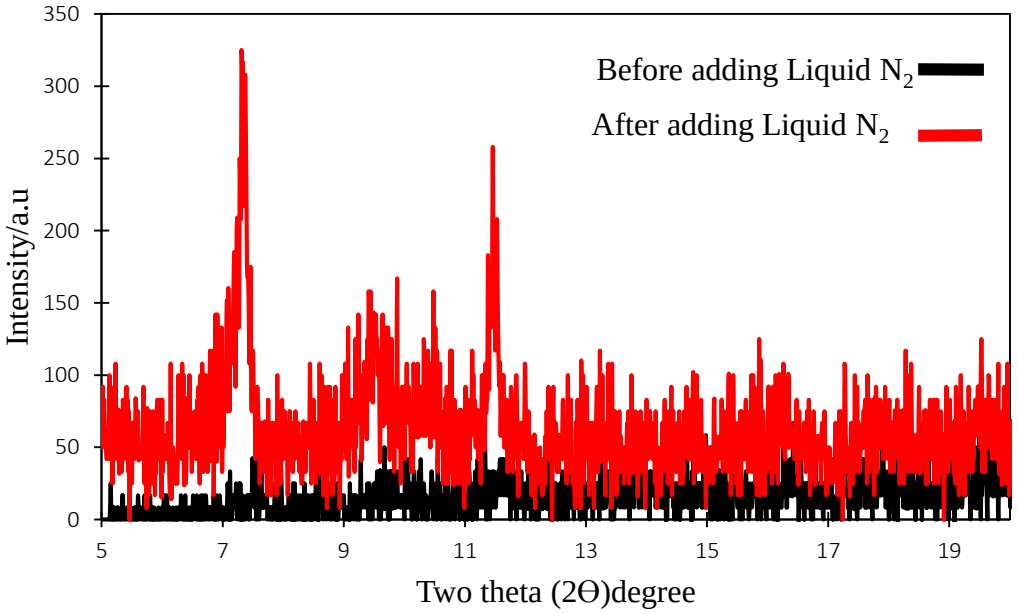

Figure 57 XRD profile on PhenDBMEu(iii)NO3 ligand contained ML material a) with treatment of Liquid Nitrogen b) without treatment of Liquid Nitrogen

differential scanning calorimetry studies

Figure 57,58,59 and 60 depicted that DSC profiles for the two different ML materials with and without treated liquid Nitrogen. Figure 57 corresponds to the DSC profile on Eu(ii)I based mechanoluminescent material before liquid nitrogen treatment. The calculation of the DSC reveal that glass transition temperature for that ML material is 19°C. However ML material after treated with Liquid Nitrogen ,DSC profile is shows glass transition temperature for that changed to 3°C.In figure 59 DSC profile reveal that PhenDBMEu(iii)NO_3 based mechanoluminescent material before liquid nitrogen treatment , according to the calculations Glass transition temperature for that -4°C.After treat with Liquid Nitrogen glass transitions

transfer to the -14°C.Carefully studying with four spectra we can see that after treated with liquid nitrogen glass transition temperature shift to lower temperature values. In this case, we can suggest that ML materials formed fully crystallize in lower temperature and because of the liquid nitrogen treatment some part contained the amorphous phase of the ML material trained to crystalized. In figure 56 XRD profile it is confirmed that PhenDBMEu(iii)NO_3 based mechanoluminescent material before the Nitrogen treatment amorphous phase and after treated with liquid Nitrogen transfer to crystallized.

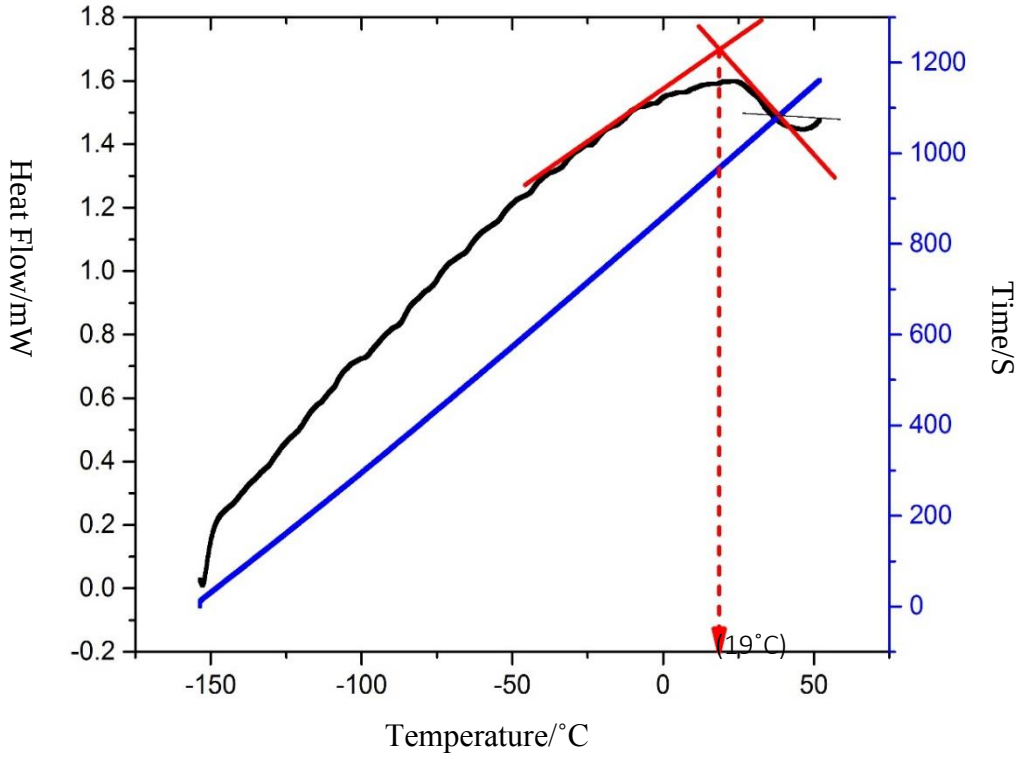

Figure 58 DSC profile on Eu(ii)I based mechanoluminescent material before liquid nitrogen treatment

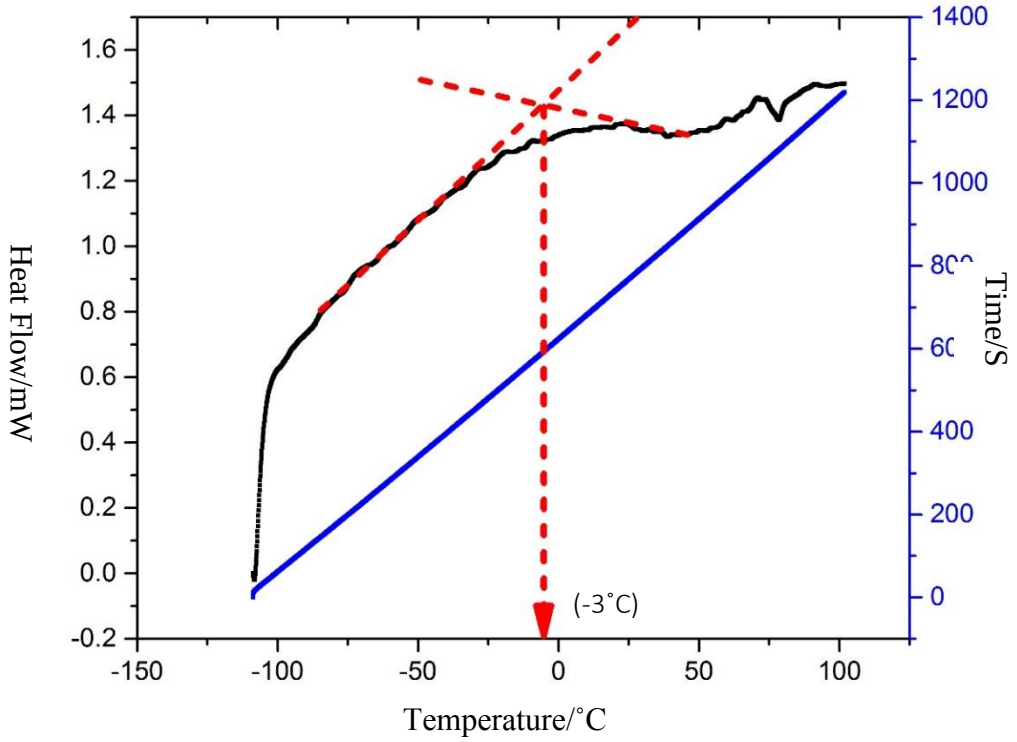

Figure 59 DSC profile on Eu(ii)I based mechanoluminescent material after liquid nitrogen treatment

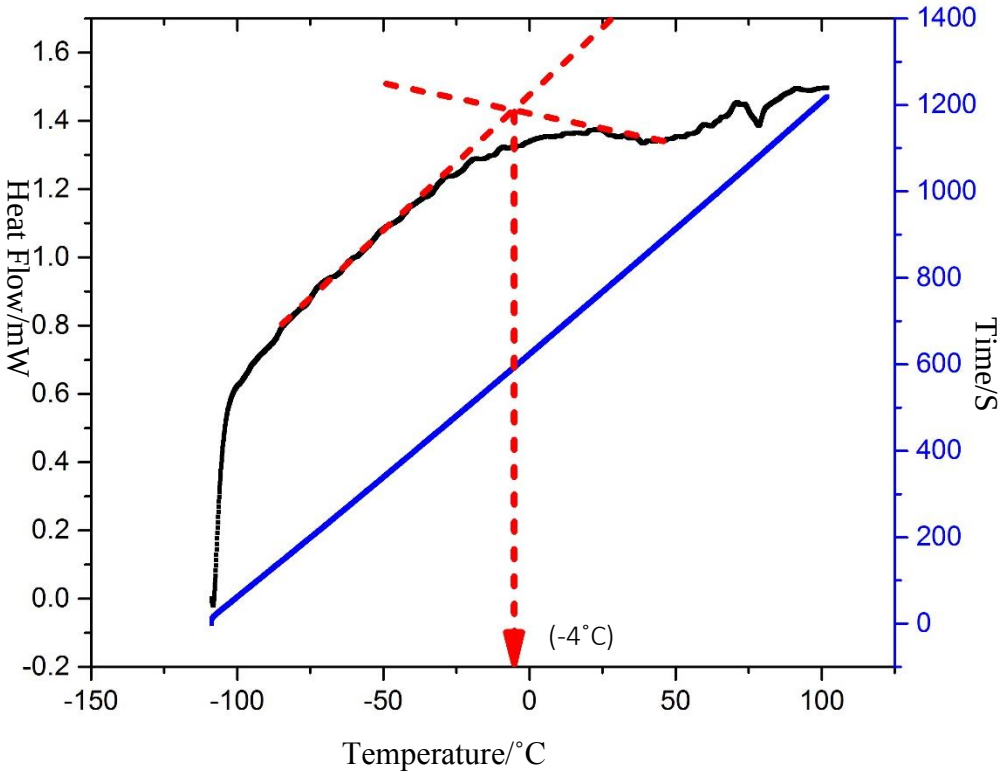

Figure 60 DSC profile on PhenDBMEu(iii)NO_3 ligand contained ML material before liquid nitrogen treatment

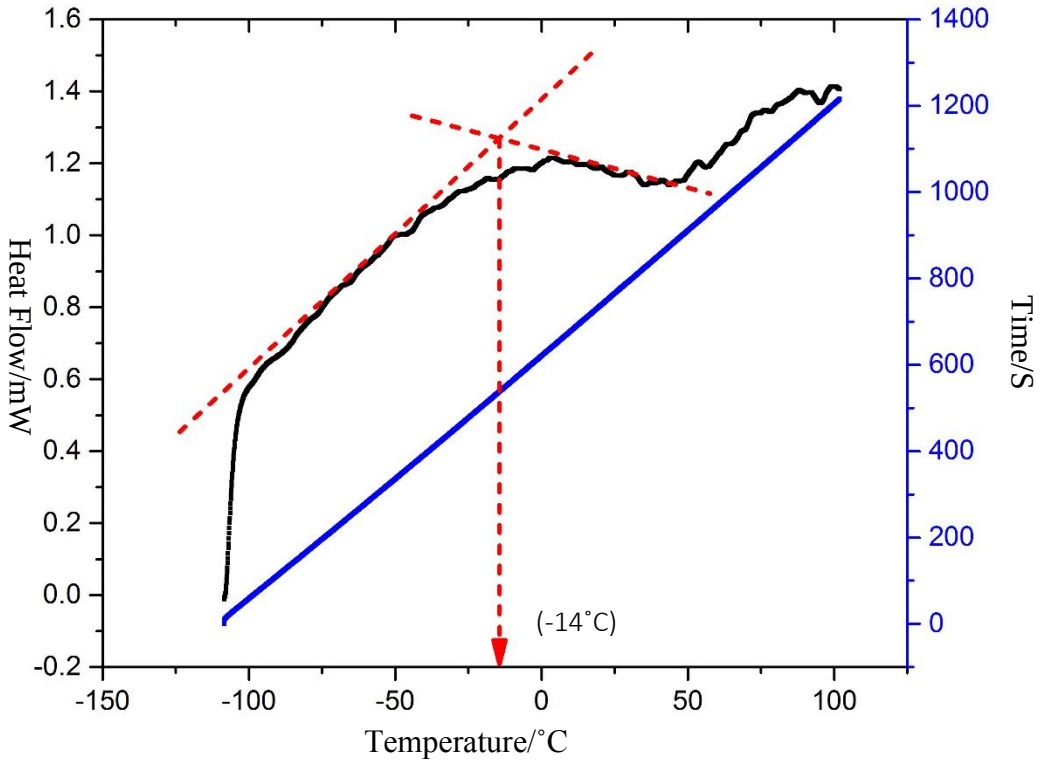

Figure 61 DSC profile on PhenDBMEu(iii)NO_3 ligand contained ML material after liquid nitrogen treatment

4.3.4 Conclusions

We have synthesized novel ML materials with three different ligands.ML intensity is increased gradually according to the electron affinity of the ligands. Highest ML intensity is reveal that Eu(ii)I contained ML material. PS data depicted that compositions od synthesized ML materials are only having C, O, Eu and Valance band structures of the ML material is confirmed that Eu^{+3} and Eu^{+2} is available in synthesized materials. DSC Profile confirmed

that after treated with liquid N glass transition temperature of the M material has changed and its confirmed that some part of the amorphous phase of the ML material has crystallized after treated with Liquid N. Increasing crystallinity peer to enhanced the ML intensity with higher electrons affinity.

4.3.5 References

79. Ohgaku, T., S. Nakamura, and K. Inabe, *Comparative study on mechanoluminescence of irradiated and non-irradiated ionic crystals.* Radiation Protection Dosimetry, 2006. **119**(1-4): p. 98-101.
80. Olawale, D.O., et al., *Introduction to Triboluminescence*, in *Triboluminescence: Theory, Synthesis, and Application*, D.O. Olawale, et al., Editors. 2016, Springer International Publishing: Cham. p. 1-16.
81. Balsamy, S., et al., *Triboluminescence and Vapor-Induced Phase Transitions in the Solids of Methyltriphenylphosphonium Tetrahalomanganate(II) Complexes.* Inorganic Chemistry, 2014. **53**(12): p. 6054-6059.
82. Takao, K., et al., *Effect of pressure on the luminescence of zinc sulphide phosphors.* Journal of Physics and Chemistry of Solids, 1966. **27**(10): p. 1577-1586.

Chapter 5 Fabrication of Mechanoluminescent Thin Film on Flexible Substrate and Effect of The PVP Concentration for the Photoluminescence and Mechanoluminescent Intensity

5.1 Introduction

Mechanoluminescence (ML) is a phenomenon that light emission induced by a mechanical action on a solid[39]. There are several forms of ML materials such as elastico, plastico and fracto, usually denoted by the method used to excite the electrons[40]. Compare with other luminescence materials elastico ML materials are most abundant of them because of continuous intensity is emitted while it is crushing[41]. Things what happen believe in here crystal bonds are broken along the planes with opposite charge, and when they are re-connected light is emitted as the charges pass through the separations created through the fractures[42]. ML also can be prepared by using peeling off the tape in a vacuum. The light is emitted by several distinct it depends on the substance and synthesized mechanism. The emission spectrum of sugar mentioned that the light comes from the atmospheric nitrogen that fills the Gap during fracture[44].Fabricate the Mechanoluminescent thin film is most notable of concern the applications of ML materials. Fabricate the Pressure-sensitive paint, earthquake detector, air bag sensor in the automobile industry and impact detector on aircraft are several applications on ML thin film. In 1999, Sage and Geddes used the property of ML, application for a sensor having the ability of locations of impact. They are used different kind

of ML materials could be utilized and arranged at various places. The main advantage of this is when an Impact takes place, its location could be identified according to corresponded wavelength emitted[45].However, consider the available mechanoluminescent materials' intensity is very low. Resulting light cannot detect easily also in dark light[83]. Nanoparticles have interested much attention due to their superior characteristics[84]. The reactions of nanoparticles with other substances can be more efficient due to their excellent surface to volumes ratios. In increasing to the leading percentage of atoms at the grain boundaries[85]. Most of the ML thin film are formed by using adhesive or resign, total ML intensity cannot obtain since of the diffraction of the resulting light. Therefore, we have focused to form the ML nanoparticles thin film without applying any resign or binder.

5.2 Experimental

The synthesis was began by 3mmol dibenzoylmethane(1,3-diphenylpropane-1,3dione, $C_{15}H_{12}O_2$), (98.0%, Wako) and 1.5 ml trimethylamine(99.0%,Wako) were dissolved in 80 ml of ethyl alcohol(99.5%,Wako) under vigorously stirred on the hot plate at 70°C for solute become completely dissolved. Then 0.3mol Europium(iii)nitratehexahydrate (99.9%,Wako) was added to the stirred solution and further stirred 20 minutes until the solution became apparent. The hot solution contained beaker was capped tightly then inserted into the thermos on treating on slow cooling effect for overnight. Precipitated synthesized ML material was filtered by using vacuumed filter and washed four-time with ethyl alcohol. Then different

concentration of polyvinylpyrrolidone (PVP) (4%w/w, 7%w/w, 9%w/w, 11%w/w, 13%w/w, 15%w/w) were dissolved in 40 ml ethanol solutions. 0.1g synthesized mechanoluminescencent material was added in to each different concentration of PVP solutions and sonicate for 5 minutes until completely dispersed. Six of Ni substrate was cleaned and heated 400˚C. Then 0.101g (0.01mol) $Al_2O_3$was dissolved in 40 ml of ethanol, and each solution was sprayed on above-heated substrates by using a spray gun. Heated substrates were kept cooling down to 130˚C.Then each ML material contained different PVP solutions were sprayed on the above-heated substrate by using a spray gun. Phase purity and crystal structure of the resulting materials were determined by X-Ray diffraction (Rigaku RINT UltimaIII XRD, Cu kα(λ=). Photoluminescence and mechanoluminescence were observed by Multichannel spectroscope(Hamamatsu-photonic) (PMA/C8808-01). X-Ray photoelectron spectra were measured by using KRATOS AXIS UltraOLD. TEM images were obtained by JEM-2100F.

5.3 Result and discussion

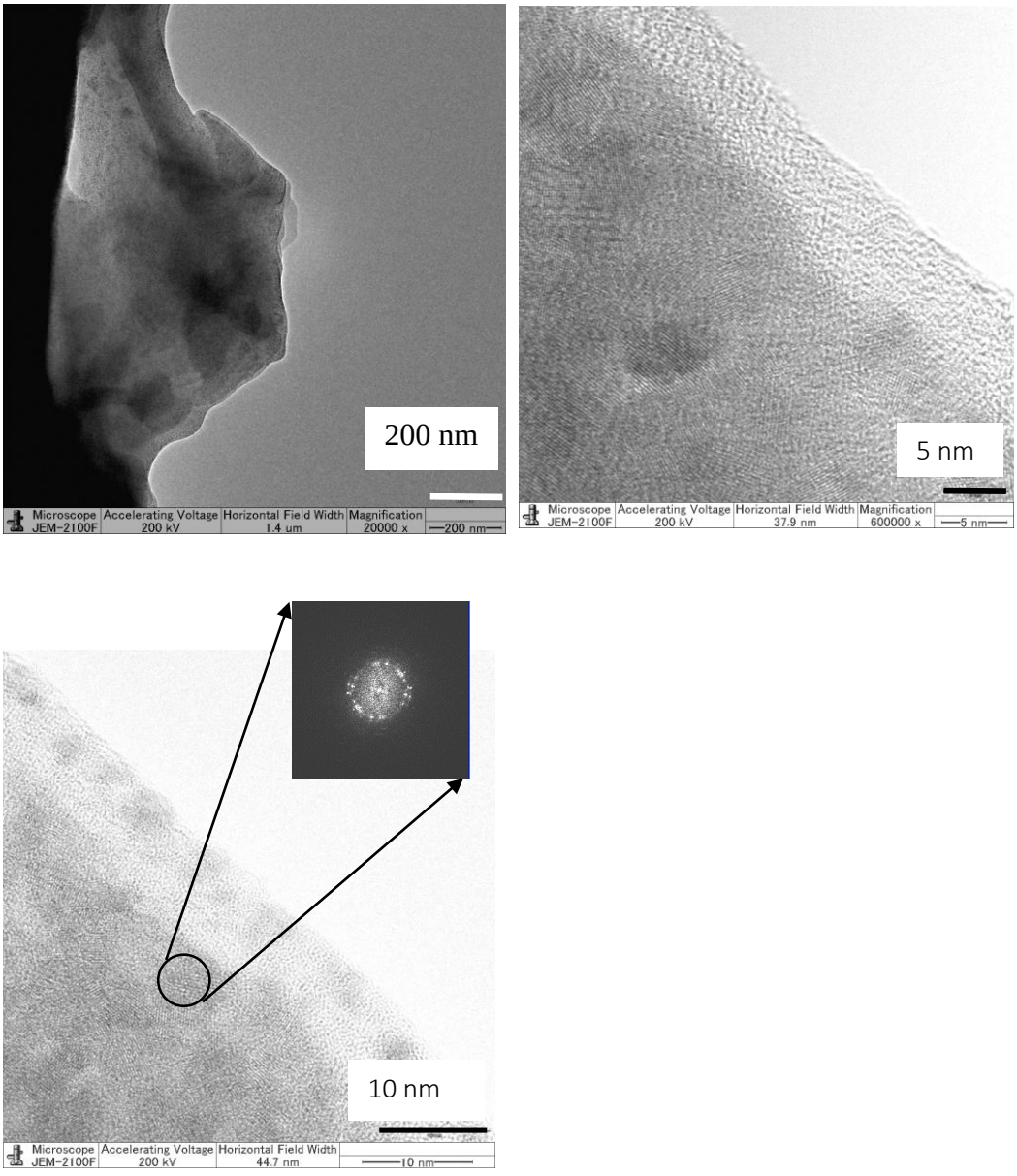

Figure 62 TEM images of Europium dibenzoylmethidetriethylammonium mechanoluminescent

Figure 60 TEM images are revealed that mechanoluminescent particles are well crystallized and particle size of those are around 2nm to 5nm.The diffraction pattern shows that content belongs to polycrystalline.

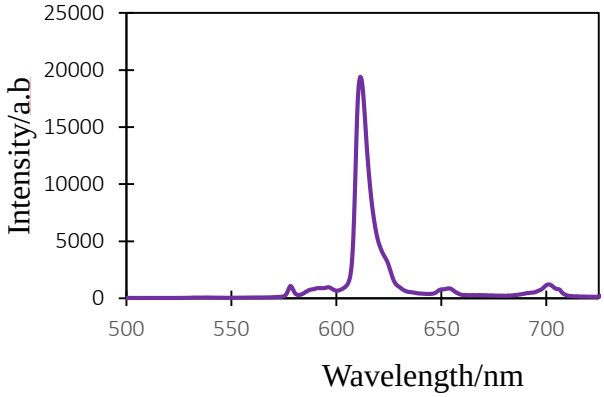

Figure 64 Photoluminescence intensity spectrum of the fabricated ML thin film

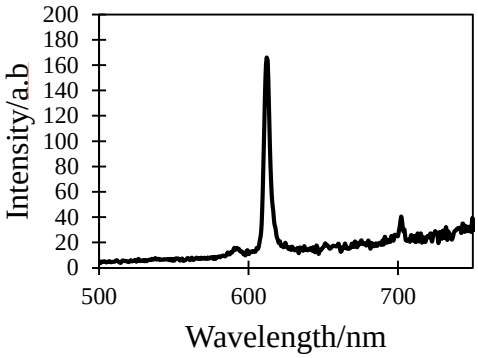

Figure 63 Mechanoluminescence intensity spectrum of the fabricated ML thin film

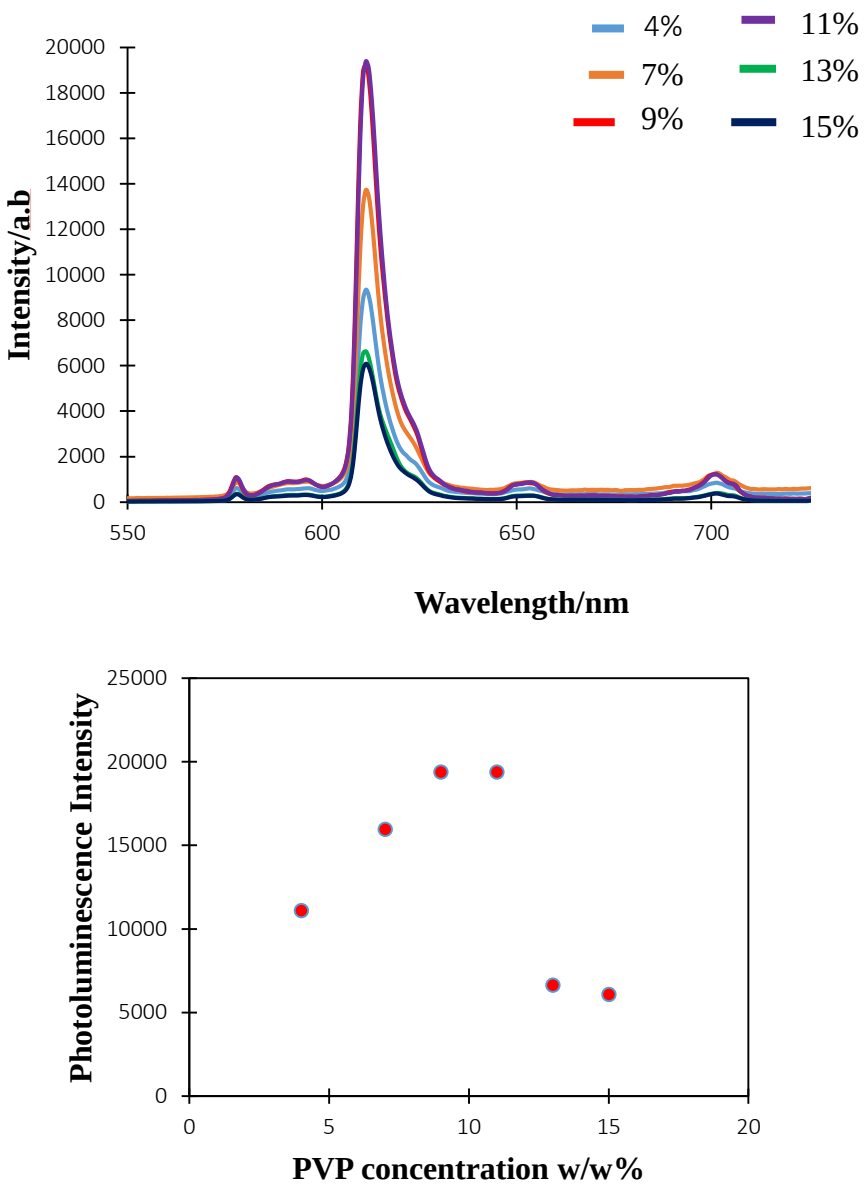

Figure 65 Photoluminescence spectrums on ML material with different pvp w/w%

Figure 61 and figure 62 have expressed mechanoluminescence (ML) and photoluminescence (PL) intensity spectrum of fabricated thin film with 11%w/w PVP concentration. Compare with other concentration this PVP concentration content thin film has higher PL and ML

intensity. ML intensity spectrums have showed bands at 592.7 nm ($^5d_0$-$^7F_1$), 612 nm ($^5D_0$-$^7F_2$), 651.2 nm ($^5D_0$-$^7F_3$), 691 nm and 701.3 nm ($^5D_0$-$^7F_4$). According to Figur**e** 62 photoluminescence intensity is increased PVP concentration from 4%w/w to 9%w/w then it is constant 9%w/w to 11%w/w and gradually decreased to 15%w/w. In mechanism can be happened when increasing the concentration of the PVP color center Eu^{+3} can be coordinate with PVP molecules, and electron transaction is increased from ligand (LUMO) to metal. Further increasing PVP can act as an impurity of the crystalline surface and cause to hinder the electron transaction to the metal ion. In this case only showing europium intra-energy state electron transaction and it is showing mainly intensity is decreasing of the ML material. Figure 64 corresponding XRD patterns reveal that changing of the crystallinity of the fabricated thin films with different concentration of the PVP. We investigated that when the concentration of the PVP from 4% w/w to 11% w/w crystallinity of the thin film is increased, and it is decreased the further increasing the PVP concentration. Compare with PL and ML intensity spectrum we investigated the intensity are in enhanced by 9%w/w to 11%w/w this is evidenced for crystallinity increasing of the material cause to the electron transaction increasing and tend to enhance the intensities of the ML material.

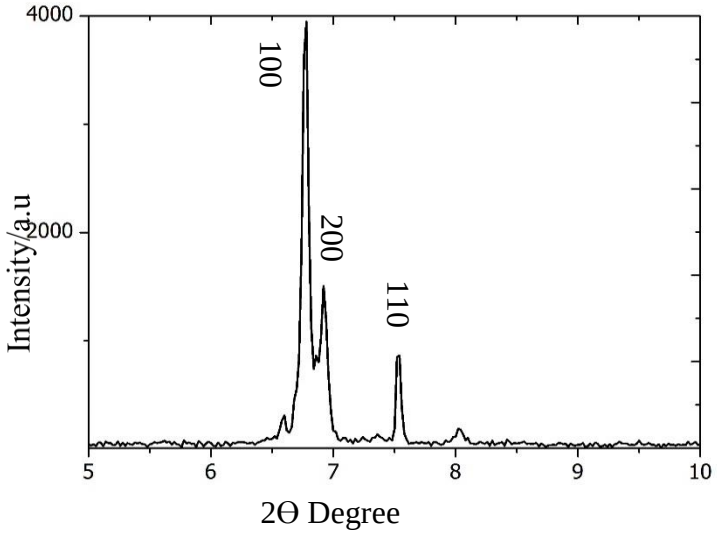
4000
2000
Intensity/a.u
100
200
110
5
6
7
8
9
10
2Θ Degree

(a)

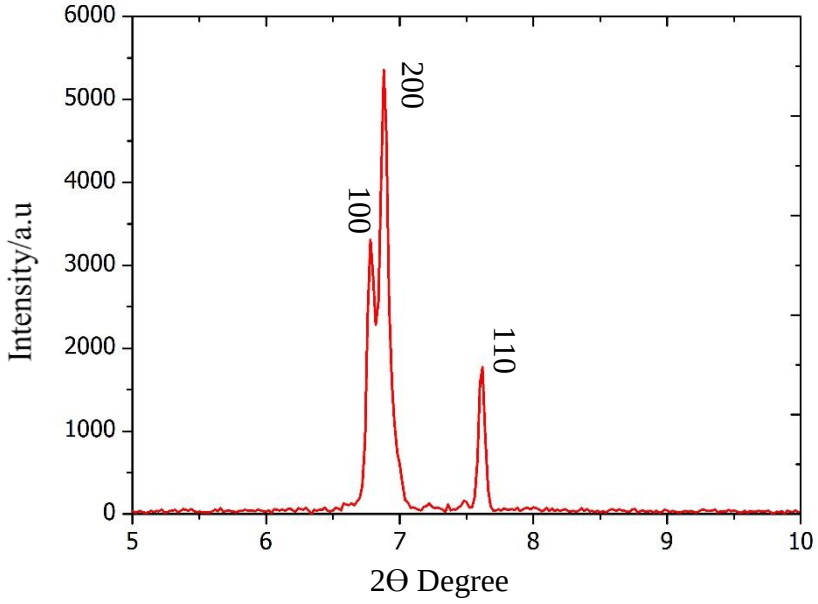
6000
5000
4000
3000
2000
1000
0
Intensity/a.u
200
100
110
5
6
7
8
9
10
2Θ Degree

(b)

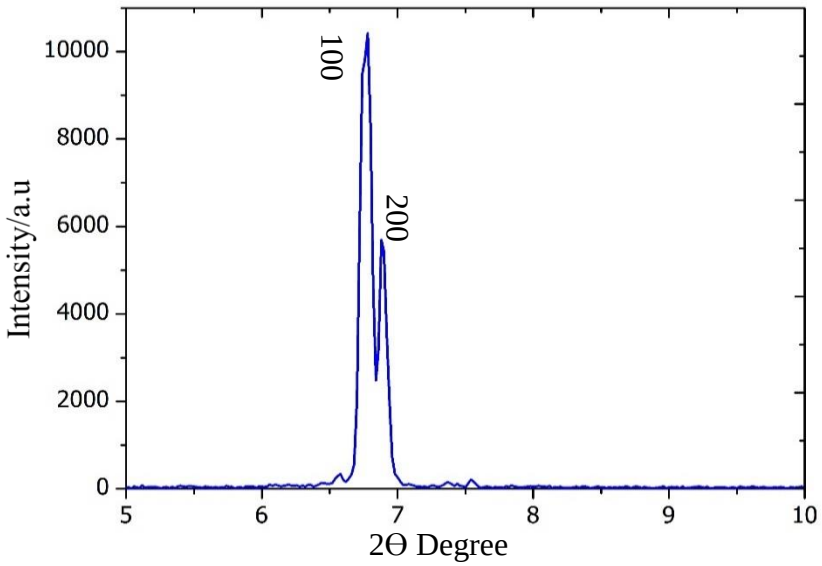
100
200
Intensity/a.u
2Θ Degree
0
2000
4000
6000
8000
10000
5
6
7
8
9
10

(c)

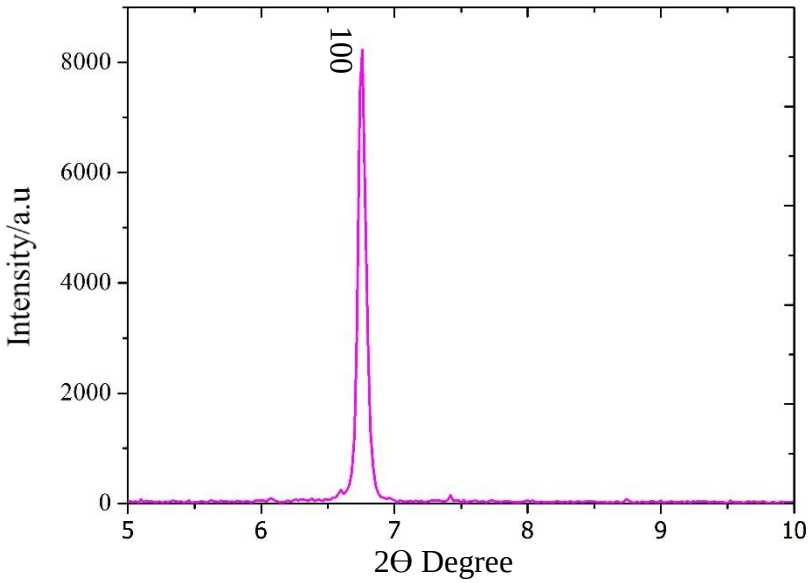
100
Intensity/a.u
2Θ Degree
0
2000
4000
6000
8000
5
6
7
8
9
10

(d)

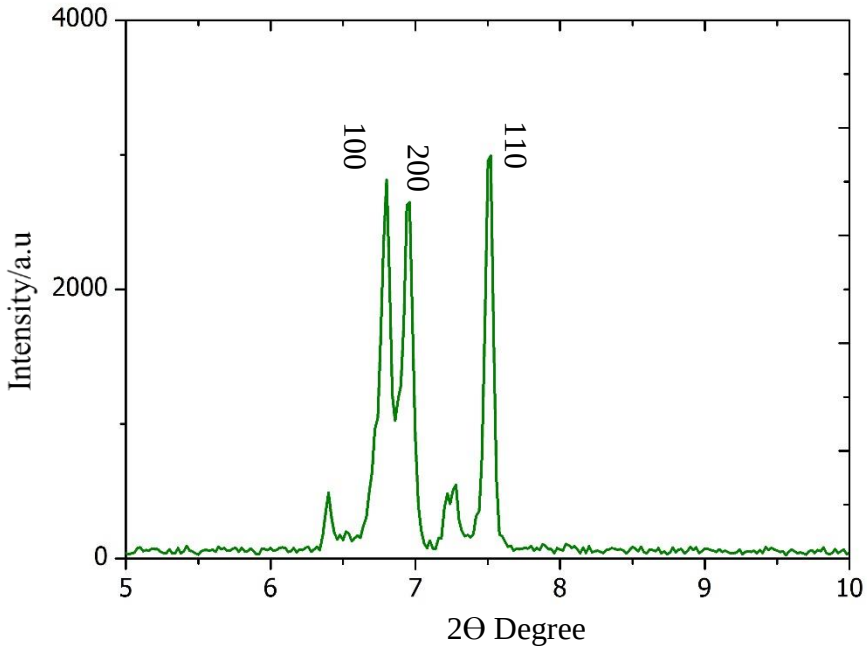

(e)

Figure 66 Corresponding XRD patterns on ML material with adding different concentration of the pvp (a) 4%w/w (b) 7%w/w (c) 9%w/w (d)11%w/w (e)15%w/w

Figure 64 corresponds XRD pattern of ML thin films with different concentration of PVP and peaks depicted on 2Θ value 6.7,6.9 belongs to the miller plane (100) and (200) (JCPDS Card No 00-054-1918).

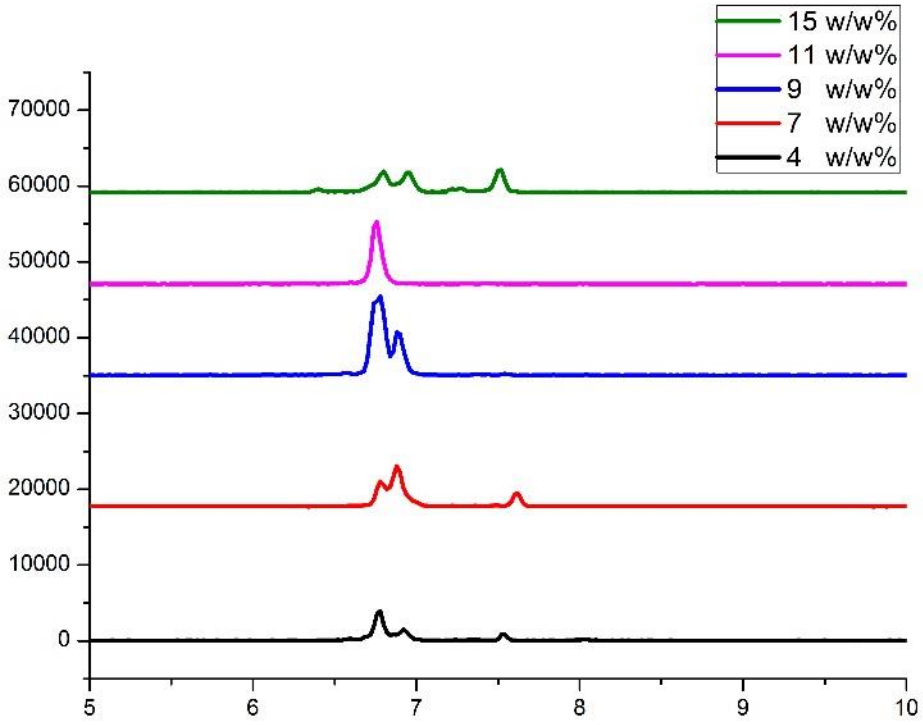

Figure 67 Stack view of Corresponding XRD patterns on ML material with adding different concentration of the pvp **(a)** 4%w/w **(b)** 7%w/w **(c)** 9%w/w **(d)**11%w/w **(e)**15%w/w

Figure 64 and 65 Corresponding XRD pattern reveals that fabricated material is well crystalline. However frequently increasing the concentration of weight percentage on PVP, Crystallinity of the material oscillating until 15%w/w. Since 9%w/w to 11%w/w planes on the material are overlapped after that, it seems to decrease. The viewpoint of this it believes that all the component corresponded to the material involved to the reaction on 11%w/w PVP concentration and some percentage of matter substance rest in a solvent which is not participating in the reaction. It is somehow disturbing to the mechanoluminescent property of the material.

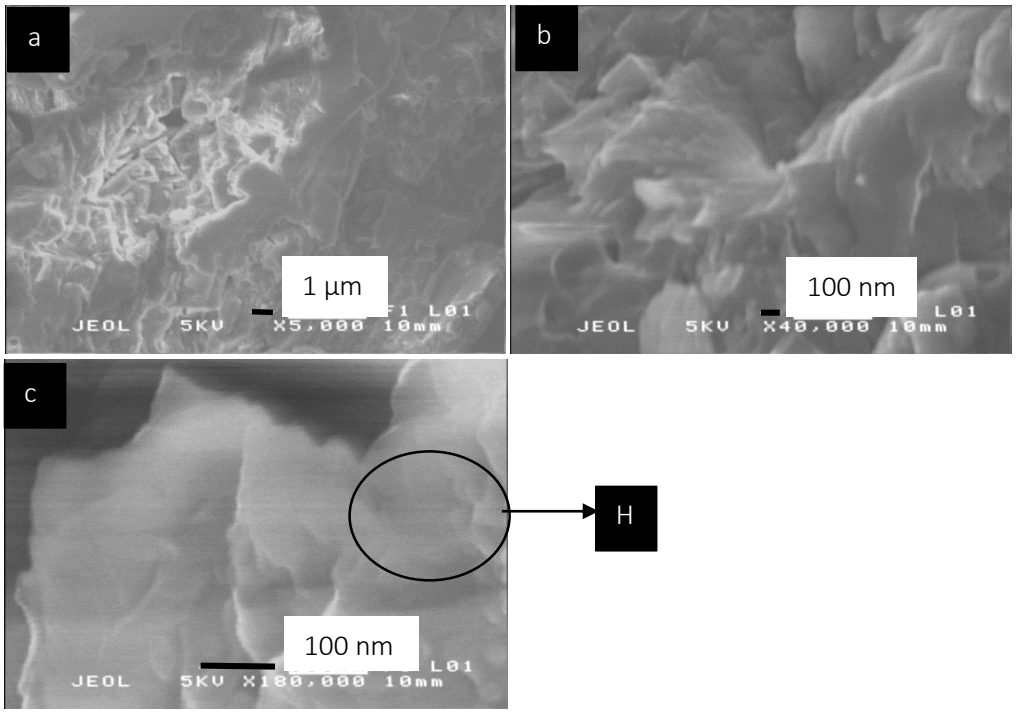

Figure 68 SEM micrographs of the fabricated ML thin film on 11% w/w pvp concentration

Figure 66 Shows the SEM micrograph of the fabricated thin film morphology on 11%w/w PVP concentration. Compare with the TEM images ML particles are tiny, approximately 2nm-5nm therefore in SEM images we cannot see the particles fluently. Part (H) we can see small particles in higher magnification. Image (a) and (b) we can see the PVP on fabricated thin film. Recently no one formed the mechanoluminescent thin film without resin and binder. In our knowledge, this is the first fabricate the mechanoluminescent thin film with higher intense.

Figure 69 Different places on Mechanoluminescent thin film stress by using glass mortar Captured by using Cannon 60D50mmf/1.8/exposure time 1/30 s iso 1200

5.4 Conclusions

We are successfully formed the organic mechanoluminescent thin film without any binder or resin. Intensity of both the mechanoluminescence and the photolumines-cence increases with the addition of polyvinylpirrolidone from 4%w/w to 11%w/w but further increase of pvp decreases the intensities due to the deteriorated crystallini-ty of material. Both the ML and the PL (excited by 357 nm) give emissions at 592.7 nm, 612 nm, 651.2 nm and 701.3 nm which correspond to 5D0 to 7Fn (n= 1,2,3,4) elec-tron transactions induced by the europium doping.

5.5 Synthesis of Mechanoluminescent Nanoparticles by Ball Milling And Fabrication of Organic-Based Novel Mechanoluminescent Thin Film

5.5.1 Introduction

Mechanoluminescence (ML) is a phenomenon that light emission induced by a mechanical action on a substantial[39]. There are several forms of ML materials such as elastico, plastico and fracto, usually denoted by the method used to excite the electrons[40]. Compare with other luminescence materials elastico ML elements are most abundant of them because of constant intensity is emitted while it is crushing[41]. The light is emitted by several distinct it depends on the material and synthesized mechanism. The emission spectrum of sugar mentioned that the light comes from the atmospheric nitrogen that fills the Gap during fracture[44].Fabricate the Mechanoluminescent thin film is most notable of concern the applications on ML materials. Manufacture the Pressure-sensitive paint, earthquake detector, air bag sensor in the automobile industry and impact detector on aircraft are several applications on ML thin film.However, Consider the available mechanoluminescent materials' intensity is very low. Resulting light cannot detect easily also in dark light[83]. Nanoparticles have captivated much consideration due to their distinct characteristics[84]. The reactions of nanoparticles with other materials can be more dynamic due to their high surface to volumes ratios. In appreciation to the great percentage of atoms at the grain terminals[85]. The major utility of the conventional ball milling is to fractures the particles and to diminish the size, e.g. increase mechanical strength, enhanced diffusivity higher specific heat and electrical resistivity compared to conventional coarse-grained

counterparts[86]. Most of the ML thin film are fabricated by using a binder or resign[63], whole the ML intensity cannot obtain because of the diffraction of the resulting light. Therefore we have focused on fabricating the ML nanoparticles thin film without using any resign or binder.

5.5.2 Experimental method

First ethyl alcohol (99.9%, Wako) was thawed to 70 °C, and then 1, 3-diphenylpropane-1, 3-dione (99%, Wako) was supplemented and stirred. After the solute was totally dissolved, europium nitrate hexahydrate (99.9%, Wako), polyvinylpyrrolidone(99.9%, Wako) and triethylamine (99.8%) were added further into the solution and retained at 70 °C for 20 minute. Then the solution vessel was capped tightly and inserted in the thermos overnight. Synthesized crystals were cleaned with ethanol in two times. 0.1g ML crystals embedded into the ball mill container, the mass ratio between ML: TiO_2 balls were 1:20 and ball milled for 5 hours. Then 1cmx1cm Ni substrate was cleaned, and heated 400˚C and 0.101g (0.01mol) Al_2O_3 powder was dissolved in 40 ml of ethanol and solution were sprayed on the above-heated substrate by using a spray gun. The heated substrate was kept to cool down to 130˚C. Finally, Ball milled ML material were dispersed 30 ml ethanol solution and sprayed on the above-heated substrate by using a spray gun.

5.5.3 Results and discussion

Figure 68 shows SEM micrograph on synthesized mechanoluminescent nanoparticles on fabricated thin film. Micrographs clearly show that mechanoluminescent particle size around 20 nm to 30 nm. Since particles size is reducing molecular orbitals are overlapping increased, and it is caused to quickly electron transaction between each energy levels. Therefore smaller particles can be easily excited by lower energy.

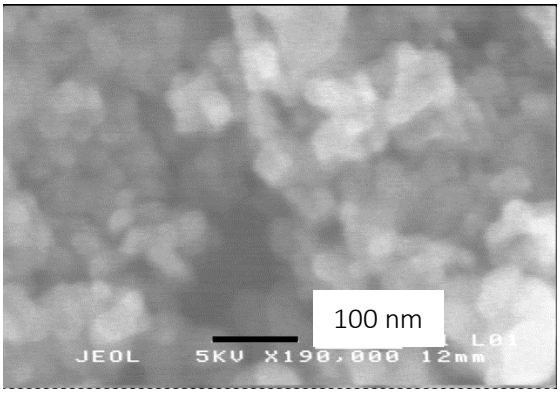

Figure 70 Scanning electron microscope Image (SEM) on Ball milled synthesized mechanoluminescent nanoparticles of fabricated thin film

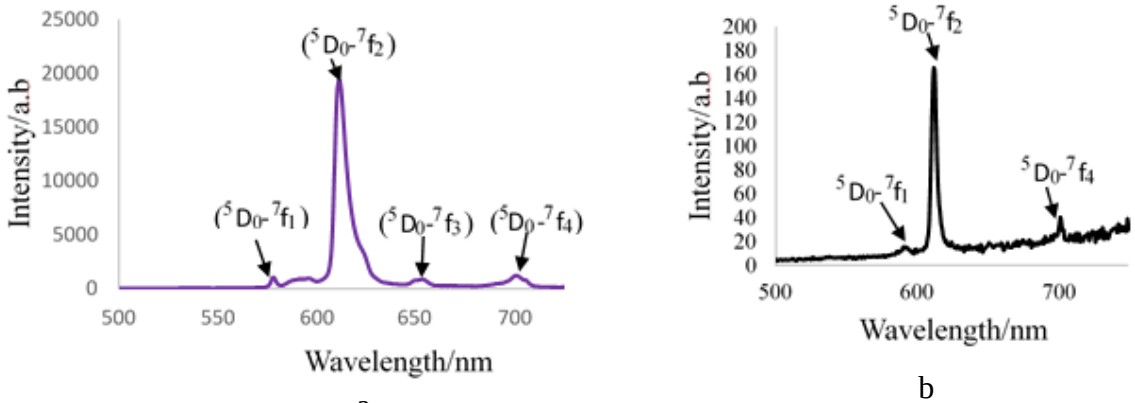

Figure 71 a) Photoluminescence spectrum on fabricated thin film **b)** mechanoluminescence spectrum on fabricated thin film

Figure 69 a) and **b)** are revealed photoluminescence and mechanoluminescence spectrums which are corresponded to fabricated thin film. The wavelength at 581nm, 612nm, 654 nm and 704nm correspond to europium $^5D_0$-$^7F_1$, $^5D_0$-$^7F_2$, $^5D_0$-$^7F_3$, and $^5D_0$-$^7F_4$ transactions. Compare with the photoluminescence and mechanoluminescence spectrums $^5D_0$-$^7F_3$ transaction we couldn't see, and it believes that electron excitation energy is not enough.

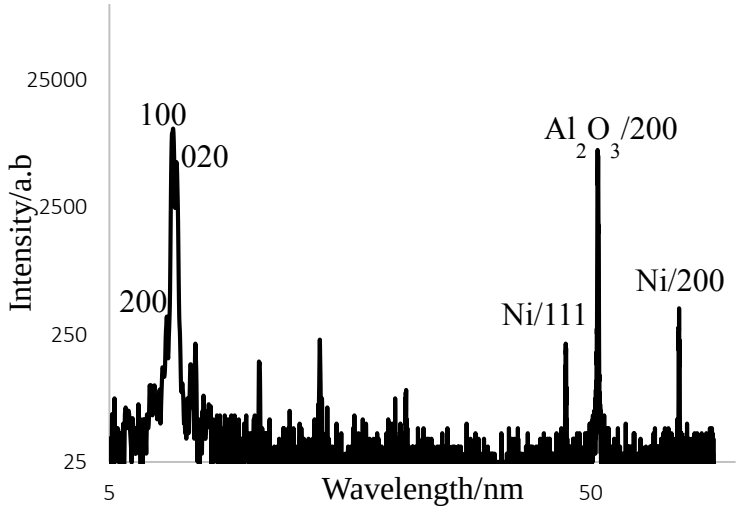

Figure 72 X-ray diffraction pattern on fabricated thin film

In Figure 70 XRD pattern reveal that Two-theta angles 6.76˚, 6.88˚ are corresponded to plane (100),(020) and belongs to the mechanoluminescent material. Two-theta angles 44.26˚, 76.4˚ are corresponded to plane 111,200 on Ni substrate, and angle 51.9˚ on plane 200 corresponded to Al_2O_3.

5.5.4 Conclusion

We are successfully fabricated mechanoluminescent thin film without mixing any resign or binder by simple hang spraying method. Photoluminescence and mechanoluminescence spectrums are revealed that fabricated thin film has intense photoluminescence and mechanoluminescence property. SEM micrograph (**Figure 68**) is evidence for synthesized mechanoluminescent particles became nanoparticles state after the ball milled. Corresponding XRD pattern is revealed that fabricated thin film is well crystalized.

5.5.5 References

39. Akiyama, M., et al., *Recovery phenomenon of mechanoluminescence from Ca2Al2SiO7:Ce by irradiation with ultraviolet light.* Applied Physics Letters, 1999. **75**(17): p. 2548-2550.
40. Chandra, B.P., *Mechanoluminescence*, in *Luminescence of Solids*, D.R. Vij, Editor. 1998, Springer US: Boston, MA. p. 361-389.
41. Fontenot, R.S., et al., *Synthesis and characterization of highly triboluminescent doped europium tetrakis compounds.* Journal of Luminescence, 2012. **132**(7): p. 1812-1818.
44. Putterman, S.J., et al., *Mechanoluminescent x-ray generator*. 2014, Google Patents.
63. Xu, C.N., et al., *Preparation and characteristics of highly triboluminescent ZnS film.* Materials Research Bulletin, 1999. **34**(10–11): p. 1491-1500.
83. Fontenot, R.S., et al., *Comparison of the triboluminescent properties for europium tetrakis and ZnS:Mn powders.* Journal of Theoretical and Applied Physics, 2012. **6**(1): p. 15.
84. Momeni, A. and M.H. Mahdieh, *Photoluminescence analysis of colloidal silicon nanoparticles in ethanol produced by double-pulse ns laser ablation.* Journal of Luminescence, 2016. **176**: p. 136-143.
85. Brandl, F., et al., *Nanoparticles with photoinduced precipitation for the extraction of pollutants from water and soil.* Nature Communications, 2015. **6**: p. 7765.
86. Loh, Z.H., A.K. Samanta, and P.W. Sia Heng, *Overview of milling techniques for improving the solubility of poorly water-soluble drugs.* Asian Journal of Pharmaceutical Sciences, 2015. **10**(4): p. 255-274.

Reference

1. Ahn, T.S., et al., *Self-absorption correction for photoluminescence quantum yields from integrating sphere measurements.* Rev Sci Instrum, 2007. **78**.
2. Janulevicius, M., et al., *Luminescence and luminescence quenching of highly efficient Y2Mo4O15:Eu3+ phosphors and ceramics.* Scientific Reports, 2016. **6**: p. 26098.
3. Dothager, R.S., et al., *Cerenkov Radiation Energy Transfer (CRET) Imaging: A Novel Method for Optical Imaging of PET Isotopes in Biological Systems.* PLOS ONE, 2010. **5**(10): p. e13300.
4. Wurfel, P., *The chemical potential of radiation.* Journal of Physics C: Solid State Physics, 1982. **15**(18): p. 3967.
5. Katsumi, Y., et al., *Thermochromism, Photochromism and Anomalous Temperature Dependence of Luminescence in Poly(3-Alkylthiophene) Film.* Japanese Journal of Applied Physics, 1988. **27**(4A): p. L716.
6. Goldberg, M.C. and E.R. Weiner, *The Science of Luminescence*, in *Luminescence Applications*. 1989, American Chemical Society. p. 1-22.
7. Enomoto, K., J.A. LaVerne, and M.S. Araos, *Heavy Ion Radiolysis of Liquid Pyridine.* The Journal of Physical Chemistry A, 2007. **111**(1): p. 9-15.
8. Liu, Y., et al., *Photophysics of Monodisperse Platinum-Acetylide Oligomers: Delocalization in the Singlet and Triplet Excited States.* Journal of the American Chemical Society, 2002. **124**(42): p. 12412-12413.
9. Reiher, M., O. Salomon, and B. Artur Hess, *Reparameterization of hybrid functionals based on energy differences of states of different multiplicity.* Theoretical Chemistry Accounts, 2001. **107**(1): p. 48-55.
10. Georgescu, S., et al., *Excited-state-absorption in low concentrated Er : YAG crystals for pulsed and cw pumping.* Journal of Luminescence, 2001. **93**(4): p. 281-292.
11. Duffy, D.M., S.L. Daraszewicz, and J. Mulroue, *Modelling the effects of electronic excitations in ionic-covalent materials.* Nuclear Instruments and Methods in Physics Research Section B: Beam Interactions with Materials and Atoms, 2012. **277**: p. 21-27.
12. Carey, F.A. and R.J. Sundberg, *Advanced Organic Chemistry: Part A: Structure and Mechanisms*. 2007: Springer Science & Business Media.
13. Widder, E.A., *Bioluminescence in the Ocean: Origins of Biological, Chemical, and Ecological Diversity.* Science, 2010. **328**(5979): p. 704-708.
14. Xu, Y., D.W. Piston, and C.H. Johnson, *A bioluminescence resonance energy transfer (BRET) system: Application to interacting circadian clock proteins.* Proceedings of the National Academy of Sciences, 1999. **96**(1): p. 151-156.
15. Matsumoto, M., *Advanced chemistry of dioxetane-based chemiluminescent substrates originating from bioluminescence.* Journal of Photochemistry and Photobiology C: Photochemistry Reviews, 2004. **5**(1): p. 27-53.

16. Rees, J.F., et al., *The origins of marine bioluminescence: turning oxygen defence mechanisms into deep-sea communication tools.* Journal of Experimental Biology, 1998. **201**(8): p. 1211.
17. Shimomura, O., F.H. Johnson, and Y. Saiga, *Extraction, Purification and Properties of Aequorin, a Bioluminescent Protein from the Luminous Hydromedusan, Aequorea.* Journal of Cellular and Comparative Physiology, 1962. **59**(3): p. 223-239.
18. Elliott, C.M., et al., *Highly Efficient Solid-State Electrochemically Generated Chemiluminescence from Ester-Substituted Trisbipyridineruthenium(II)-Based Polymers.* Journal of the American Chemical Society, 1998. **120**(27): p. 6781-6784.
19. Leland, J.K. and M.J. Powell, *Electrogenerated Chemiluminescence: An Oxidative - Reduction Type ECL Reaction Sequence Using Tripropyl Amine.* Journal of The Electrochemical Society, 1990. **137**(10): p. 3127-3131.
20. Jiang, Q., et al., *Chemiluminescent energy transfer conjugates and their uses as labels in binding assays*. 2000, Google Patents.
21. Weiser, H.B., *Crystalloluminescence.* The Journal of Physical Chemistry, 1917. **22**(7): p. 480-509.
22. Chung, C.T., et al., *Organic electro-luminescence element used in a display device*. 2005, Google Patents.
23. Toyama, T., et al., *Hot-electron induced electroluminescence and avalanche multiplication in hydrogenated amorphous silicon.* Journal of Non-Crystalline Solids, 1996. **198**: p. 198-201.
24. Kido, J. and T. Matsumoto, *Bright organic electroluminescent devices having a metal-doped electron-injecting layer.* Applied Physics Letters, 1998. **73**(20): p. 2866-2868.
25. Karg, S., et al., *Transient electroluminescence in poly(p-phenylenevinylene) light-emitting diodes.* Synthetic Metals, 1994. **67**(1): p. 165-168.
26. Mariano, A.N. and P.J. King, *Europium-activated cathodoluminescence in minerals.* Geochimica et Cosmochimica Acta, 1975. **39**(5): p. 649-660.
27. Wu, X.L., et al., *Photoluminescence and cathodoluminescence studies of stoichiometric and oxygen-deficient ZnO films.* Applied Physics Letters, 2001. **78**(16): p. 2285-2287.
28. Werts, M.H.V., *Making sense of lanthanide luminescence.* Science Progress, 2005. **88**(2): p. 101-131.
29. Vanheusden, K., et al., *Mechanisms behind green photoluminescence in ZnO phosphor powders.* Journal of Applied Physics, 1996. **79**(10): p. 7983-7990.
30. Prosperetti, A., *A new mechanism for sonoluminescence.* The Journal of the Acoustical Society of America, 1997. **101**(4): p. 2003-2007.
31. Nakashima, K., et al., *Thermoluminescence mechanism of dysprosium-doped β-tricalcium phosphate phosphor.* Journal of Luminescence, 2005. **111**(1–2): p. 113-120.
32. Watanabe, S., et al., *Thermoluminescence Mechanism In Li2B407:Cu.* Radiation Protection Dosimetry, 1996. **65**(1-4): p. 79-82.
33. Chandra, B.P., et al., *Fracto-mechanoluminescence and mechanics of fracture of solids.* Journal of Luminescence, 2012. **132**(8): p. 2012-2022.
34. Carpenter, M.A., et al., *Elastic anomalies due to structural phase transitions in mechanoluminescent SrAl2O4:Eu.* Journal of Applied Physics, 2010. **107**(1): p. 013505.
35. Chandra, B.P. and A.S. Rathore, *Classification of Mechanoluminescence.* Crystal Research and Technology, 1995. **30**(7): p. 885-896.
36. Dickinson, J.T., et al., *Fracto-emission from deuterated titanium: Supporting evidence for a fracto-fusion mechanism.* Journal of Materials Research, 2011. **5**(1): p. 109-122.

37. Chandra, V.K., B.P. Chandra, and P. Jha, *Models for intrinsic and extrinsic elastico and plastico-mechanoluminescence of solids.* Journal of Luminescence, 2013. **138**: p. 267-280.
38. Chandra, B.P., V.K. Chandra, and P. Jha, *Piezoelectrically-induced trap-depth reduction model of elastico-mechanoluminescent materials.* Physica B: Condensed Matter, 2015. **461**: p. 38-48.
39. Akiyama, M., et al., *Recovery phenomenon of mechanoluminescence from Ca2Al2SiO7:Ce by irradiation with ultraviolet light.* Applied Physics Letters, 1999. **75**(17): p. 2548-2550.
40. Chandra, B.P., *Mechanoluminescence*, in *Luminescence of Solids*, D.R. Vij, Editor. 1998, Springer US: Boston, MA. p. 361-389.
41. Fontenot, R.S., et al., *Synthesis and characterization of highly triboluminescent doped europium tetrakis compounds.* Journal of Luminescence, 2012. **132**(7): p. 1812-1818.
42. Fontenot, R., et al., *Luminescent properties of lanthanide dibenzoylmethide triethylammonium compounds.* Journal of Theoretical and Applied Physics, 2013. **7**(1): p. 1-10.
43. Chandra, V.K. and B.P. Chandra, *Suitable materials for elastico mechanoluminescence-based stress sensors.* Optical Materials, 2011. **34**(1): p. 194-200.
44. Putterman, S.J., et al., *Mechanoluminescent x-ray generator*. 2014, Google Patents.
45. Fontenot, R., et al., *Comparison of the triboluminescent properties for europium tetrakis and ZnS:Mn powders.* Journal of Theoretical and Applied Physics, 2012. **6**(1): p. 1-9.
46. Hurt, C.R., et al., *High Intensity Triboluminescence in Europium Tetrakis (Dibenzoylmethide)-triethylammonium.* Nature, 1966. **212**(5058): p. 179-180.
47. Sweeting, L.M. and A.L. Rheingold, *Crystal disorder and triboluminescence: triethylammonium tetrakis(dibenzoylmethanato)europate.* Journal of the American Chemical Society, 1987. **109**(9): p. 2652-2658.
48. Zhang, J.-C., et al., *Elastico-mechanoluminescent enhancement with Gd3+ codoping in diphase (Ba,Ca)TiO3:Pr3+.* Optical Materials Express, 2014. **4**(11): p. 2300-2309.
49. Liu, Y. and C.-N. Xu, *Influence of Calcining Temperature on Photoluminescence and Triboluminescence of Europium-Doped Strontium Aluminate Particles Prepared by Sol−Gel Process.* The Journal of Physical Chemistry B, 2003. **107**(17): p. 3991-3995.
50. Kaur, J., et al., *Optical properties of rare earth-doped barium aluminate synthesized by different methods-A Review.* Research on Chemical Intermediates, 2015. **41**(4): p. 2317-2343.
51. Chandra, B.P., et al., *Mechanoluminescence glow curves of rare-earth doped strontium aluminate phosphors.* Optical Materials, 2011. **33**(3): p. 444-451.
52. Watanabe, T., C. Xu, and M. Akiyama, *Triboluminescent inorganic material and a method for preparation thereof*. 2000, Google Patents.
53. Tsuguo, I., et al., *Fracto-Luminescence of Rare Earth Element-Doped Hexacelsian (B a A l 2 S i 2 O 8).* Japanese Journal of Applied Physics, 1997. **36**(6B): p. L781.
54. Chandra, B.P., V.K. Chandra, and P. Jha, *Models for intrinsic and extrinsic fracto-mechanoluminescence of solids.* Journal of Luminescence, 2013. **135**: p. 139-153.
55. Chandra, V. and B. Chandra, *Dynamics of the mechanoluminescence induced by elastic deformation of persistent luminescent crystals.* Journal of Luminescence, 2012. **132**(3): p. 858-869.
56. Zhang, J.-C., et al., *Controlling elastico-mechanoluminescence in diphase (Ba,Ca)TiO3:Pr3+ by co-doping different rare earth ions.* RSC Advances, 2014. **4**(77): p. 40665-40675.

57. Mathur, V.K. and J.L. Price, *Color switchable stress-fracture sensor for damage control*. 2007, Google Patents.
58. Tiwari, N., V. Dubey, and R.K. Kuraria, *Mechanoluminescence Study of Europium Doped CaZrO3 Phosphor.* Journal of Fluorescence, 2016. **26**(4): p. 1309-1315.
59. Jha, P. and B.P. Chandra, *Survey of the literature on mechanoluminescence from 1605 to 2013.* Luminescence, 2014. **29**(8): p. 977-993.
60. Chandra, B.P., et al., *Sensing of shock-wave velocity and pressure using shock-wave induced mechanoluminescence of crystals.* Sensors and Actuators A: Physical, 2015. **235**: p. 203-209.
61. Teotonio, E.E.S., et al., *Mechanoluminescence of Coordination Compounds*, in *Triboluminescence: Theory, Synthesis, and Application*, O.D. Olawale, et al., Editors. 2016, Springer International Publishing: Cham. p. 39-63.
62. Reynolds, G.T. and R.H. Austin, *Mechanoluminescence of plastic scintillation counters.* Journal of Luminescence, 2000. **92**(1–2): p. 79-82.
63. Xu, C.N., et al., *Preparation and characteristics of highly triboluminescent ZnS film.* Materials Research Bulletin, 1999. **34**(10–11): p. 1491-1500.
64. Takada, N., et al., *Mechanoluminescence from piezoelectric crystals of an europium complex.* Synthetic Metals, 2000. **111–112**: p. 587-590.
65. Chandra, B.P., *Mechanoluminescence and high pressure photoluminescence of (Zn, Cd) S phosphors.* Pramana, 1982. **19**(5): p. 455-465.
66. Chandra, B.P., V.K. Chandra, and P. Jha, *Microscopic theory of elastico-mechanoluminescent smart materials.* Applied Physics Letters, 2014. **104**(3): p. 031102.
67. Jeong, S.M., et al., *Mechanoluminescence Color Conversion by Spontaneous Fluorescent-Dye-Diffusion in Elastomeric Zinc Sulfide Composite.* Advanced Functional Materials, 2016. **26**(27): p. 4848-4858.
68. Botterman, J., et al., *Mechanoluminescence in BaSi2O2N2:Eu.* Acta Materialia, 2012. **60**(15): p. 5494-5500.
69. Chandra, B.P., et al., *Real-time mechanoluminescence sensing of the amplitude and duration of impact stress.* Sensors and Actuators A: Physical, 2012. **173**(1): p. 9-16.
70. Wang, X., et al., *Dynamic Pressure Mapping of Personalized Handwriting by a Flexible Sensor Matrix Based on the Mechanoluminescence Process.* Advanced Materials, 2015. **27**(14): p. 2324-2331.
71. Rahimi, M.R., et al., *Effects of persistent luminescence decay on mechanoluminescence phenomena of SrAl2O4:Eu2+, Dy3+ materials.* Optics Letters, 2013. **38**(20): p. 4134-4137.
72. Li, D.G., N.S. McAlpine, and D. Haneman, *Surface barriers and potentials from luminescence on cleaved Si, GaAs, and InP.* Surface Science, 1993. **281**(1): p. L315-L320.
73. Lin, Y.-H., et al., *Studies on mechanoluminescence from SrAl2O4:Eu, Dy phosphor.* Materials Chemistry and Physics, 2003. **80**(1): p. 20-22.
74. Chandra, B.P., et al., *Strong mechanoluminescence induced by elastic deformation of rare-earth-doped strontium aluminate phosphors.* Journal of Luminescence, 2009. **129**(7): p. 760-766.
75. Imai, Y., R. Momoda, and C.-N. Xu, *Elasticoluminescence of europium-doped strontium aluminate spherical particles dispersed in polymeric matrices.* Materials Letters, 2007. **61**(19–20): p. 4124-4127.

76. Sharma, R., et al., *Mechanoluminescence and thermoluminescence of Mn doped ZnS nanocrystals.* Journal of Luminescence, 2011. **131**(10): p. 2089-2092.
77. Pust, P., et al., *Narrow-band red-emitting Sr[LiAl3N4]:Eu2+ as a next-generation LED-phosphor material.* Nat Mater, 2014. **13**(9): p. 891-896.
78. Schneider, C.A., W.S. Rasband, and K.W. Eliceiri, *NIH Image to ImageJ: 25 years of image analysis.* Nat Meth, 2012. **9**(7): p. 671-675.
79. Ohgaku, T., S. Nakamura, and K. Inabe, *Comparative study on mechanoluminescence of irradiated and non-irradiated ionic crystals.* Radiation Protection Dosimetry, 2006. **119**(1-4): p. 98-101.
80. Olawale, D.O., et al., *Introduction to Triboluminescence*, in *Triboluminescence: Theory, Synthesis, and Application*, D.O. Olawale, et al., Editors. 2016, Springer International Publishing: Cham. p. 1-16.
81. Balsamy, S., et al., *Triboluminescence and Vapor-Induced Phase Transitions in the Solids of Methyltriphenylphosphonium Tetrahalomanganate(II) Complexes.* Inorganic Chemistry, 2014. **53**(12): p. 6054-6059.
82. Takao, K., et al., *Effect of pressure on the luminescence of zinc sulphide phosphors.* Journal of Physics and Chemistry of Solids, 1966. **27**(10): p. 1577-1586.
83. Fontenot, R.S., et al., *Comparison of the triboluminescent properties for europium tetrakis and ZnS:Mn powders.* Journal of Theoretical and Applied Physics, 2012. **6**(1): p. 15.
84. Momeni, A. and M.H. Mahdieh, *Photoluminescence analysis of colloidal silicon nanoparticles in ethanol produced by double-pulse ns laser ablation.* Journal of Luminescence, 2016. **176**: p. 136-143.
85. Brandl, F., et al., *Nanoparticles with photoinduced precipitation for the extraction of pollutants from water and soil.* Nature Communications, 2015. **6**: p. 7765.
86. Loh, Z.H., A.K. Samanta, and P.W. Sia Heng, *Overview of milling techniques for improving the solubility of poorly water-soluble drugs.* Asian Journal of Pharmaceutical Sciences, 2015. **10**(4): p. 255-274.

Chapter 6 Conclusions

6.1 Conclusions

In this thesis, we have succeeded to synthesized the ML material at low temperature and increased the ML and PL intensity with adopted different additives. First time we have succeed to fabricated the ML thin film without using any binder or resin. Further we have observed the structure of the novel ML material with utilizing different characterizations. Our research objectives have achieved.

1. We have successfully synthesized organic based ML materials at a low temperature at 70°C without addition and with an addition of PVP.

ML and PL intensity are defined by using Multichannel spectroscope (Hamamatsu Photonics, PMA). PL spectrum with 357 nm excitation consists of emission lines at 592.7 nm, 612.0 nm, 651.2 nm including 701.3 nm. This discharge wavelength belongs to electron transition between $^{5}D_{0}$ to $^{7}F_{n}$ (n=1,2,3,4) energy levels. Corresponded XRD and TEM patterns are evidence for novel material have good crystallinity rather than without PVP material. More electron orbital over lapping, the flexibility of ligand molecules and higher dipole moment of the PVP caused to increase the ML, and PL intensity of the novel synthesized ML material.

2. Structural formation is observed by using NMR, XRD instrumentation and HOMO and LUMO molecular orbital energy distributions of the molecules are investigated by using Gaussian DFT calculations.

For the first time, we have investigated the minimum ratio between TEA and DBM (1:3) from an analysis of ^{1}H and ^{13}C NMR spectra. The XRD characterization carried out for 2θ values from 5˚ to 40˚, and the prominent XRD peaks were observed in the range of 5˚to 10˚. In Figure 3, the 2θ values at 6.68, 6.87, 7.00 and 7.60 correspond to the (100), (200), (110) and (011) Millar planes, respectively, and in good agreement with JCPDS card no: 96-711-8092. The XRD measurements confirmed that the crystal structure similar to the europium, 2,2′-bipyridine 5,5′-dicarboxylic acid ($C_{36}Eu_2N_6O_{17}$) compound and the crystal system is monoclinic. The Miller planes (100), (200) reveal that the structure has grown along the vertical c plane and when other two planes, (110) and (011), are considered it can be concluded that the material has a rod-like structure.

The XPS results indicate that the materials have peaks that correspond to C, O, N and Eu. The ML and PL intensities were characterized using a Multichannel spectroscope (Hamamatsu Photonic/PMA).

The corresponding TEM images have confirmed that the material has a rod-like structure, and a histogram confirmed particle sizes at approximately 4 nm. The histogram from the TEM micrographs and XRD results of the material without PVP confirm a mean value of grain size from approximately 7 nm to 10 nm. After the addition of PVP, a decrease in the particle size was confirmed. The fine particle size and crystallinity of the synthesized

ML material enabled a higher overlap in the electron orbitals. The greater electron orbital overlap, a flexibility of the ligand molecules and a higher dipole moment of PVP resulted in an increase in the ML and PL intensities of the synthesized ML material.

Since the novel material has a higher ML intensity, it can be applied to defect detection in pipes, stress sensor analyses, real- time visualization of the stress distribution in solids, internal visualization of artificial legs, real-time visualization of the aquadynamic crack-propagation in solids, novel ML-driven solar cell systems, and real-time visualization of the stress field near the tip of a crack and used as an ML light source.

3. We have investigated the enhanced the intensity of the ML material with changing the ligands and observed that with XRD characterization crystallinity of the ML material is enhanced with changing the ligands. XPS data confirmed that HOMO and LUMO energy difference of the ML material peer to change according to changing the ligands.

DSC observation are confirmed that after treatment with liquid nitrogen glass transition temperature of the ML materials are changed. It is confirmed that after the treatment some amorphous phase of the materials have turned to crystalized and lead to increase the intensity of ML materials.

4. For the first time, we have succeeded to fabricated the intense ML thin film without using any binder or resin on a flexible Ni substrate.

Spray technique is cost effective energy saving simple method to formed ML thin film with higher intense. Corresponding ML spectrum reveal that band at 592.7 nm,652.2 nm, 691 nm, 701.3 nm are Europium $^5D_0$-$^7F_4$ energy transitions.

Photoluminescence intensity of the ML thin film is increased gradually with PVP concentration from 4% w/w to 9% w/w then it is decreased to 15% w/highest ML and PL intensity is corresponds to 11% w/w PVP included ML thin film and it has good crystallinity.

6.2 Expectations

About the future research, the following strategies should be taken in to consideration.

1). As the pressure sensitivity hope to analysis the ML intensity variations with different pressure by using ML setup.

2). Hope to synthesize the novel ML materials with tunable light emission by using combination of the lanthanide elements.

List of Figures